ASE-2017

SURVEY OF EXTRATERRESTRIAL NON-SOLAR X-RADIATION BY ROCKET BORNE INSTRUMENTS

By H. Gursky, R. Giacconi and J. R. Waters

Prepared under Contract No. NAS w-898 by
AMERICAN SCIENCE AND ENGINEERING, INC.
11 Carleton Street, Cambridge, Massachusetts 02142

for

NATIONAL AERONAUTICS AND SPACE ADMINISTRATION

FOREWORD

This document represents the final report on NASA Contract NAS w-898 The program initiated under this contract called for the design, construction and integration into Aerobee rockets of two fully instrumented payloads in order to perform observations of X-rays originating from outside the solar system. The program also called for the reduction and analysis of the data obtained during the rocket flight of these payloads. The scientific objectives were to survey the directional intensity of non-solar cosmic X-rays, obtain a rough survey of their spectral composition between 10 A and 0. 1A, distinguish between a thermal and non-thermal component, and correlate regions of strong intensity with optical and radio objects of special interest. The work outlined above has been completed. The payloads developed under this program were successfully flown on NASA designated Aerobees 4. 122 CG and 4. 123 CG. The results from these rocket flights, as well as descriptions of the instrumentation have been published in the scientific literature. The published reports are attached as appendices to this document.

The principal investigator for this program was Dr. Riccardo Giacconi of AS&E. Co-investigators have been Dr. Herbert Gursky, Dr. Oscar Manley, Dr. John Waters of AS&E and Professor Bruno Rossi of M. I. T. The project scientist at AS&E was Dr. Gursky.

Payload engineering and integration was the responsibility of Mr. Donald Fryklund and Mr. Gerald Sinnamon. The project electrical engineer was Mr. Stanley Mickiewicz. The project mechanical engineer was Mr. Albert DiCaprio. Mr. Gerald Ouellette and Mr. Michael Bate

were responsible for numerical analysis and computer programming. The above-named individuals are staff members at AS&E.

Certain phases of this program have been carried out as a collaborative effort with scientists associated with the Physics Department at M.I.T. The modulation collimator was conceived at M.I.T. and the first models were constructed there. Additional efforts have been involved in the analysis of portions of the data and in the authorship of research papers. The individuals participating in this collaboration at M.I.T. have been George Clark, Gordon Garmire, Minoru Oda and Masami Wada. Professor Oda is on leave from the Institute for Nuclear Study of the University of Tokyo, and Professor Wada is on leave from the Institute of Physical and Chemical Research in Tokyo.

ACKNOWLEDGEMENTS

As with any space research effort, the success of this program has depended on the conscientious effort of many individuals in several agencies. We gratefully acknowledge the contribution of the rocket sounding branch of the Goddard Space Flight Center, which had the responsibility for providing the telemetry system, integration of the payload with the rocket, coordinating flight operations, and providing high quality recorded data. The vehicle manager for this program was Mr. George Kraft, and the telemetry engineer was Mr. William Fortney.

We also acknowledge the support given us by the group at the U. S. Navy Ordnance and Missile Test Facility at the WSMR, who were actually responsible for launching the rocket. That group was directed by Chief Warrant Officer Bieber.

TABLE OF CONTENTS

		Page
1.0	INTRODUCTION	1
2.0	EXPERIMENT PLAN	5
3.0	INSTRUMENTATION	9
4.0	ROCKET FLIGHTS	19
5.0	DATA REDUCTION AND ANALYSIS	23
6.0	CONCLUSIONS AND RECOMMENDATIONS	29
REFERENCES		32
APPENDICES		

LIST OF FIGURES

		Page
FIGURE 1	ASSEMBLED PAYLOAD	10
FIGURE 2	ASSEMBLED PAYLOAD	10
FIGURE 3	ASSEMBLED PAYLOAD WITH OGIVE	11
FIGURE 4	BANKS OF GEIGER COUNTERS MOUNTED IN ROCKET	12
FIGURE 5	SCINTILLATION COUNTER	13
FIGURE 6	PHOTOELECTRIC DETECTOR	15
FIGURE 7	STAR ASPECT SENSOR	16
FIGURE 8	TELEMETRY RECORD	18

1.0 INTRODUCTION

At the initiation of this program the observational status of X-ray astronomy was that a strong X-ray source had been detected in the constellation Scorpius and that weaker sources had been observed in Cygnus and Taurus. Also a general background of X-radiation had been observed that could be of celestial origin. The source in Scorpius had been detected from three independent rocket experiments flown during June 1962[1], April 1963[2], and June 1963[3] by groups of scientists at AS&E and at NRL. These observations had clearly established the existence of intense celestial sources of X-rays. The astrophysical implications of the existence of these sources had been examined by a number of authors. At the time of the original discovery, it was suggested that the X-rays represent synchrotron radiation of a high energy (10^{18} ev) electron component of galactic cosmic rays[1]. Other possibilities arose. These were:

1) Inverse compton effect as a source of background (4)
2) Cumulative effect of external galaxies as a source of background (5)
3) "Hot" intergalactic electrons as a source of background (6)
4) Suprathermal electrons in the vicinity of the galactic centre (5)
5) Neutron stars (7, 8)

The problem in accounting for celestial X-rays is that the fluxes observed at the earth (10^{-7} - 10^{-8} ergs/cm^2 -sec in the energy range 1 - 10 Kev) requires source emissivity between 10^{33} - 10^{38} ergs/sec at reasonable stellar distances. Such an energetic source implies a configuration of matter that is not anticipated on the basis of visible light or radio observations.

The objectives of a program of X-ray astronomy from sounding rockets as we saw them early in 1964 were as follows:

1. All sky survey with moderate angular resolution. If one could increase the X-ray detection sensitivity by an order of magnitude, more sources might be expected to be revealed, as well as allowing more precise location of known sources.

2. Moderate resolution spectral data. Any given mechanism for X-ray production makes a prediction as to the spectral shape.

In order to perform this program two rocket payloads were instrumented for flight from Aerobee 150 rockets. The flights took place on 29 August 1964 and 27 October 1964.

The data from these rocket flights have served to establish the following facts regarding celestial X-rays.

1. A cluster of sources exists in the vicinity of the galactic center. These sources are distinct from ScoX-1, the strong source in Scorpius.

2. At least two sources near the galactic center were isolated (SgrX-1, ScoX-2) and their position given within 1^{o}.

3. ScoX-1 was located within $1/2^{o}$.

4. The angular diameter of ScoX-1 was established to be less than seven arc minutes.

5. Spectral data indicates that X-radiation from the group of sources near the galactic center extended to about 30 Kev whereas the radiation from ScoX-1 fell off rapidly above 15 Kev. In the range 1 - 10 Kev, the spectrum was well represented by a distribution (ergs/cm^2-sec-(c/s)) of the form E^{-1} (E = energy of the X-rays) for both source regions.

6. The only sources observed were those near the galactic center and ScoX-1. No other sources exist in the region of scan with intensity of as much at 1/20 ScoX-1.

Given these results, along with results of rocket experiments performed by the other groups of scientists, the following picture of the X-ray sources emerges.

1) With the exception of ScoX-1, which lies at a galactic latitude of $+25^{\circ}$, all known sources are confined to within a few degrees of the galactic equator.

2) The observed distribution indicates that most, if not all, the known X-ray sources belong to the local galaxy. Those clustered near the galactic center, probably are about 8000 p. c. from the earth. ScoX-1 may be very close (several hundred p. c.).

3) An extragalactic origin cannot be excluded for one or more of the sources.

4) The only known object that has been observed to emit measurable fluxes of X-rays is the Crab Nebula (9, 10). The remaining objects do not correlate with strong radio sources or peculiar visible light objects.

5) Spectral data has been obtained on several objects. Significant fluxes of X-rays have been observed from the Crab Nebula out to about 60 Kev (10); and from the sources near the galactic center out to about 30 Kev. The radiation from ScoX-1 drops sharply beyond about 15 Kev.

These new observations are not sufficiently quantitative to allow an unambiguous identification of the nature of the X-ray sources, but they have served to limit the choices. It is not possible to reconcile the observations with neutron stars as they are currently thought to occur. Where there is spectral data, a blackbody spectrum can be ruled out, and furthermore, except for the Crab Nebula, none of the known supernova remants is observed to emit X-rays. If one still wishes to consider neutron stars as a possible explanation for the X-ray sources, new theories must be developed that

allow for their evolution without a supernova phase, and also allow for a substantial fraction of their radiation output to arise from non-thermal processes.

The Crab Nebula may represent a distinct class of X-ray emitters compared to the other objects since no other radio sources or supernova remnants are observed to emit X-rays. Furthermore the X-radiation from the Crab cannot be simply ascribed to an extension of the synchrotron radiation from that object. The lifetime of the electrons giving rise to such X-rays would be extremely short (~year) and implies the existence of a very efficient acceleration mechanism.

On the other hand it has become apparent that hot plasmas could be the sources of the X-rays. With a temperature of the order of $10^{7}{}^{o}K$, a plasma will radiate primarily in the 1 - 10 Kev X-ray range, without necessarily radiating more strongly in the visible light or radio regions of the spectrum. One can easily derive the physical conditions required of such plasmas (density, size, etc.). There is no evidence (except for the X-ray data) for the existence of such objects; however, the solar corona, the earth's magnetosphere and planetary nebulae are examples of hot plasmas which do exist, even though they do not apparently represent the state of matter necessary to comprise an X-ray source of the kind that are observed.

2.0 EXPERIMENT PLAN

Given the objectives of the program as outlined in the introduction, we planned to perform the following experiment from the Aerobee rockets. To insure a small precession cone and to maintain the angular momentum axis close to vertical, the rocket would be allowed to maintain a high (2 rps) spin rate during its flight above the atmosphere. Four banks of geiger counters would be incorporated in the payload; the counters would be collimated to yield a field of view 10° x 20° (10° in the direction of the spin) and directed so that the centers of the field of view of each bank made angles of 10°, 20°, 30° and 40°; respectively, with respect to the rocket equator. Thus, during the flight, the hemisphere above the horizon between 0° and 50° elevation (comprising about 75% of the observable portion of the celestial sphere) would be scanned for X-ray sources.

To obtain spectral data two filters were to be mounted in front of two of the banks of counters (the four banks of counters were mounted in pairs on opposite sides of the rockets). During the flight the filters would drop from the bank of counters in front of which they were initially mounted to the bank of counters immediately below. In this way data would be recorded from each counter bank with no filter, one filter, and two filters interposed.

Additional spectral information was to come from independent detectors. A NaI scintillation counter would record X-rays with energies greater than about 10 Kev; a photoelectric detector would record data from X-rays with energies below several Kev. An anthracene scintillation counter was incorporated to record the charged particle contribution.

Rocket aspect was to be determined from data given by a pair of star sensors sensitive to third magnitude stars. Magnetometers were included in the payload to aid in the problem of star identification.

After the program had been initiated, we modified our objectives on the basis of the invention by Prof. Minoru Oda of M.I.T. of the modulation collimator (10). The collimator allows the observation of small angular diameters of the X-ray sources. On the basis of the device we decided to make an attempt to measure the angular size of ScoX-1. The collimator is described in Appendix A, which details as well the manner in which we intended to use it in the rocket. The principal advantage of the modulation collimator is its broad field of view for acquiring a source. The field of view of a conventional mechanical collimator is equal to its angular resolution; thus in a scanning experiment, the observation time of a given source is directly proportional to the angular resolution of the collimator. In any given experiment there is a limitation on how narrow a field of view can be used, based on the requirement that a reasonable number of counts be detected from the source. The modulation collimator, with its broad field of view, is not affected by this requirement in the experiments we had planned. We modified the payload by providing two banks of geiger counters with modulation collimators. The remaining two banks of geiger counters, as well as the other instrumentation, remained unchanged.

The first rocket flight (Aerobee 4.122) was planned for a sidereal time of 21 hr, at which time the galactic equator was almost directly overhead running on a north-south line. The flight allowed for a maximum separation in the scan direction between ScoX-1 and the galactic center. The results from that flight indicated that a cluster of sources existed near the galactic center and along the galactic equator. It also indicated that much higher angular resolution was required than the $10 \times 20^{\circ}$ used in the first flight in order to resolve these sources. Accordingly we modified

the payload planned for the second flight to the following extent. Two banks of geiger counters with the center of their field of view at 0° and 20° respectively, were fitted with slat collimators with a field of view of $1.5^{\circ} \times 10^{\circ}$ FWHM. The 1.5° was in the elevation direction and the 10°, in the scan direction. These counters viewed a very narrow swath of the sky per rotation, and the precession of the rocket spin axis would cause this swath to move across the sky. We planned to fly at a sidereal time (21 hr) such that the counters would scan along the galactic equator during the precession motion. A third bank of counters was fitted with $1.5 \times 15^{\circ}$ FWHM collimators with the center of the field of view at 10° elevation. The 1.5° was in the direction of scan. The fourth bank of counters was fitted with a modulation collimator. The remaining instrumentation was unchanged from the first flight.

3.0 INSTRUMENTATION

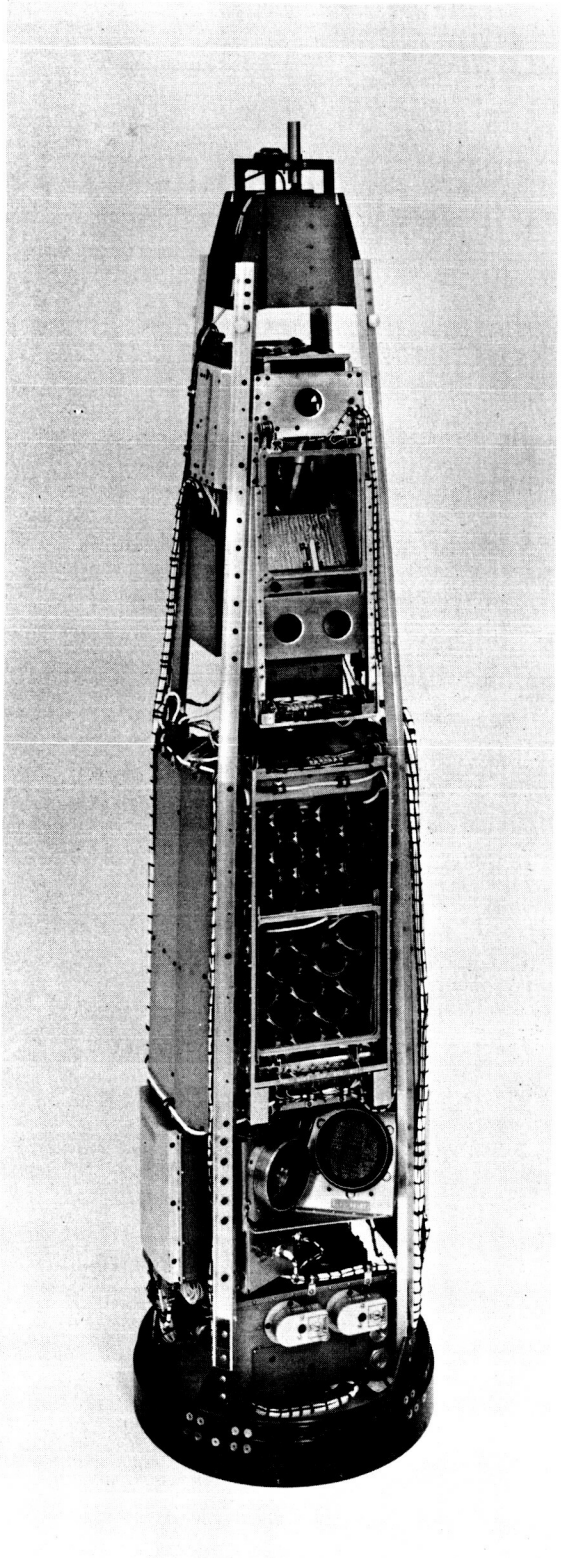
The payload developed for this program is shown in Figures 1 and 2 with the ogive removed, and in Figure 3 with the ogive and doors in place. The following instruments were incorporated in the payload.

1. Geiger counters (four banks). Each bank consisted of 12 or 13 individual end window counters. The sensitive area of each counter was a 1" diameter circle. The filling gas was argon-methane at one atmosphere pressure, and the entrance window was 0.002" of beryllium. Two banks of counters are shown mounted in the payload in Figure 4.

2. Anticoincidence Scintillation Counter. All four banks of geiger counters were mounted in an anticoincidence shield which was used to eliminate the cosmic ray portion of the geiger counter response. The scintillation material was NE 102 (plastic) which was viewed by two type 7818 CBS Photomultipliers.

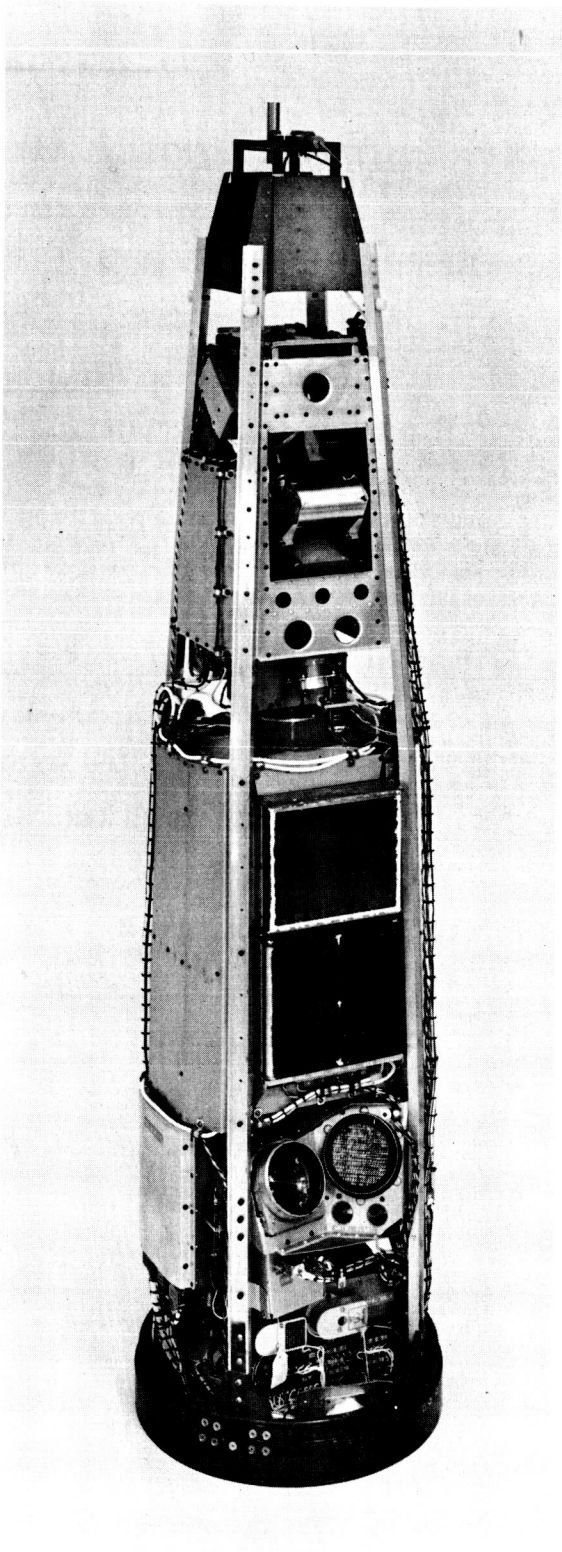
3. Scintillation Counters. Two were used in the payload, one using a NaI scintillation crystal, the other, an anthracene crystal. In both cases the crystal housing was directly mounted on the face of a 3" CBS photomultiplier (type 7818). One of the counters is shown in Figure 5.

4. Photoelectric Detector. This device is an open window, X-ray sensitive photomultiplier. The photocathode is a layer of KCl which is viewed by an electron multiplier. The device has an "O" ring sealed door that is kept closed until the rocket reaches altitudes, at which point the door is opened, and the cathode is exposed to radiation. A thin film of aluminized formvar is used to exclude ambient plasma. The detector volume is kept evacuated on the



CH-015

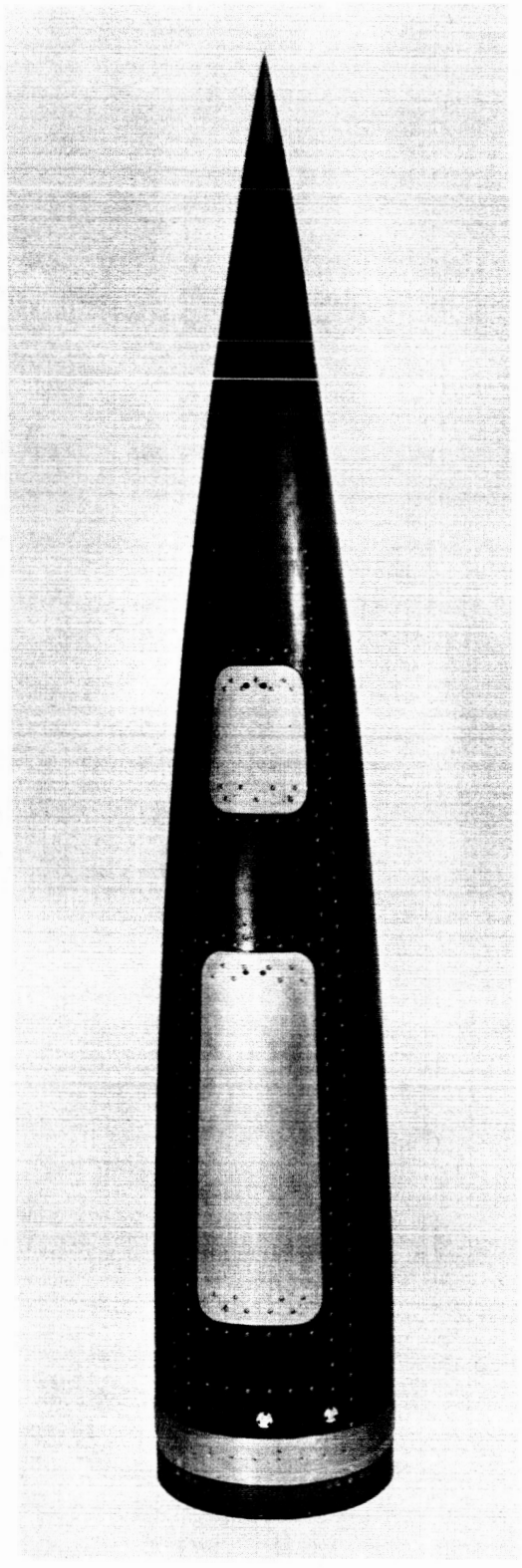
Fig. 1



CH-014

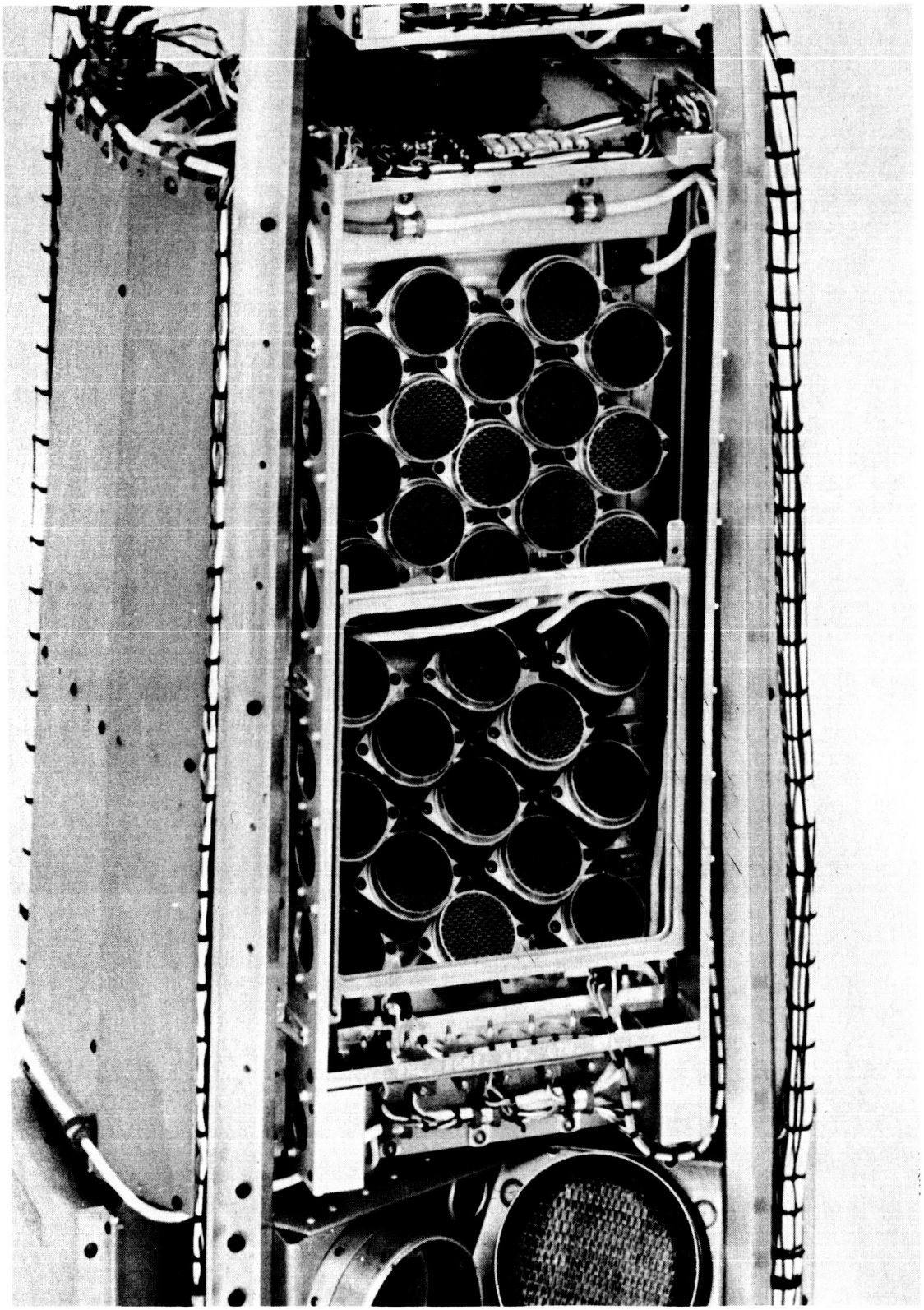
Fig. 2

ASSEMBLED PAYLOAD



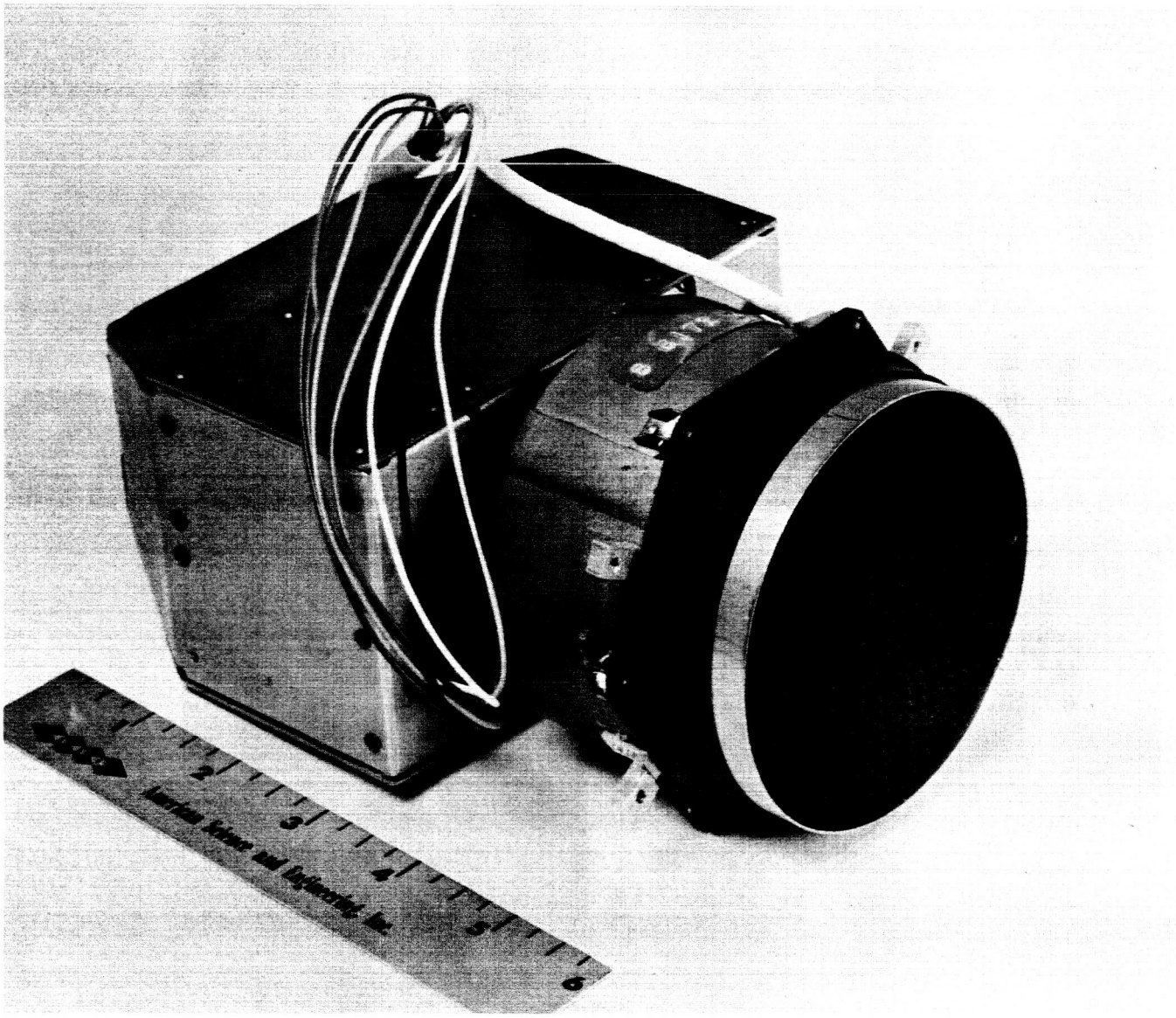
CH-016A

Fig. 3 ASSEMBLED PAYLOAD WITH OGIVE



CH-015A

Fig. 4 BANKS OF GEIGER COUNTERS MOUNTED IN ROCKET



CH-006

Fig. 5 SCINTILLATION COUNTER

ground by a 0.4 liter/second getter-ion pump. The device is shown in Figure 6.

5. Star Sensors. Two star sensors were incorporated in the payload. They consisted of an RCA type C70129B photomultiplier whose photocathode was placed at the focus of a 2.5 diameter fresnel lens. The photocathode defined the field of view (1.5^{o} x 10^{o}) of the lens. The star sensor is shown in Figure 7.

The electronics used for these instruments represent conventional amplifiers, gating circuits, scalers and power supplies. The geiger counter electronics was somewhat unconventional. The outputs of all counters in a bank were required to be mixed then presented to scale of 8 counter arranged as a D/A converter. The output consisted of a discrete voltage level corresponding to the state of the scaler. When a count occurred the voltage level changed. If a signal was present simultaneously from the anticoincidence scintillator, the input to the scaler was blocked. The mixer circuit that received the counter pulses would block the output of any pair of counters if the counting rate from that pair exceeded some preset value. This rejection was necessary to prevent a failure in a single counter that resulted in an excessively high count rate from mixing in with the outputs of the remaining operational counters.

The scintillation counter output was sent through a preamplifier than into a circuit that stretched the signal for one millisecond and blocked the input for 2 milliseconds. The stretched signal was telemetered directly.

The photoelectric detector electronics was identical with that used for the geiger counters with the exception that no mixer was involved and a high gain preamplifier was used to amplify the signal before its presentation to the scaler circuit.

The star sensor output consisted of a D.C. amplifier that converted the anode current of the photomultiplier into a voltage level that was telemetered directly. D.C. amplification was used to allow rapid recovery

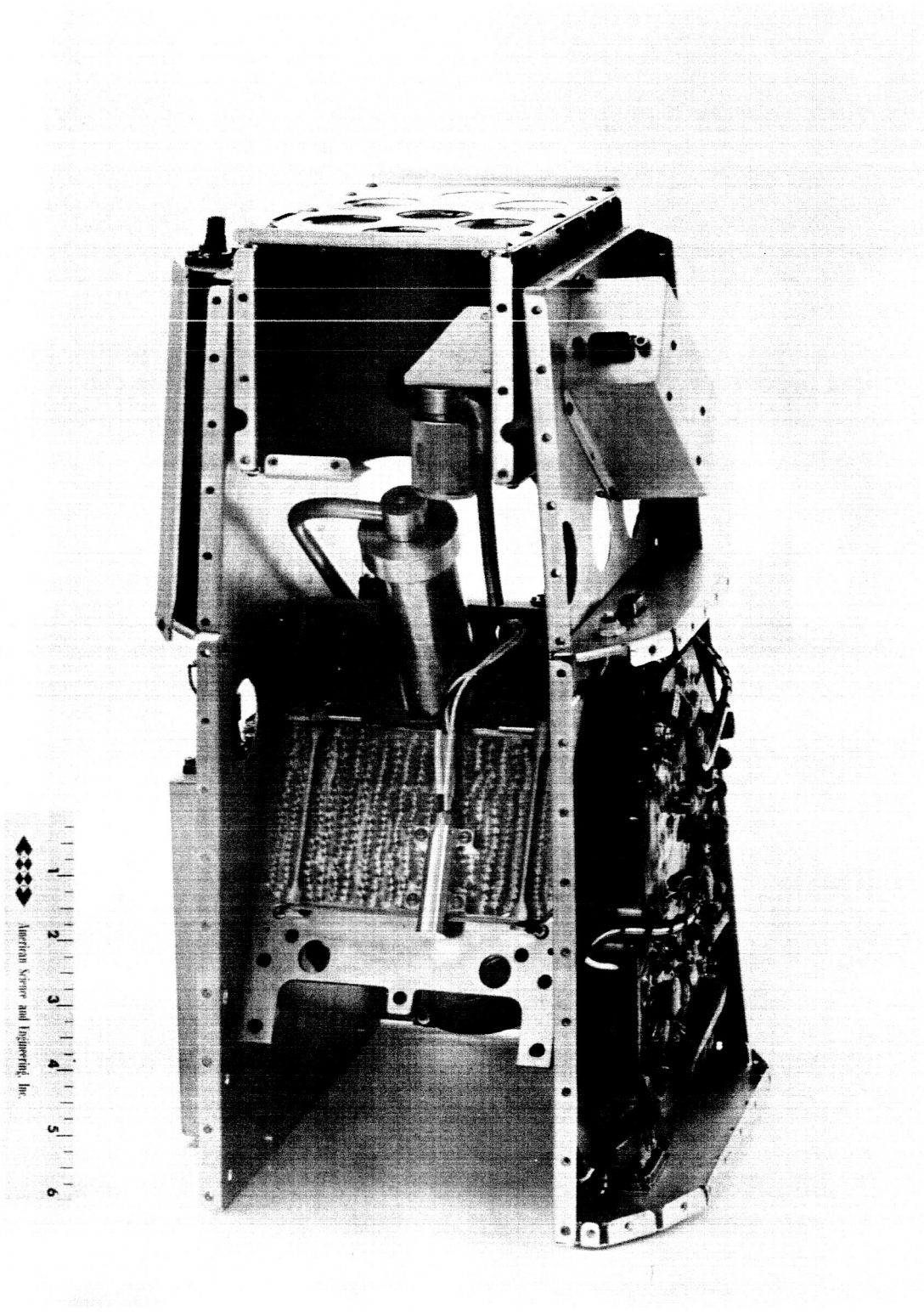
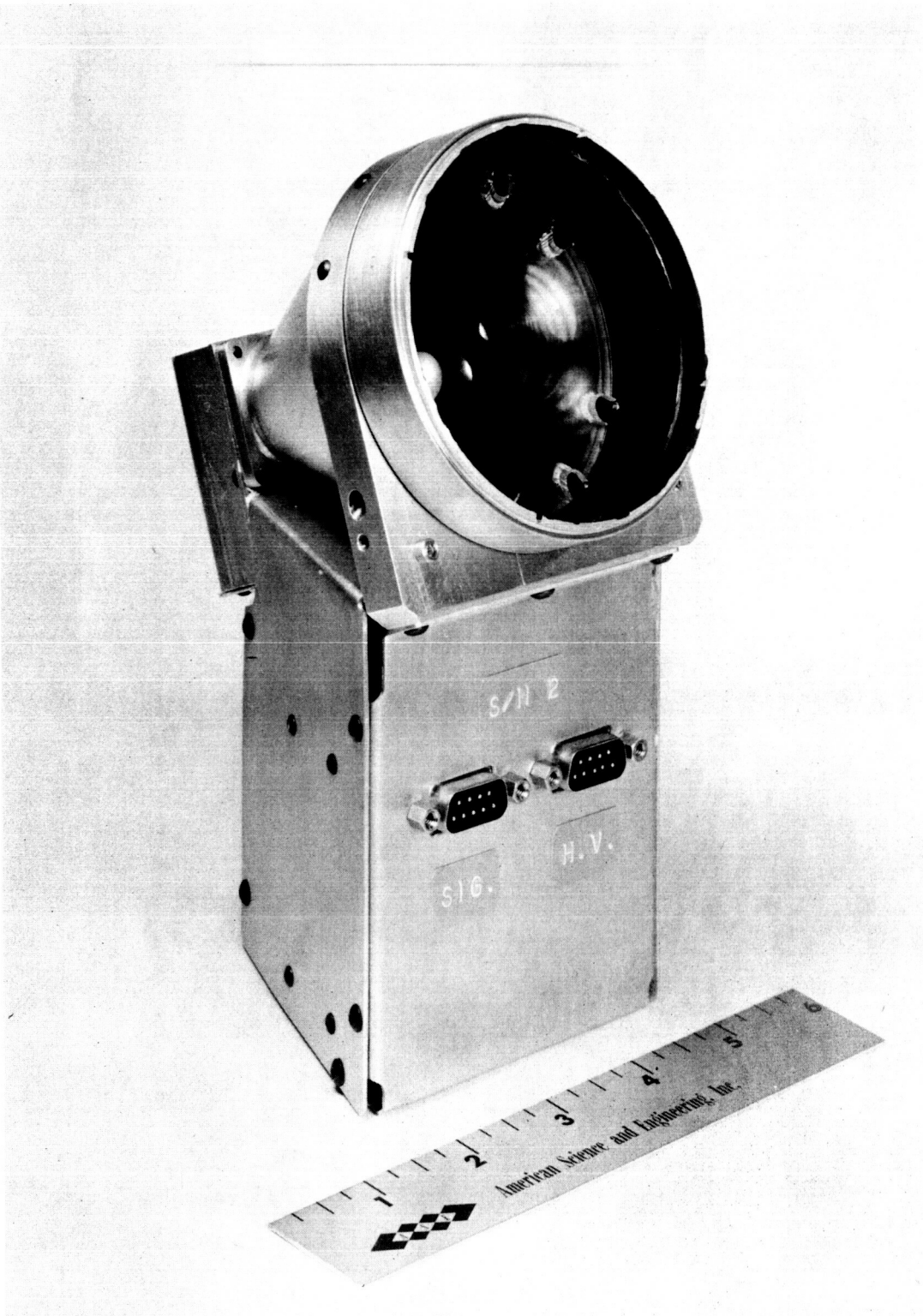


Fig. 6 PHOTOELECTRIC DETECTOR



CH-005

Fig. 7 STAR ASPECT SENSOR

following exposure to intense light sources. On one flight the moon was observed and in the other flight the sun was observed. In spite of the presence of these extremely bright objects the star sensors yielded useful data.

The above instrumentation was common to both payloads flown during this program. The changes that occurred were restricted to choice of collimators and view angles. The telemetered output as it was seen on a paper record is shown in Figure 8.

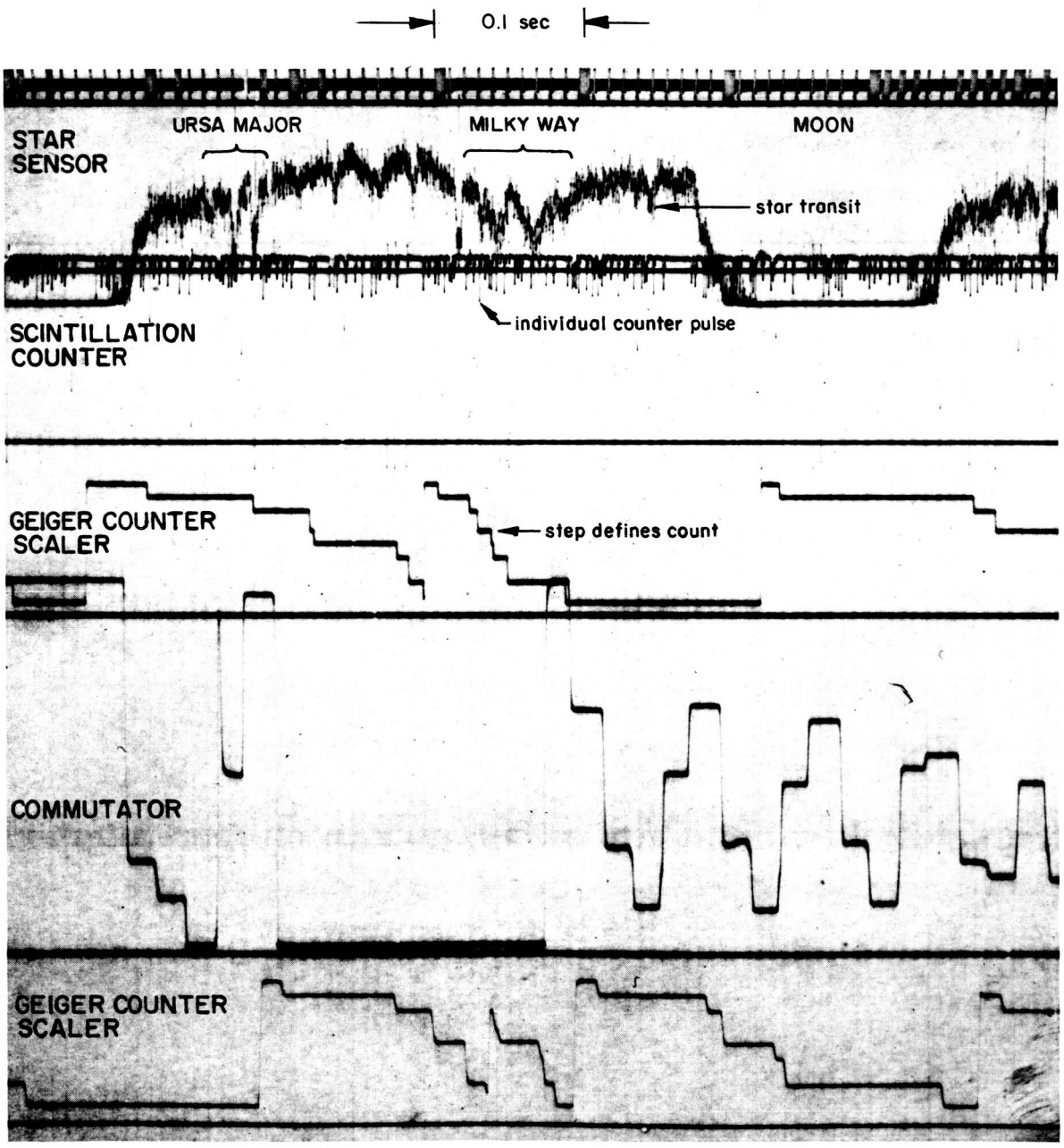


Fig. 8 TELEMETRY RECORD

4.0 ROCKET FLIGHTS

Two Aerobee rockets, NASA designations 4.122 CG and 4.123 CG were flown under this program. Both flights took place from the WSMR. Aerobee 4.122 was launched at 22:30 MST on 29 August 1964. The sidereal time at launch was 21 hour. The rocket reached an altitude of 178 km and traveled downrange for a distance of 95 km. The instrumentation incorporated in this flight was as follows:

1. GT 10 - Geiger counters
2. GT 20 - " "
3. GT 30 - " "
4. GT 40 - " "
5. Photoelectric Detector
6. NaI scintillation detector
7. Anthracene scintillation detector
8. 30^{o} Star Sensor
9. 0^{o} Star Sensor
10. Magnetometers (two axes)

The orientation and view angles of these instruments was as given in Table I.

TABLE I. Instrumentation on Rocket 4.122

Instrument.	Field of View	Rocket Coordinates	
		Elevation	Azimuth
GT 10	10 x 20° FWHM	10°	180°
GT 40	10 x 20°	40°	180°
GT 20	Modulation Collimator Resolution = 30'	20°	0°
GT 30	Modulation Collimator Resolution = 10'	30°	0°
Photoelectric Detector	10° x 40°	30°	180°
NaI Detector	10° x 40°	30°	162°
Anthracene	10° x 40°	30°	338°
30° Star Sensor	1.5 x 10°	30°	16°
0° Star Sensor	1.5 x 10°	0°	209.5°

Two filters were mounted initially in front of GT 40; one filter was 7.04 mg/cm^2 of beryllium, the other was 1.72 mg/cm^2 of mylar.

The orientation of the instruments (azimuth and elevation) are given in a coordinate system where elevation is measured up from the rocket equator (the plane normal to the rocket spin axis) and azimuth is measured ccw in the plane of the rocket equator.

The bulk of the telemetered data from this flight was useful for analysis. One significant failure occurred. High voltage arcing damaged the input transistor of the photoelectric detector preamplifier, and resulted in the loss of all data from that instrument. Some geiger counter data were lost because of the failure of several individual counters.

The data from this flight yielded the following information.

1. Either a group of sources or a single extended source existed along the galactic equator in the vicinity of the galactic center.
2. Spectral data in 1 - 10 Kev region was obtained for ScoX-1 and for the source region near the galactic center.

3. The angular diameter of ScoX-1 was determined to be less than 7 arc minutes.

The second flight (4.123 CG) took place at 17:58 MST on 27 October 1964. The sidereal time at launch was 20 hr. 20 min. The rocket reached a peak altitude of 192 km and traveled downrange for a distance of 73.3 km. The instrumentation incorporated in this flight was as follows:

1. GTHO - Geiger Counters
2. GTH20 - Geiger Counters
3. GTV10 - Geiger Counters
4. GTMCO - Geiger Counters with modulation collimator.

The remaining instruments were identical with those listed as 5 - 10 for the first flight.

The orientation and view angles of the geiger counters were as given in Table II.

TABLE II. Instrumentation on Rocket 4.123

		Rocket Coordinates	
Instrument.	Field of View	Elevation	Azimuth
GTHO	$15^{\circ} \times 1.4^{\circ}$	0°	180°
GTH20	$15 \times 1.5^{\circ}$	20°	180°
GTV10	$1.4^{\circ} \times 20^{\circ}$	10°	0°
GTMCO	Modulation Collimator Resolution 30'	0°	0°

The remaining instruments were unchanged from the first flight.

Virtually all possible data were recovered during this flight. The only failure that occurred was in one of the two magnetometers.

The data from this flight yielded the following information:

1. The sources along the galactic equator and near the galactic center all lie within 3° of the galactic equator.
2. ScoX-1 represents a distinct source; there is no significant emission between ScoX-1 and the galactic equator.

3. Two of the sources along the galactic equator were localized and given accurate positions.

4. ScoX-1 was located precisely.

5. High energy spectral data was obtained for ScoX-1 and for the sources along the galactic equator.

The flight of 4.123 completed the observational portion of the program.

5.0 DATA REDUCTION AND ANALYSIS

The telemetered data obtained during the rocket flights was recorded on magnetic tape and played back and recorded on paper in a CEC recorder. The paper records, produced at a recording rate of 10 and 20 inches/second were used to reduce the flight data. Approximately 300 seconds of data at altitude was obtained from each flight. The reduction of the data consisted of recording the time at which events occurred; an event being defined as a count in the X-ray detectors (geiger counters, scintillation counter and photoelectric detectors) or a star signal in the star sensors. In the case of the geiger counters and photoelectric detector the count was defined by a transition (step) in the output voltage, the magnitude of the step being about 0.5 volts. In the case of the scintillation counters, the count consisted of a pulse of 1 ms duration (the pulse was somewhat broadened by the telemetry and recording system), of varying amplitude. With the star sensor, no pulse shaping was done on board and the record was quite noisy. Any signal that appeared to be above noise was recorded as a "star" and subsequent analysis was used to distinguish noise from star signals.

The pulse amplitude of the scintillation counter signals was recorded as well as the onset time of pulse. For the magnetometer data we recorded the amplitude of the signal at arbitrary times during the flight.

Information was transformed from the paper records to IBM punched cards via a Benson-Lehner A/D converter (Oscar). The time resolution was 0.5 ms with the records run at 20 inches/sec. and was limited by the resolution of the A/D converter. The punched cards were processed and analyzed in an IBM 1620 computer. The initial analysis of both counter data and star sensor data consisted of converting the onset time of the signal to rocket spin azimuth assuming a spin period for the rocket.

The signals were then summed according to azimuth to reduce the large number of rotations effectively to a single rotation (the small precession cone angle makes this possible, if the precession angle was large it would be necessary to consider every rotation independently). The spin period was modified until the best possible summation of data was obtained. By best we mean the one yielding the sharpest peaks in the counting rate corresponding to the transit of a source. The technique amounts to performing an autocorrelation on cyclic data; the cycle in this case being the rocket rotation. In a given flight it was necessary to determine the correct spin period for only one of the detectors and then applying that spin period to the remaining sensors.

When this summation was performed on the star sensor data, the signals from stars were grouped at unique azimuths, whereas noise was scattered randomly through the data. It was possible to detect close to fourth magnitude stars in this way, even though a third magnitude or brighter star was required to give a recognizable signal on a single transit.

The aspect of the rocket was obtained by the following sequence of analysis:

1. Magnetic aspect was obtained from the magnetometer data which yielded a first estimate of the spin period, precession period and precession cone angle; as well as limiting the spin axis to a small circle in the sky.
2. Stars were identified by their azimuthal separation. The identification was facilitated by using a rocket heading based on the magnetometer data and by checking the magnetic aspect of the star against the magnetometer data.
3. The heading of the rocket axis throughout the precession cycle was determined by noting the appearance and disappearance of stars from the field of view of the star sensor.

4. The heading of any axis at any given time was determined by relating it to the transit of stars occurring within several seconds of the given time.

This completed the reduction of the raw data. Further analysis involved the following:

1. Location of any observed sources on the celestial sphere.
2. Analysis of data obtained with the modulation collimater in order to obtain angular size.
3. Pulse height (energy) distribution of data obtained in scintillation counter.
4. Analysis of data obtained with filters.

The results of these analyses are contained in four articles that have been published in Nature. These articles are incorporated as appendices in this report. The first article (Appendix B) reports the discovery of a region of sources near the galactic center; the second article (Appendix C) reports the analysis of modulation collimator data leading to a determination of the angular size of ScoX-1; the third paper (Appendix D) deals with the accurate location of three X-ray sources; and the fourth paper (Appendix E) reports the spectral data on the X-ray sources. A review article (Appendix F) which discusses all the above results plus the data obtained by other experimenters will be published as part of proceedings of the International School of Physics "Enrico Fermi", held at Varenna, Italy in 1965.

We have studied the relation of the celestial X-ray sources to known objects, concentrating on the possibility that the X-rays represent the radiation from a hot plasma ($T \approx 10^7$ degrees Kelvin). The results are contained in a paper (Appendix G) that is scheduled for publication in the Astrophysical Journal. Appendix H contains the results of the calculation of the position of the moon during the rocket experiment

of the NRL group (9) intended to observe the Crab Nebula in X-rays during its occulation by the moon. The position data given by the NRL group in their paper was in error since it neglected the motion of the rocket relative to the earth. The more precise data changes both the width and location of the X-ray source in the Crab.

As an adjunct to the analysis of the data on this program, a number of computer programs were developed. Many of these are highly specialized in that they are concerned with assembling data of a given form; some of the programs, however, are sufficiently general to be useful in other applications.

The most important of these programs are documented in Appendix I. Other significant programs that were written include:

1. Automatic star identifier. Given a catalog of stars visible to the vehicle and acquisitions by a photoelectric star finder, it identifies the acquisitions.

2. Star catalog utility programs. One of these writes a star catalog. Another generates a subset of the star catalog for a specific rocket flight. This involves elimination of stars that are below the horizons, or close to the sun or moon. Corrections for nutation, precession, proper motion, and aberration are applied.

3. Yaw parameter star finder differential corrector. This program differentially corrects those rocket aspect parameters that describe yaw. It is similar to the star finder differential corrector described in Appendix I, but is formulated so that a knowledge of spin parameters is not necessary.

4. Azimuthal distribution program. This produces an output showing count intensity as a function of spin phase as observed from a measuring instrument that shows discrete events. The program sums several successive spins together. It includes an automatic peak finder feature.

5. Azimuthal distribution collating program. Adds together successive azimuthal distributions produced by the azimuthal distribution program, so that the output will represent the sum of many consecutive spins.

6. Pulse height analysis program. Processes data from the proportional type of radiation detector, which generates an output pulse whose voltage level (height) is proportional to the energy level of the incoming particle. This program shows number of particles detected as a function of height.

7. Azimuthal and pulse height distribution program. Processes data from the proportional detectors. Produces a two dimensional grid showing number of particles detected as a function of spin phase and pulse height. Any number of spin periods are added together to form the output.

8. Benson-Lehner Oscar utility program. This processes data generated in free form by reading telemetry strip charts on the Benson-Lehner Oscar reader. It checks for errors, and punches the data in a format compatible with the computer programs used to reduce the data.

9. X-ray absorption analysis. Simulates the effects of various combinations of filters on an input X-ray spectrum.

Appendix J is a description of the calculational methods used to determine the residual atmospheric mass along a line of sight from the rocket (a point above the Earth at altitude between 80 km and several hundred km) to a point on the celestial sphere. The calculation takes account of the diurnal bulge in the atmosphere that results from solar heating.

6.0 CONCLUSIONS AND RECOMMENDATIONS

The present status of X-ray astronomy is summarized in the Introduction and in Appendix F. It is clear from current observational data that the study of celestial X-rays has become a well defined branch of astronomy; it is not at all clear however, how the X-rays fit in with the radio and visible light picture of the Universe. Regarding the future of X-ray astronomy, we note that the following observations can be performed:

1. Survey for weak X-ray sources.
2. Determination of angular size and structure.
3. Location on the celestial sphere.
4. Measurement of the spectral content.
5. Measurement of polarization.

The following kinds of vehicles are available for making observations:

1. Sounding rockets (observation time ≈ 300 sec)
2. High altitude balloons (observation time ≈ 8 hrs)
3. Unmanned spacecraft (" " ≈ 1 year)
4. Manned spacecraft (" " ≈ 1 month)

The following instruments are currently available to make such observations:

1. Large area gas counters (1 - 10 Kev)
2. Modulation collimators
3. Focussing X-ray telescope
4. Flow proportional counters (< 1 Kev)
5. Photoelectric detectors (< 1 Kev)

The following instruments are under development and should find application in X-ray astronomy.

1. Lithium scatterer for measuring polarization (12)
2. Slitless spectrometer using a transmission grating in conjunction with a focussing X-ray telescope (13)

There is no doubt that other instruments will be devised for making observations.

The observational requirements and potential have been extensively documented in the report of the working group on X-ray and Gamma-ray astronomy which studied the field under the auspices of the Space Science Board of the National Academy of Sciences. The group included scientists from AS&E who have contributed technical portions of that report and assisted in formulating the recommendations made by the group. Rather than make specific recommendations for future work in this document, we list programs in which AS&E is currently engaging. These are:

A. Celestial X-rays.

1. OSO-D Wheel Experiment. Survey experiment using small area (40 cm^2) detectors and low angular resolution (10^o).

2. Sounding Rocket. Two flights, one a reflight of the payload described in this report; the other flight will be a new payload utilizing a high angular resolution (40") modulation collimator.

3. Apollo X-ray Experiment. An experiment to be performed to accurately locate existing X-ray sources and to measure the emission from known objects. This experiment is severely limited by onboard radioactive sources used in the Apollo fuel monitoring system.

B. Solar X-ray Astronomy.

1. OSO-D Pointed Experiment. Utilizes a focussing X-ray telescope to scan the sun for X-ray emission.

2. Solar X-ray Rocket. Utilizes a telescope mounted in a biaxial solar pointing control on an Aerobee rocket to photograph the sun in X-rays.

3. AOSO Experiment. Has included the development of an instrument, consisting of a large area (20 cm^2 collection area) focussing telescope and a high resolution X-ray imaging device.

The program in solar X-ray astronomy, although in a field in itself, involves the development of instruments and techniques that will be applied to observations of celestial X-ray sources.

In addition to the above approved programs, AS&E has submitted proposals to NASA for the following programs.

1. Sounding Rockets. The program calls for study of X-ray sources with high resolution instruments currently being developed.

2. X-ray Explorer. The program calls for the development of a special purpose satellite for surveying the celestial sphere for weak X-ray sources. The sensitivity of the instruments should be several orders of magnitude higher than any of the other X-ray experiments.

3. Follow-on Apollo Experiment. Instrumentation similar to that now being developed for Apollo would be utilized in a later flight.

4. Apollo Telescope. A large area X-ray telescope to be used during an Apollo mission. Both celestial and solar experiments have been proposed.

Without the current and past sounding rocket programs it would not have been possible to engage in the various satellite activities. Sounding rockets have provided the basic observational data from which more extensive experiments could be planned, and they allow testing of new instruments and theories as they arise.

REFERENCES

1) Giacconi, R. et al: Phys. Rev. Lett. 9, 439 (1962)

2) Bowyer, S. et al: Nature 201, 1307 (1964b)

3) Gursky, H. et al: Phys. Rev. Lett. 11, 530 (1963)

4) Folter, J. E., and Morrison, P.: Phys. Rev. Lett. 10, 453 (1963)

5) Gould, R. J., and Burbidge, G. R.: Astrophys. J. 138, 969 (1963)

6) Hoyle, F.: Astrophys. J. 137, 993 (1963)

7) Chiu, H. Y.: Ann. Phys. (N. Y.) 26, 364 (1964)

8) Morton, D. C.: Astrophys. J. 140, 460 (1964)

9) Bowyer, S. et al: Science, 146, 912 (1964c)

10) Clark, G.: Phys. Rev. Lett. 14, 91 (1965)

11) Oda, M.: J. Appl. Opt. 4, 143 (1964b)

12) Novick, Robert: Columbia University. Private Comm.

13) Gursky, H., and Zehnpfennig, T: "An Image Forming Slitless Spectrometer for Soft X-ray Astronomy", submitted for publication to Reviews of Scientific Instruments. December 1965.

APPENDIX A

ASE-637

Notes on

A COLLIMATOR SUITABLE FOR MEASURING THE ANGULAR DIAMETER OF A RADIATION SOURCE

Dr. Minoru Oda
Massachusetts Institute of Technology
Cambridge, Massachusetts

and

Dr. Herbert Gursky
American Science and Engineering, Inc.
Cambridge 42, Massachusetts

Prepared for

National Aeronautics and Space Administration
Washington 25, D. C.

22 June 1964

I. Basis for Collimator Design.

1. Collimator geometry

The Oda collimator consists of two sets of parallel wires arranged so that there is modulation; i.e., alternate transmission or obscuration, of incident radiation depending on the angle of incidence of the radiation. The degree of modulation depends on the angular spread of the radiation, being maximum for parallel radiation and falling to zero as the angular spread approaches a critical value determined by the dimensions of the collimator. The collimator thus is sensitive to the angular size of the radiation source. The device is illustrated in Figure 1. The coordinate system is defined so that the Z axis lies in the plane of the wires and normal to long axis (X) of the wires. The modulation is determined by the angle measured with respect to the Z axis of the wires and is independent of the angle measured in the azimuthal plane (X, Y plane) of the wires. Additional mechanical collimation (not shown) is used to limit the field of view in the azimuthal direction.

In the frame of reference of the rocket, the collimator could be mounted so that the rocket spin axis coincides with the Z axis of the wires. In this case, as the rocket rotates past a source the angle, θ, that the radiation makes with the Z axis of the wire does not change, and during a spin cycle the collimator will either only transmit or only obscure depending on the value of θ. If the rocket yaws or if the spin axis is not parallel to the wire Z axis, then θ will

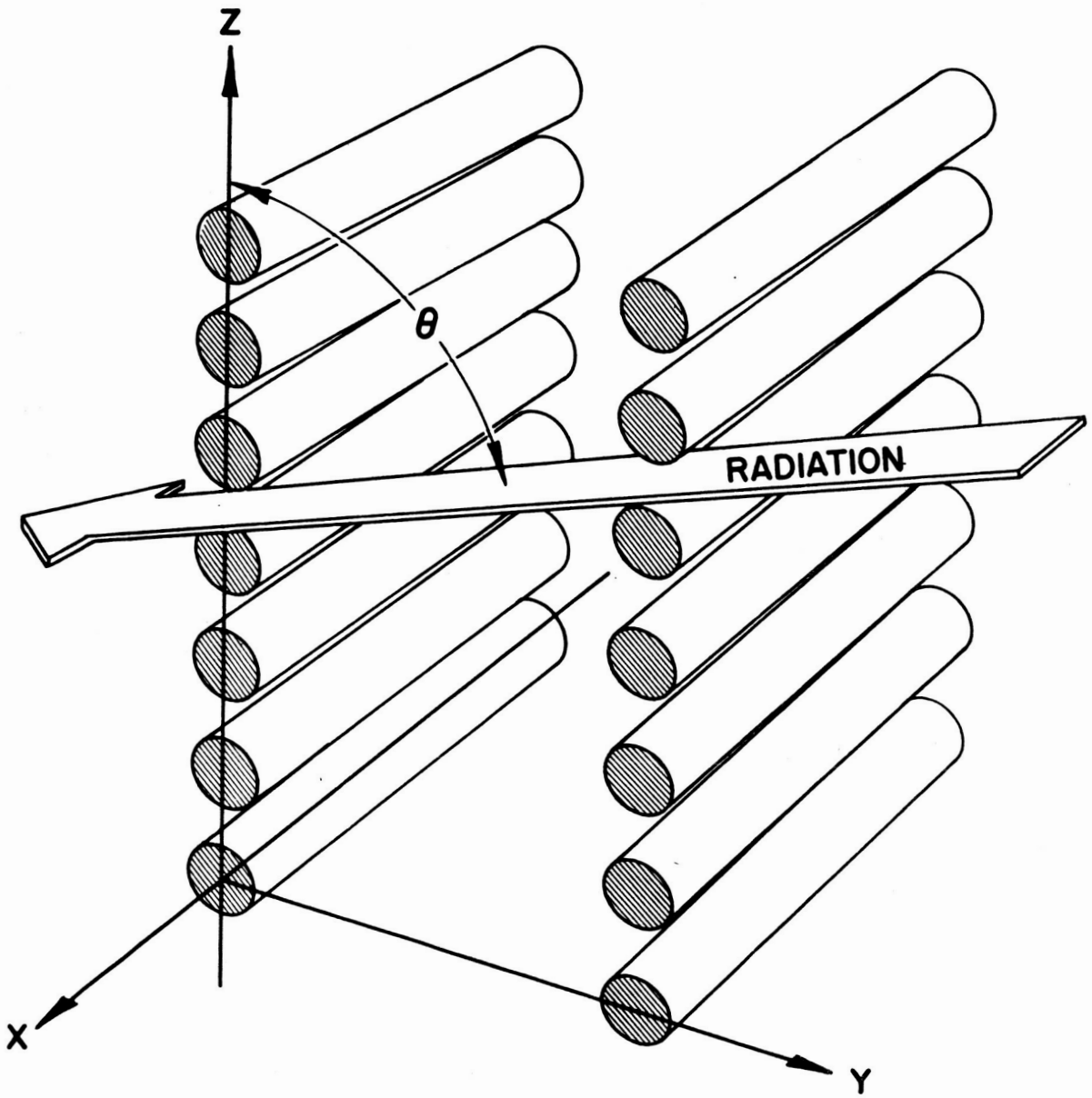


Fig. 1 Collimator Geometry

not remain constant but will change during a spin cycle and the radiation will be subject to modulation, either within one rocket rotation or between successive rotations. The rate of the modulation is directly a function of the time rate of change of θ.

Meaningful data will be obtained provided the following conditions are met: 1) the rate of change of θ is such that at least several modulation cycles occur during the rocket flight, and such that no more cycles occur during a single rotation of the rocket than one is allowed to observe because of bandwidth limitations (approximately 20 per rotation); 2) a sufficient amount of data is obtained from the radiation source. It is not easy to define "how much" is sufficient but it is probably the order of twice what one needs to establish that a source exists at all.

2. Expected Counting Rate

We can develop the following relations to determine the accumulated number of counts during the rocket flight. The peak instantaneous counting rate is given by:

$$\frac{dN}{dt} = A \epsilon \phi$$

A = detector area

ϵ = detector efficiency

ϕ = source flux

During a single rotation of the rocket the number of accumulated counts will be:

$N = \frac{A \epsilon \phi}{4} \Upsilon \left(\frac{\Omega}{2\pi}\right)$, where Υ is the spin period and $\frac{\Omega}{2\pi}$ is the fraction of the rotation during which the source is observed. The Oda collimator reduces the number of counts by another factor of 4 - one factor of two results from the collimation resulting from the wires

alone, and an additional factor of 2 results from the loss of area because of the presence of the wires. In the case of X-1 (the Scorpius source) and for our detector - $A = 100\ cm^2$, $\tau = 0.5$ sec.

$\phi = 20\ cm^{-2} sec^{-1}$, $\epsilon = 0.5$, $\Omega = 0.5$ radians

$$N = \frac{100\ (.5)\ (20)}{4} \quad (.5) \quad \frac{.5}{2\pi} \cong 10 \text{ cts/rotation}$$

For 300 seconds of data collection time (600 rotations of the rocket) the total number of counts will be the order of 6000. Since probably only the order of 100 cts will be sufficient to establish the existence of source, the number of counts should be much in excess of what is necessary to establish an effect of the collimator for X-1. This number is so large that even the lesser sources (for which ϕ is 1/5 to 1/10 that of X-1) should yield significant data. Thus point (2) above is satisfied.

3. Rate of Modulation

The number of modulation cycles that occur during the rocket flight is directly a function of $\frac{d\theta}{dt}$, where θ has been previously defined as the angle between the source and the Z axis of the wires of the collimator. In the case where this axis coincides with the spin axis of the rocket, the presence of rocket yaw will result in an average $\frac{d\theta}{dt}$ to the extent defined below: $\frac{d\theta}{dt} = \frac{2\Theta}{T}$

where Θ is the full opening angle of the yaw cone and T is the yaw period. Assuming typical values, $\Theta = 20^\circ$, $T = 80$ sec, $\frac{d\theta}{dt} = \frac{40}{80} = 1/2^\circ/\text{sec} = 30'/\text{sec}$
$15'/\text{rotation}$

The two collimators we plan to use have resolutions of 10 arc minutes and 30 arc minutes. Thus allowing an even larger yaw cone, the number of modulation cycles will not exceed one per rocket rotation.

On the other hand if little or no yaw occurs, very few modulation cycles would be observed during the rocket flight. To insure against such a possibility the collimators are fabricated so that the Z axes are not parallel to the rocket axis, and that at least two modulation cycles will occur during each rotation of the rocket past the source.

II. Experimental Tests of Collimator

1. Autocorrelation method of analysis

Because of the manner in which the collimator is fabricated, while the source passes through the field of view of the collimator during the spin of the rocket, modulation of at least two times is expected. Data was artifically manufactured using a Monte Carlo method for various combinations of counts per spin and cycle of modulation per spin to see how an autocorrelation method works for the analysis of data. Counts are added at random as the background. Figure 2 a)b)c) show the results of the autocorrelation for the combination of the average counts, the cycle of the modulation and the total operating period indicated respectively.

Although both the number of counts and the operating time are made much shorter than is really expected, the effect of the modulation is very clear.

2. The Modulation Effect

The set-up shown in Figure 3 was used to see the effect of the modulation of radiation by the collimators. Visible light was used instead of soft X-rays, since the former is expected to simulate the latter quite well.

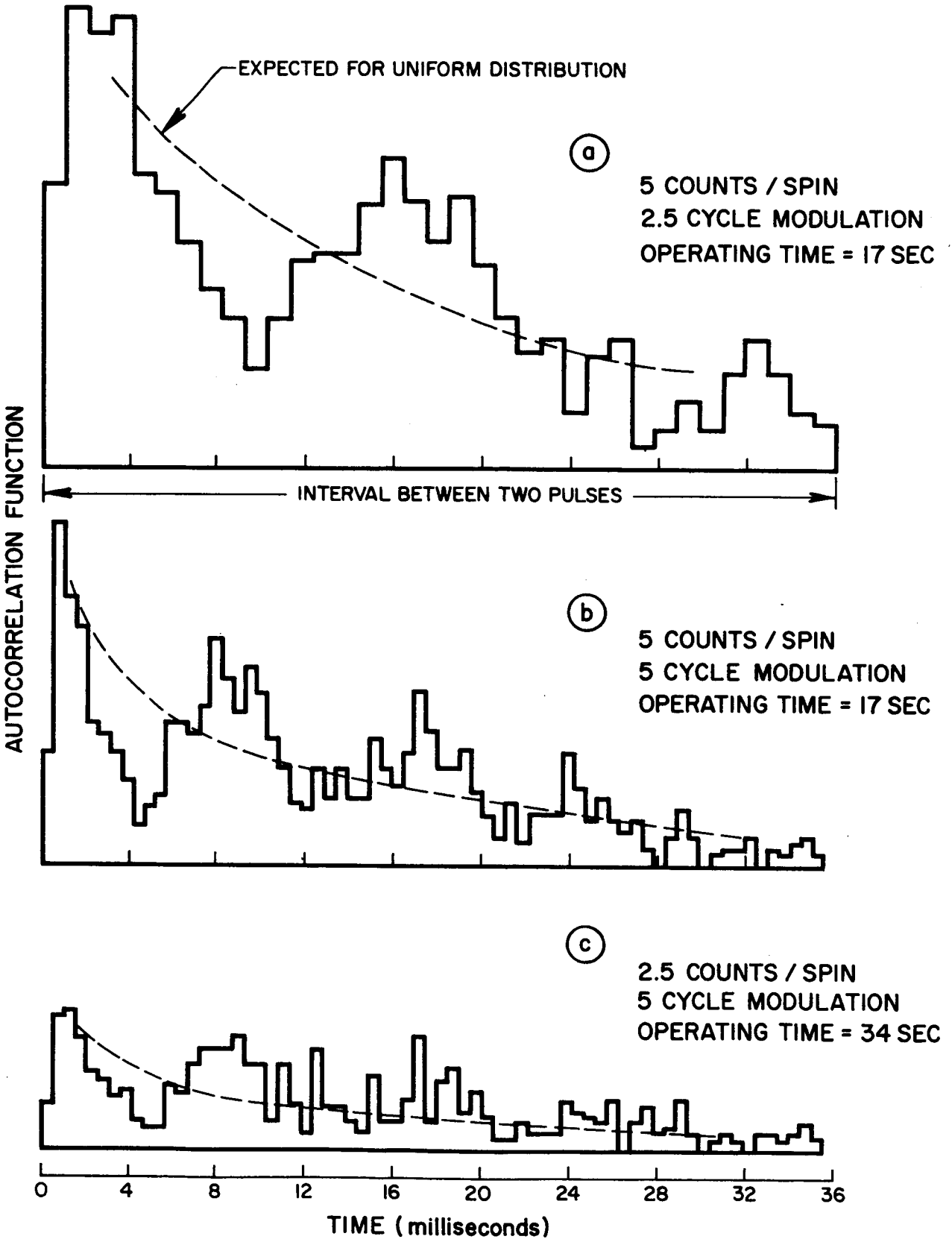


Fig. 2 Results of an Autocorrelation of Data

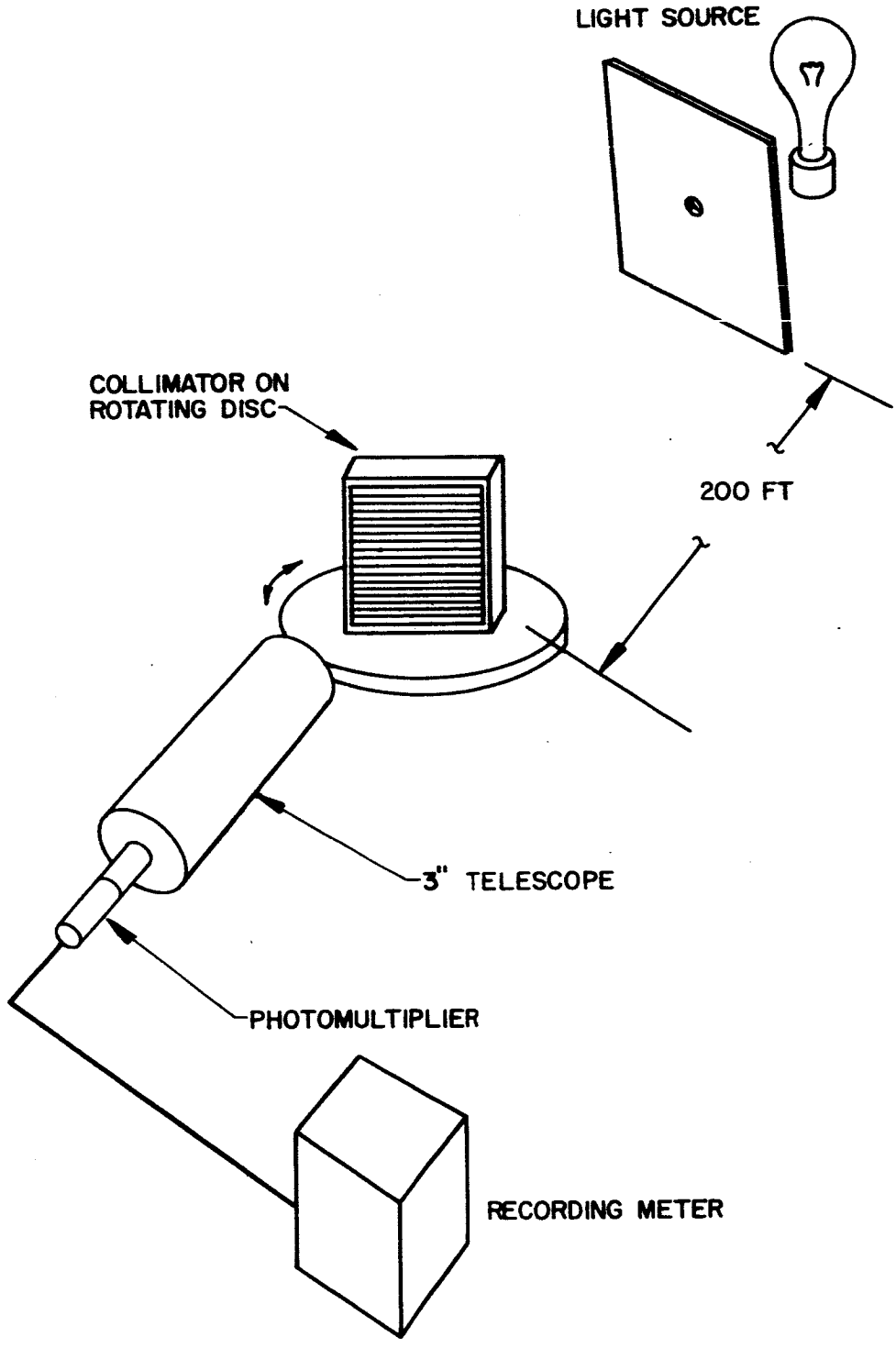


Fig. 3 Test Set Up for Measuring Modulation

Figure 4 is the copy of a record which represents the variation of the light intensity at the telescope by the rotation of the collimator. Modulation of 80 - 95% is recognized when the light source is essentially a point source. When the source is large or diffuse, the modulation is lost.

3. Visual Test of the Collimator

Figure 5 is a picture of the 30' collimator mounted in front of a diffuse background of light. The shadow pattern is caused by parallax, and the angle subtended to the eye by the width of the shadow corresponds to the typical angular resolution of the collimator. When one walks back from the collimator, the number of cycles of the shadow decreases and eventually one observes either transmission or obscuration. The same measurement using the telescope and photomultiplier as described before was done as well as the microphotometry to check the modulation. The results all agree.

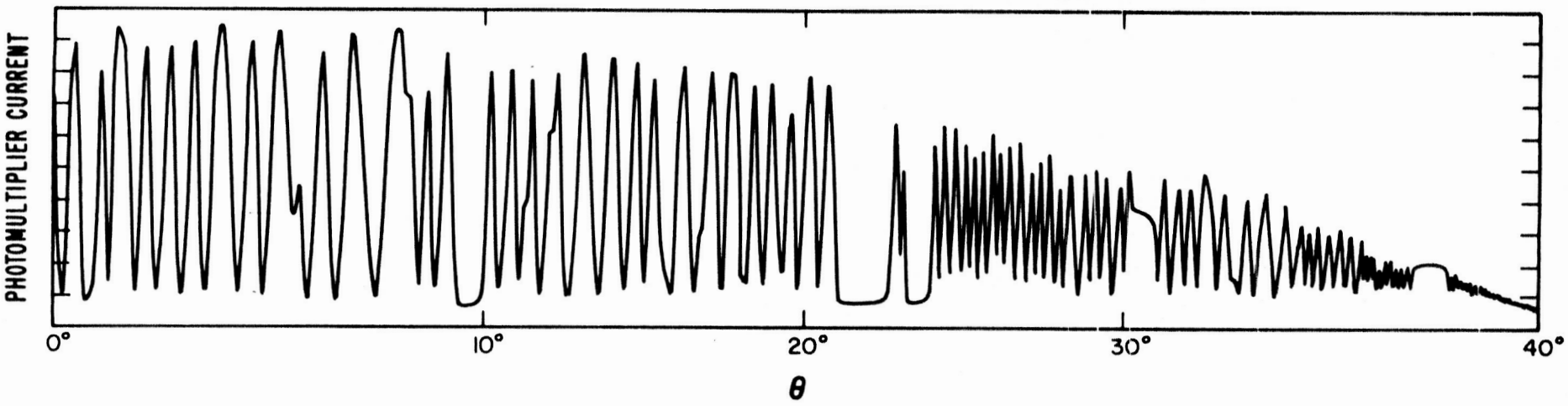


Fig. 4 Modulation Effect of the Collimator
Taken From Strip Chart Recorder

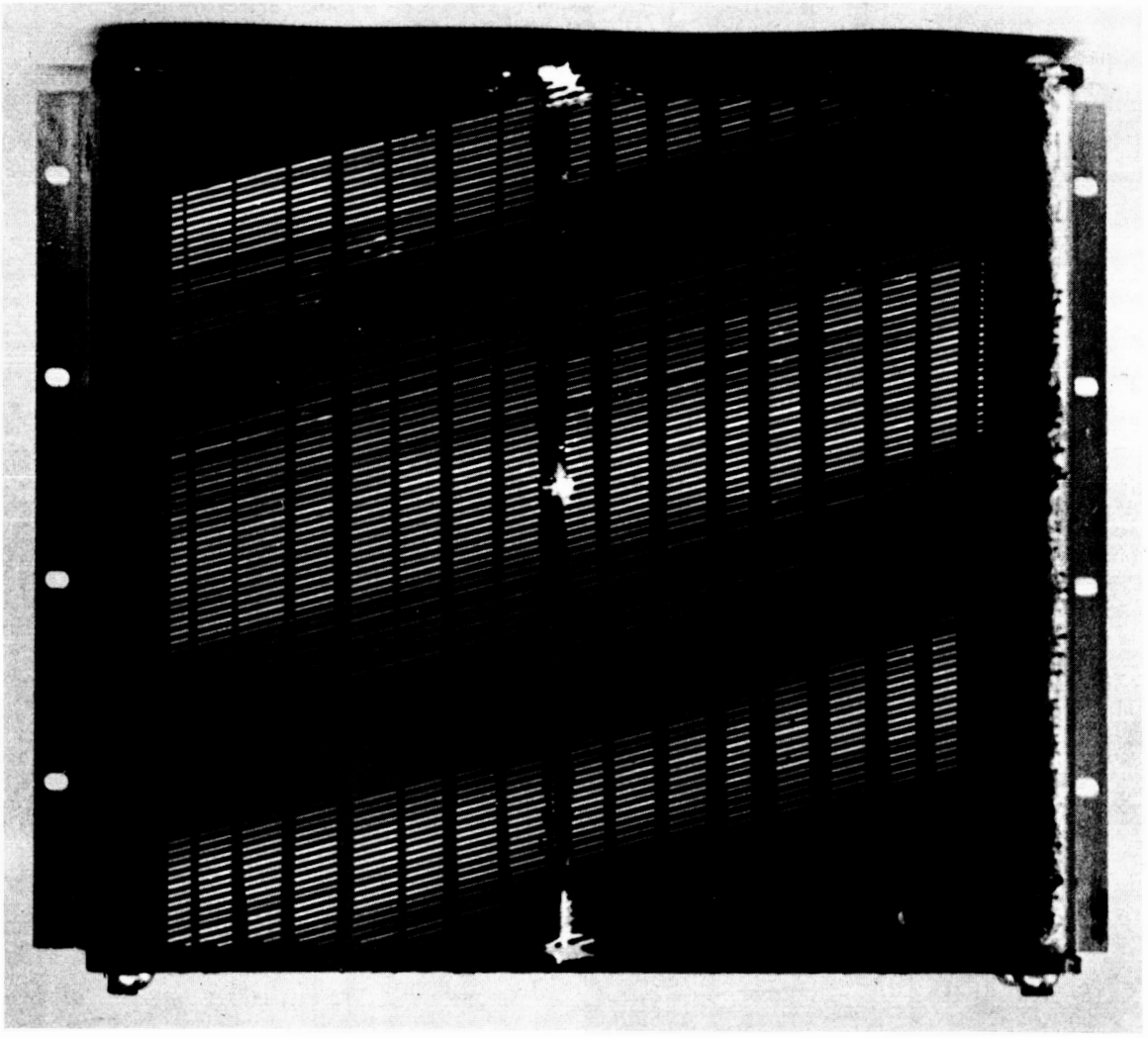


Fig. 5 30 Arc Minute Collimator

No. 4962 December 5, 1964 NATURE

LETTERS TO THE EDITOR

ASTROPHYSICS

Two Sources of Cosmic X-rays in Scorpius and Sagittarius

We have observed two separate and intense sources of cosmic X-rays in the region of the constellations Scorpius and Sagittarius during a rocket experiment launched on August 28, 1964. This is the same general region of the sky from which non-solar cosmic X-rays were first detected in June 1962 by Giacconi *et al.*[1]. In that earlier work a Geiger tube detector of large area and wide angular response was mounted, looking out of the side of a spinning rocket. A strong maximum in the counting rate was observed when the detector pointed in a southerly direction. A detailed discussion of the results led to the conclusion that the X-rays were of non-terrestrial origin, and that they emanated from a source close to, but apparently not coincident with, the galactic centre. These conclusions were confirmed in two later rocket flights, also employing wide-angle detectors[2]. In April 1963 Bowyer *et al.* conducted a rocket experiment using a detector with a field of view 10° wide at half maximum intensity[3]. At the time of that flight the galactic centre was below the horizon. They gave a location for the source in Scorpius at about 16 h 15 min right ascension and −15° declination and stated that its angular diameter is less than 5°.

The results reported here are based on an analysis of data received from one of several detectors in a payload carried aloft by an *Aerobee* rocket from White Sands, New Mexico (latitude, 32·4°, longitude, 106° W.) at 05: 30 G.M.T. (sidereal time, 20 h 56 min). This particular detector was a bank of argon-filled Geiger tubes with 0·002 in. thick beryllium windows, and a total sensitive area of 70 cm². The X-ray sensitivity of the detector extends from 1 to 9 Å. A rectangular honeycomb collimator with a field of view of 15° × 21·5° at half maximum intensity was mounted in front of the detector, with its long dimension coplanar with the rocket spin axis. The normal to the detector made an angle of 80° with the rocket axis. The orientation of the rocket during the flight was established from data obtained by two star sensors which registered the passage of stars across narrow rectangular fields of view. During the observations the rocket motion was a rapid spin about its long axis, and a slow precession of the spin axis around a yaw cone of small opening angle.

The presence of two sources in the band of directions scanned by the X-ray detector is evident from the data presented in Fig. 1. In this figure the number of counts is plotted as a function of angle around the spin axis for each of several intervals around the yaw cycle. Fig. 2 shows the traces of the normal to the detector across the sky at the mid-point of each of the time intervals for which the data were compounded to give the results given in Fig. 1. The numbers along the traces correspond to the angle around the spin axis as shown in Fig. 1. The left-hand peak (between angles 175° and 200°) appears to be due to the source in Scorpius. The other peak (between 200° and 225°) is due to a source in Sagittarius and may be coincident with Sgr *A*, the radio centre of the galaxy. The shape of the double peak can be accounted for entirely in terms of the angular response of the detector, which implies that the angular widths of the sources are smaller than 5° in the scan direction.

The maximum counting rates recorded when the normal to the detector came closest to the two sources were 12·6 counts cm^{-2} sec^{-1} for the Scorpius source and 5·5 counts cm^{-2} sec^{-1} for the Sagittarius source. If we tentatively assume an effective wave-length of 3 Å (that is, a wave-length near the peak of the spectral response curves of the detectors) we compute for these rates energy fluxes of 1·0 × 10^{-7} and 0·44 × 10^{-7} ergs cm^{-2} sec^{-1}, respectively.

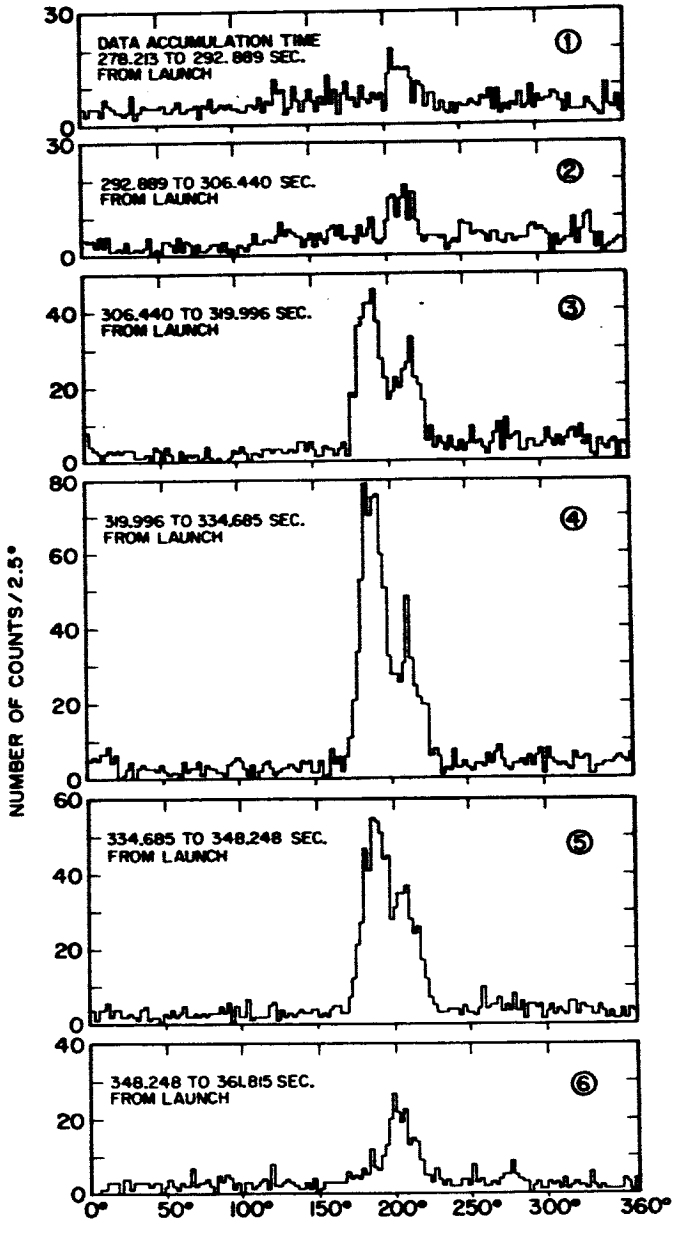


Fig. 1. Number of counts obtained in six time intervals plotted as a function of the angle around the rocket spin axis

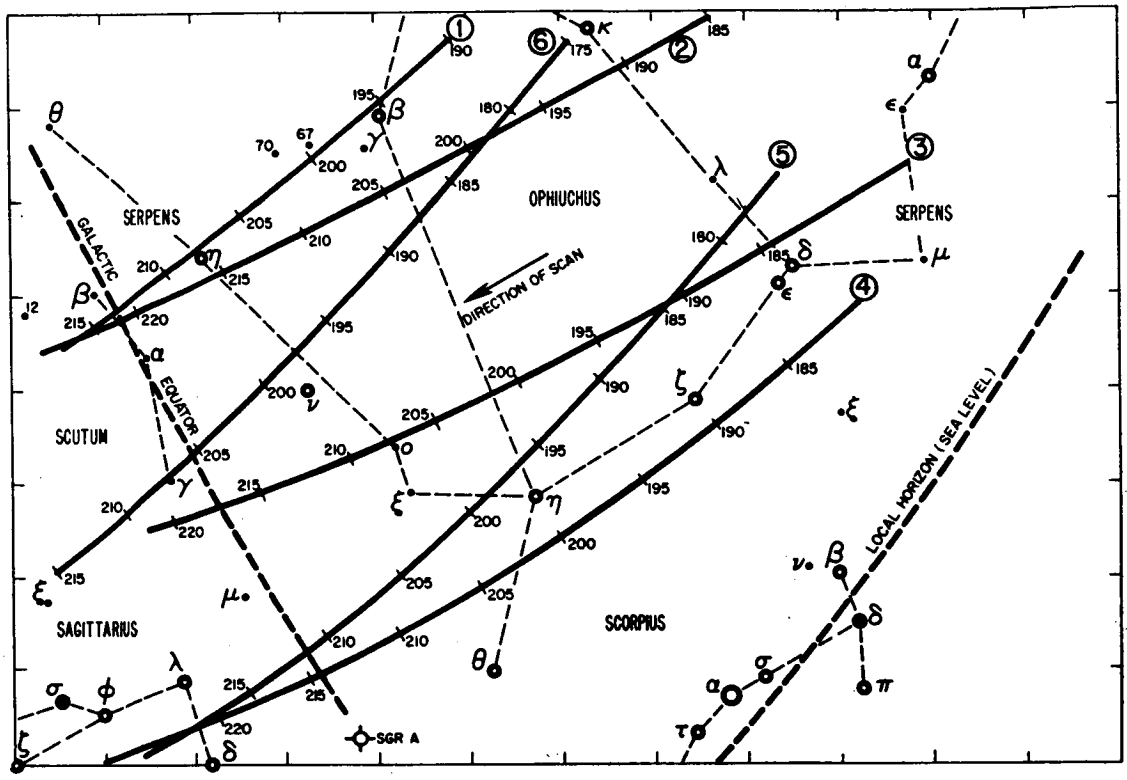


Fig. 2. Traces of the detector axis are shown in the region of the celestial sphere containing the two sources. The circled numbers refer to correspondingly numbered distributions in Fig. 1. The angles given along the traces correspond to those in Fig. 1

This work was supported by the U.S. National Aeronautics and Space Administration, Office of Space Sciences, under contract *NASw*–898.

R. Giacconi
H. Gursky
J. R. Waters

American Science and Engineering, Inc.,
Cambridge, Mass.

G. Clark
B. Rossi

Massachusetts Institute of Technology,
Cambridge, Mass.

[1] Giacconi, R., Gursky, H., Paolini, F. R., and Rossi, B. B., *Phys. Rev. Letters*, **9**, 439 (1962).
[2] Gursky, H., Giacconi, R., Paolini, F. R., and Rossi, B. B., *Phys. Rev. Letters*, **11**, 530 (1963).
[3] Bowyer, S., Byram, E. T., Chubb, T. A., and Friedman, H., *Nature*, **201**, 1307 (1964).

APPENDIX C

(Reprinted from Nature, Vol. 205, No. 4971, pp. 554-555, February 6, 1965)

ANGULAR SIZES OF THE X-RAY SOURCES IN SCORPIO AND SAGITTARIUS

By M. ODA*, G. CLARK, G. GARMIRE and M. WADA†
Laboratory for Nuclear Science, Massachusetts Institute of Technology, Cambridge, Massachusetts
AND
PROF. R. GIACCONI, DR. H. GURSKY and J. WATERS
American Science and Engineering Inc., Cambridge, Massachusetts

THE angular diameters of the X-ray source regions in the constellations Scorpio and Sagittarius respectively have been investigated in two rocket experiments conducted on August 28, 1964 (flight I), and October 24, 1964 (flight II), at the White Sands Missile Range. These sources were first observed by Giacconi *et al.*[1] as a single unresolved source of cosmic X-rays with wave-lengths around 3 Å and located near the galactic centre. Subsequent observations by Friedman *et al.*[2] and by Giacconi *et al.*[3] established the existence of two separate sources, in this part of the sky, one located near right ascension $16^h\ 15^m$, declination $-15°$, and the other near or coincident with the radio centre of the galaxy. In the present experiments we observed these two sources with a detector using a special collimator which has a high angular resolving power and at the same time a large field of view.

Flight I was launched at a sidereal time of 20 h 56 min, and flight II at a sidereal time of 20 h 20 min. In both flights, the rocket motion consisted of a rapid spin about its long axis and a slow procession of the long axis around a yaw cone of small opening angle. The detectors themselves were banks of Geiger–Müller tubes with beryllium windows 0·002 in. thick. Each bank had a sensitive area of approximately 100 cm². The collimators, which have been described elsewhere[4], consist of two grids of parallel wires. Each wire is separated from the adjacent wires by slightly less than one wire diameter, and the two grids are mounted one in the back of the other and separated by a distance of 1·5 in. (as dictated by the available space in the instrument section of the rocket). Parallel radiation falling on the collimator casts a shadow of the wires forming the front grid on to the back grid. The transmission of the incident radiation passing through the back grid and into the detectors is determined by whether the shadow coincides with the back wires or with the openings between. As the apparatus is rotated around an axis parallel to the wires, the intensity transmitted by the collimator is modulated in a way that is determined by the dimensions of the wire grids and the rate of rotation. On the other hand, if the incident radiation is not parallel, as in the case of radiation from an extended source, then the shadow is diffuse, and the degree of modulation observed as the collimator is rotated is correspondingly reduced. It is apparent that the modulation is large or small depending on whether the angular size of the source is large or small compared with the effective angular resolution which is the angle subtended by a wire diameter at the distance of separation between the two grids in the collimator. In this experiment the rotation of the collimator was provided by the motion of the rocket and the angular resolutions of the two collimators were 1/2° and 1/8°, respectively, for flight I, and 1/2° for flight II.

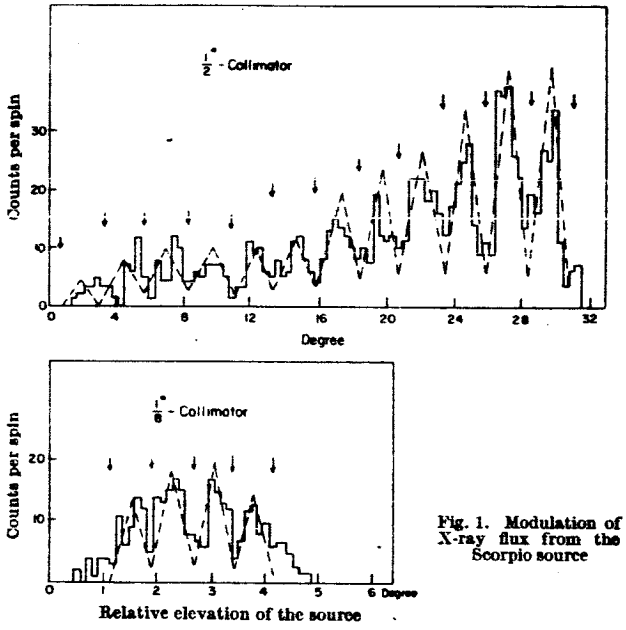


Fig. 1. Modulation of X-ray flux from the Scorpio source

The collimators for flight I were provided with baffles parallel to the spin axis of the rocket defining a field of view with a 30° full width and a triangular response. The wires of the collimator were tilted at an angle to the spin axis in such a way as to produce three modulation cycles as a source crossed the 30° field of view of the baffles. The orientation of the collimator was such that it measured the size of a source in the direction parallel to the spin axis of the rocket.

* On leave from the Institute for Nuclear Study, University of Tokyo.
† On leave from the Institute of Physical and Chemical Research, Tokyo.

Because the Scorpio source provided only about five counts per spin and the rocket's motion was complicated by the precession of the spin axis, it was necessary to analyse the aspect of the rocket in detail before it was possible to combine data from each spin. Fig. 1 shows the superposition of about 200 sec of flight after corrections have been made for the shift in phase of the modulation pattern caused by the precession of the spin axis. It is clear that there is a modulation of the X-ray flux due to the change of relative elevation of the Scorpio source with respect to the detector. The arrows indicate the expected positions of the minima in the modulation pattern as determined from the design parameters of the collimator. The dashed lines represent the expected modulation for a source of less than 1/2° and 1/8° angular diameter respectively, including the smearing effect of the background radiation and the partial transmission of the 1/8° collimator for a point source.

In flight II the collimator had an angular resolution of 1/2° and was provided with a narrower field of view with a 15° full width in order that the two source regions would be well separated. The wires this time were made perpendicular to the direction of the spin axis of the rocket. The modulation was thus expected to occur not as the result of the rotation of the rocket, but rather as the result of the variation in the elevation of the source with respect to the collimator axis caused by the precession of the rocket's spin axis. The source was seen 5 times during one yaw cycle. It is estimated that at least 90 per cent of the flux at the maximum is obscured at the minimum.

Similar analyses were made for the Sagittarius source region. The modulation is not so clear as in the case of the Scorpio source. A test analysis of artificial data generated by Monte Carlo simulation, with the isotropic background taken into consideration, showed that, in spite of the smearing effect of the background, a true modulation should have been clearly seen. The failure to observe a clear modulation, therefore, leads to the conclusion that the Sagittarius source is an extended source, or several sources distributed within a region of angular diameter larger than the resolution of the collimator.

We conclude from the foregoing analysis that the extension of the Scorpio source along the direction approximately parallel with the galactic plane is definitely less than 1/2° and probably smaller than 1/8°. Although we cannot rule out the possibility that the source extends in the direction perpendicular to the galactic plane, the fact that the modulation was seen throughout all phases of the yaw cycle while the axis of the rocket varied by 25° sets an upper limit of about 1° along the perpendicular direction to the galactic plane. We also conclude that the flux from Sagittarius does not all come from a single point source. Rather, it is spread over a region more than 30 min of arc in diameter and is either an extended source or is composed of more than a single source.

We are grateful to Prof. Bruno Rossi for many helpful discussions in connexion with this experiment.

This work is supported in part through funds provided by the National Aeronautics and Space Administration under contract *NASw*-898 and grant *NsG*-386 and in part by the U.S. Atomic Energy Commission *AT*(30-1)2098.

[1] Giacconi, R., Gursky, H., Paolini, F., and Rossi, B., *Phys. Rev.*, L, **9**, 439. (1962).

[2] Friedman, H., Liège conference on "Astronomy from Space Vehicles" (1964).

[3] Giacconi, R., Gursky, H., Waters, J., Clark, G., and Rossi, B., *Nature*, **204**, 981 (1964).

[4] Oda, M., *Applied Optics* (to be published).

Printed in Great Britain by Fisher, Knight & Co., Ltd., St. Albans.

APPENDIX D

(*Reprinted from Nature, Vol. 207, No. 4997, pp. 584 587, August 7, 1965*)

POSITIONS OF THREE COSMIC X-RAY SOURCES IN SCORPIO AND SAGITTARIUS

By G. CLARK, G. GARMIRE, M. ODA* and M. WADA†

Laboratory for Nuclear Science and Department of Physics, Massachusetts Institute of Technology

AND

R. GIACCONI, H. GURSKY and J. R. WATERS

American Science and Engineering, Inc.

WE have determined the positions of three cosmic X-ray sources in the constellations of Scorpio and Sagittarius within uncertainty areas of 1·2–3 square degrees. Positions for these sources were reported earlier by us at the Austin Conference on Relativistic Astrophysics on the basis of a preliminary analysis of the same data[1]. One of these sources is *ScoX*-1, which was first detected by Giacconi *et al.* in 1962 (ref. 2). (Our designations specify the constellation and the order of discovery, for example, *ScoX*-2 for second X-ray source in Scorpio.) The other two, *SgrX*-1 and *ScoX*-2, lie near the galactic plane in the complex of sources the existence of which was reported in a previous publication[3]. We have also located a probable fourth source to within 1° of a segment of a great circle that is almost parallel to and about 4° below the galactic equator. The Kepler supernova remnant *SN*1604 was scanned and no evidence of an X-ray source at its position was found.

We obtained the data with a rocket that was launched from White Sands, New Mexico, on October 26, 1964, at a sidereal time of 20h 20m, and reached an apogee of 224 km. Above the atmosphere the rocket spun around its long axis with an almost constant angular velocity of approximately 806 deg sec. The spin axis precessed with an angular velocity of 5·51 deg sec around a circular cone the apex angle and spatial orientation of which did not vary by more than 0·3° during the 260 sec when useful X-ray data were obtained.

The effects of the rocket motion on the observations are most easily visualized in the rocket frame of reference which we define to be a co-ordinate system fixed in the rocket with its z-axis parallel to the spin axis. During each spin any given point on the celestial sphere moved through 360° of azimuth in the rocket frame at an almost constant angle of elevation with respect to the rocket equator. In addition, the precession caused the elevation angle of an object to vary periodically with an amplitude equal to one-half of the apex angle of the precession cone. Thus an object was observed repeatedly in successive spins whenever it moved within the elevation range of a given detector's field of view.

In describing our analysis, we shall refer to the precession frame of reference which we define to be a co-ordinate system the z-axis of which is parallel to the axis of the precession cone, and the x-axis of which is in the direction of the vector product $\hat{z}_C \times \hat{z}_P$, where $\hat{z}_C$ and $\hat{z}_P$ are unit vectors parallel to the z-axes of the celestial and precession co-ordinate systems, respectively. We define the spin azimuth of a direction to be its azimuthal angle measured around the spin axis from the direction of $\hat{z}_P \times \hat{z}_S$, where $\hat{z}_S$ is a unit vector in the direction of the spin axis. We define the bearing of a direction to be the sum of its spin azimuth and the precession azimuth of the spin axis. During one complete precession cycle the spin azimuth of a given direction fixed in space decreases non-uniformly by 360°. In the same period the precession azimuth of the spin axis increases uniformly by 360°. Therefore, the bearing of a fixed direction varies about a mean value which, as one can easily see, differs by 90° from the azimuth of the fixed direction in the precession frame. The amplitude of this variation is determined by the angle of the precession cone and the elevation of the direction with respect to the precession equator.

The rocket carried a variety of instruments, among which were several X-ray detectors and two star sensors. The data consisted essentially of the occurrence times of pulses from these detectors and sensors. Four of the X-ray detectors were banks of Geiger tubes, each having sensitive areas of 70 cm², beryllium windows 9 mg cm⁻² thick, and argon fillings giving a gas thickness of 5·4 mg cm⁻². Three of the banks had slat collimators that gave rectangular fields of view with full widths of 3·0° in the narrow dimension, and 30° (detectors *GH*0 and *GH*20) or 40° (detector *GV*10) in the wide dimension. The narrow dimensions of detectors *GH*0 and *GH*20 were perpendicular to the rocket equator, while that of detector *GV*10 was parallel. The fourth bank, detector *GMC*0, had a modulation collimator[4] the response function of which, in the direction perpendicular to the rocket equator, was a sawtooth function with maxima at rocket elevation angles given by the formula 1·4° ± arc tan (0·0417n), where n is an integer. In the direction parallel to the rocket equator the response function of detector *GMC*0 was triangular with a base width of 15°. The star sensors, *SS*0 and *SS*30, had effective fields of view of 1·0° × 5·2°,

* On leave from the University of Tokyo.

† On leave from the Institute of Physical and Chemical Research, Tokyo.

with their long dimensions perpendicular to the rocket equator. In our detector designations the number following the letter code specifies the nominal elevation in degrees of the centre of its field of view above the rocket equator. We determined the actual orientations of the detectors and star sensors in the rocket frame of reference to accuracies of ± 0·3° in elevation and azimuth by optical measurements on the ground before and after the flight.

We solved the problem of determining the orientation of the rocket in the celestial frame of reference at any given instant in the following way. We first made use of the fact that *ScoX*-1 was within the elevation range of the modulation collimator throughout the precession cycle. We could therefore determine the amplitude of its variation in elevation from the observed modulation caused by the motion of *ScoX*-1 back and forth over the saw-tooth response function. This amplitude, which is equal to the full apex angle of the precession cone, was found to be 5·1 ± 0·1°. (This angle could also be determined from the star sensor data, though not with as high accuracy as from the modulation collimator data.) From the relative times of the signals from the star sensor *SS*0, we identified seven stars between the second and fourth magnitude as the sources of the signals. We then determined the orientation of the precession cone axis and the phase of the precession motion which minimized the mean square difference between the predicted and observed times when these seven stars entered and left the elevation range of the star sensor during the precession cycle. We found that the precession axis lay in the direction with right ascension 302·2° ± 0·5° and declination 38·2° ± 0·3°. From these data we could calculate the celestial orientation of the spin axis at any given instant. Analysis of the nearly periodic pulses from *SS*0 produced by various stars repeatedly crossing the field of view showed that the spin frequency increased approximately linearly with time by about 0·2 per cent during the useful period of the flight. Thus the bearing of the axis of any given detector, which for constant precession and spin frequencies would be a linear function of time, could be expressed by a quadratic function of time. The average deviation between the computed and the actual bearing was less than ± 0·5° over the useful observation period.

To determine the relative bearings of the X-ray sources and reference stars, we plotted the numbers of counts per bearing interval from each of the detectors as a function of the bearing of the detector's axis, reduced modulo 360°. The data accumulated over four precession periods are shown in Fig. 1. The main peak of the distribution for detector *GV*10 in Fig. 1*a* is due to *ScoX*-1. The difference between its average bearing and that of the star β-Cetus, observed by the star sensor *SS*0, is 239·8° ± 0·3°.

Table 1. Positions (Epoch 1950.0) of Three X-ray Sources
The preliminary values of the position co-ordinates given earlier in ref. 1 are shown in parentheses

Source	Right ascension		Declination	
ScoX-1	16h 12m or 16h 19m		−15·6° −14·0	
ScoX-2	16h 50m	(16h 50m)	−39·6°	(−41°)
SgrX-1	17h 44m	(17h 37m)	−23·2°	(−24°)

A segment of the great circle through the precession axis direction with this azimuth relative to β-Cetus is marked *A* in Fig. 3. We conclude that *ScoX*-1 lies within 0·3° of this segment.

The second, broader peak in Fig. 1*a* is due to the complex of sources near the galactic centre. From the fact that the ratio of the amplitude to the area of the peak is less than one-half times that of the *ScoX*-1 peak we conclude that it contains more than two sources. Arcs *B* and *C* in Fig. 3 are loci of positions the average bearings of which are equal to the values marked *B* and *C* in Fig. 1*a*. They are segments of great circles drawn through the precession axis, and they bound the region within which these sources lie. The Kepler's supernova remnant *SN*1604 lies 2° outside this region, and the radio source *SgrA* at the galactic centre is just barely within it. The separate peak, the average bearing of which is marked *D* in Fig. 1*a*, is 3·5σ above the background. It is probably caused by a separate source that lies somewhere along the great circle segment marked *D* in Fig. 3.

The bearing distribution for the *GMC*0 detector is shown in Fig. 1*b*. It has separate peaks due to *ScoX*-1 and the galactic centre complex, but it has a low angular resolution and does not improve the bearing determinations already made with the *GV*10 data.

Figs. 1*c* and 1*d* show the bearing distributions for the two detectors *GH*0 and *GH*20 the fields of view of which were narrow slits parallel to the rocket equator. Both show the presence of sources which are a part of the complex between circles *B* and *C*, and which lie within the two 8-degree wide elevation bands scanned by the detectors during the precession cycle. These bands are bounded by the small circles marked *GH*0 and *GH*20 in Fig. 3. It is apparent from the absence of a peak at the bearing of *ScoX*-1 in either distribution that *ScoX*-1 does not lie within either of these bands.

To obtain more precise information about the elevation of a source with respect to the precession equator we examined the precession variation in the rates of counts in an appropriate bearing interval round the average bearing of the source. At any fixed bearing the precession elevation of a detector axis varied with an amplitude equal to one-half the apex angle of the precession cone. If a source lay in the region scanned, this variation in elevation caused a variation in the X-ray counting rates

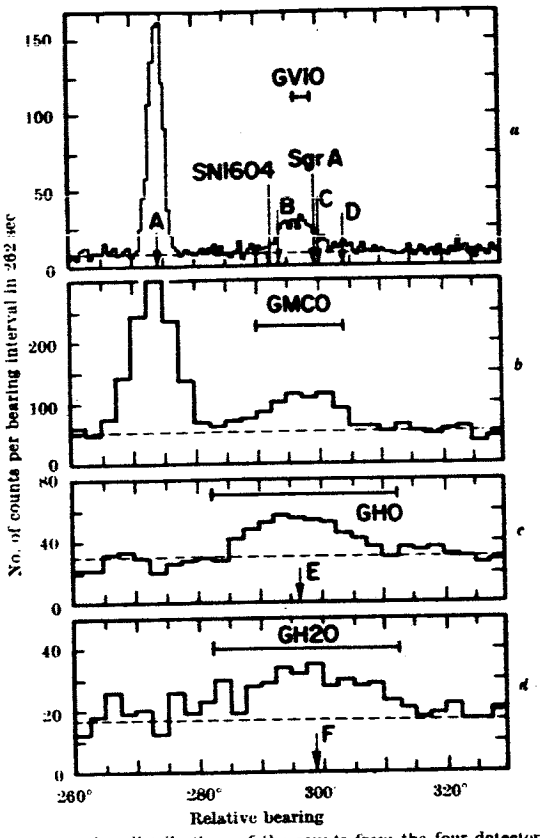


Fig. 1. Bearing distributions of the counts from the four detectors in the vicinity of *ScoX*-1 and the galactic centre complex. The full widths of the fields of view are indicated under the label of each detector. The background levels are indicated by the dashed lines

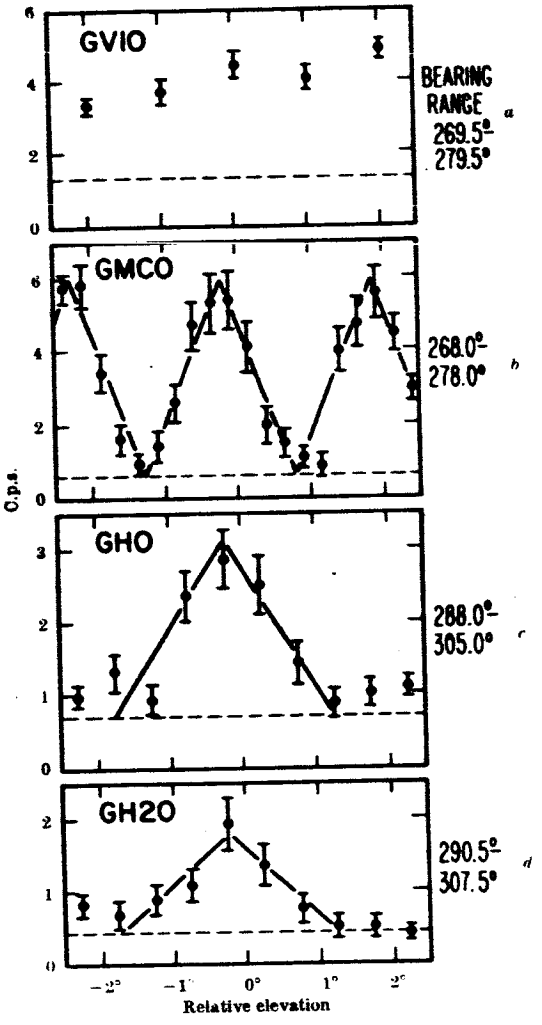


Fig. 2. Variation of the counting rates with the relative elevation of the detector axis at the midpoint of the indicated bearing interval. The background levels are indicated by the dashed lines

that could be fitted to the known response curve of the detector by a proper choice of the elevation of the source with respect to the precession equator. Fig. 2*a* shows the results for the *GV*10 detector. The abscissa is the relative elevation which we define to be the precession elevation of the detector axis at the centre of the indicated bearing interval minus its fixed rocket elevation. The fact that the counting rate was a maximum at the maximum relative elevation of the spin axis shows that *ScoX*-1 is above the maximum precession elevation of the *GMC*0 axis, which limit is indicated by the dashed line that crosses the bearing circle *A*. On the other hand, *ScoX*-1 cannot lie above the band bounded by the *GH*20 lines because the observed elevation variation is too small. Therefore, *ScoX*-1 must lie between the dashed line and the lower boundary of the *GH*20 band.

To refine the elevation determination of *ScoX*-1 we used the *GMC*0 data the elevation variation of which is shown in Fig. 2*b*. From the completeness of the modulation, as well as that of the modulation observed in a previous experiment with a similar but higher resolution collimator, it was possible to conclude that the angular diameter of *Scox*-1 is less than 7 arc min (ref. 5). One sees

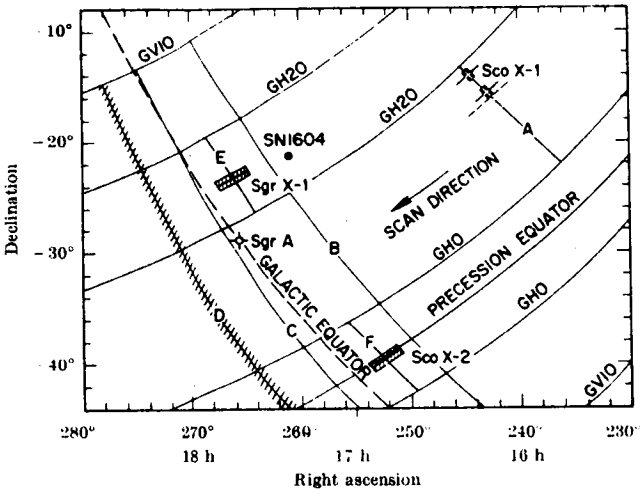


Fig. 3. Mercator projection of the celestial sphere in the region of the galactic centre. The cross-hatched areas show the locations of the sources as determined in this experiment. The small circles labelled *GV*10, *GH*0, etc., are the extreme boundaries of the regions scanned by the corresponding detectors

here that *ScoX*-1 lines on one of the maxima of the response function when the precession elevation of the *GMC*0 axis is $-2{\cdot}3°$, $-0{\cdot}2°$ or $+1{\cdot}8°$. The solid lines crossing the bearing circle *A* show the positions of the two maxima which fall between the limits previously determined. We are not able to choose between the two intersections on the basis of the data from this experiment. The boxes around each of the two intersections are 0·6° wide by 1·0° long, and they indicate the estimated errors in the bearing and elevation determinations, respectively.

Figs. 2*c* and 2*d* show the elevation variation of the counts from the sources observed by the *GH*0 and *GH*20 detectors. In both cases the sources appear to lie about 0·3° below the midpoint of the elevation scan as indicated by the line crossing the bearing circles *D* and *E*. We determined these latter bearing circles using only the data from the parts of the precession cycle when the sources gave the highest counting rates. As before, the boxes around each intersection indicate the estimated errors in the position determinations.

The two alternative positions we find for *ScoX*-1 are both within the uncertainty circle of 2° radius around the position published by the *NRL* group[6]. The lower of the two is within 0·5° of the position given by Fisher *et al.*[7].

SgrX-1 is 5° away from the Kepler supernova remnant *SN*1604. The absence of a significant peak at the average bearing of *SN*1604 in the *GV*10 data in Fig. 1*a* shows that any X-ray emission from this remnant must be several times smaller than that of the nearby sources. Therefore, our observations do not support the identification of an X-ray source with *SN*1604, as suggested by the *NRL* group[6] on the basis of data obtained with an instrument of lesser angular resolution.

ScoX-2 lies more than 5° away from the position of the nearest source reported by the *NRL* group[6].

Two of the circular arcs along which Fisher *et al.*[7] have located sources pass within 1° of our locations for *SgrX*-1 and *ScoX*-2, respectively.

Finally, we note that there is a striking lack of symmetry with respect to the galactic centre in the distribution of the general X-ray emission from this region. The centre line of the emission region between lines *B* and *C* in Fig. 3 passes the galactic centre at a galactic latitude of $b_{II} = +2{\cdot}5$. It is also apparent that the radio centre of the galaxy, *SgrA*, is at most a weak X-ray source compared with the other sources nearby.

This work was supported in part by the National Aeronautics and Space Administration under contracts *NASw*-898 and *NsG*-386 and in part by the U.S. Atomic Energy Commission under contract *AT* (30–1) 2098.

[1] Giacconi, R., *Proc. Austin Conf. Relativistic Astrophysics*, Dec. 1964 (to be published).
[2] Giacconi, R., Gursky, H., Paolini, F., and Rossi, B., *Phys. Rev. Letters*, **9**, 439 (1962).
[3] Giacconi, R., Gursky, H., Waters, J. R., Clark, G., and Rossi, B., *Nature*, **204**, 981 (1964).
[4] Oda, M., *App. Optics*, **4**, 143 (1965).
[5] Oda, M., Clark, G., Garmire, G., Wada, M., Giacconi, R., Gursky, H., and Waters, J., *Nature*, **205**, 554 (1965).
[6] Bowyer, S., Byram, E. T., Chubb, T. A., and Friedman, H., *Science*, **147**, 394 (1965).
[7] Fisher, P. C., Johnson, H. M., Jordan, W. C., Meyerott, A. J., and Acton, L. W. (preprint).

Printed in Great Britain by Fisher, Knight & Co., Ltd., St. Albans

APPENDIX E

(*Reprinted from Nature, Vol. 207, No. 4997, pp. 572 575, August 7, 1965*)

SPECTRAL DATA FROM THE COSMIC X-RAY SOURCES IN SCORPIUS AND NEAR THE GALACTIC CENTRE

By R. GIACCONI, H. GURSKY and J. R. WATERS

American Science and Engineering, Inc., Cambridge, Massachusetts

DURING two rocket flights conducted from White Sands Missile Range on August 28, 1964 (flight I), and October 26, 1964 (flight II), we have obtained information regarding the spectral composition of the X-ray source in Scorpius (*ScoX*-1) and those along the Galactic equator in the vicinity of the Galactic centre. The results were obtained from two separate detectors and extend over the spectral region 1–25 keV. We find that the radiation from *ScoX*-1 extends from 15 keV to at least 2·5 keV, and that the spectral distribution is not consistent with black-body radiation. The radiation from the region along the Galactic centre extends to about 25 keV. The latter region apparently contains several distinct X-ray sources as reported by Giacconi *et al.*[1], Bowyer *et al.*[2] and Fisher *et al.*[3].

Since the discovery of cosmic X-ray sources by Giacconi *et al.*[4] in 1962, only gross information regarding the spectral composition of the radiation has been reported. In the same paper an effective wave-length near 3 Å was reported based on atmospheric attenuation and the difference in counting rate in two separate Geiger counters. Giacconi *et al.*[5] afterwards reported that the spectrum was consistent with a black-body temperature of about 10^7 °K. Bowyer *et al.*[6] attempted to measure the spectral composition of radiation from the Crab Nebula between 1 and 10 keV by making observations in two independent Geiger counters. Later, they published[2] a critical evaluation of their experiment which showed that one of the counters did not function as expected. In the same paper they presented results on the atmospheric attenuation of X-radiation from the Scorpius source which was consistent with a black-body temperature of $2–3 \times 10^6$ °K. In another experiment X-radiation from the Crab has been observed between 20 and 60 keV by Clark[7] using balloon-borne instrumentation.

Discussions of the source mechanism for the generation of the observed X-rays has centred on three possibilities: (1) black-body radiation from a neutron star; (2) radiation from an optically thin hot plasma; (3) synchrotron radiation from high-energy electrons in a weak magnetic field. Specific literature citations appear in refs. 5 and 7 cited here and in a review article by Giacconi and Gursky[8].

We are reporting here spectral data obtained by placing absorbers in front of the Geiger counters during flight I and by performing a pulse height analysis of the output of a sodium iodide (NaI) scintillation counter during flight II. The several sources along the Galactic equator could not be resolved with these counters and all contribute to the spectral data from that region. Other results from these rocket flights have been reported by Giacconi *et al.*[9], which demonstrated the separation between *ScoX*-1 and the sources near the Galactic centre, and by Oda *et al.*[10], which presented the results of the measurement of the angular diameter of *ScoX*-1.

The Geiger counter detector used during flight I of this experiment was a bank of twelve individual argon-filled counters with beryllium windows of 9·0 mg/cm² thickness and a total sensitive area of about 70 cm². The efficiency, calculated as the product of the absorption in the gas filling and the transmission of the window, lies above 10 per cent between 17 keV and 1·2 keV and peaks at between 3 and 4 keV. This computed efficiency was checked experimentally by exposing counters to the beam from a tungsten target, windowless X-ray tube operated from 1·8 to 10 kV. The observed counting rates were in agreement over the entire range of voltage with those predicted using thick target yield curves and the computed counter efficiency.

The Geiger counters were equipped with rectangular collimators which limited the field of view to 15° full width at half maximum (FWHM) in the direction of rotation of the rocket and 20° FWHM in the direction of the rocket long axis. The counter bank was mounted so that its axis of maximum sensitivity made an angle of 80° with respect to the long axis. Two filters, *F*1 of 7·04 mg/cm² of beryllium and *F*2 of 1·72 mg/cm² of mylar, were placed in front of the detector and were sequentially removed during the flight to allow measurements for approximately equal time-intervals of the X-ray fluxes with *F*1 and *F*2 in place, *F*1 alone in place, and no filter.

The motion of the rocket during this flight (flight I) consisted of a rapid rotation with a period of 0·55 sec about the long axis plus a slow precession of the rotation axis with a period of 83 sec along a cone of a small opening angle. The X-ray source regions were observed during each rotation but, because of the low counting rates, data from successive rotations were added in order to obtain sufficient statistical precision.

During each rotation the detector swept out a band on the celestial sphere the width of which, 20°, equalled that of the collimator. The precession results in an approxim-

Table 1. Counting Rate observed in the Two-source Regions with and without Filters

Filter condition	Source region	Counting rate measured c.p.m.	Attenuation relative to no filter
No filter	*ScoX*-1	620 ± 20	1
*F*1	*ScoX*-1	440 ± 18	0·71 ± 0·04
*F*1 + *F*2	*ScoX*-1	350 ± 17	0·56 ± 0·03
No filter	Gal cen	350 ± 18	1
*F*1	Gal cen	240 ± 18	0·70 ± 0·06
*F*1 + *F*2	Gal cen	210 ± 15	0·62 ± 0·05
Typical background rate		30 c.p.m.	

ately sinusoidal variation of the angle of closest approach of a given celestial object to the centre of this band. During each precession cycle the centre of the band came within 2° of *ScoX*-1 and moved along the Galactic equator between $l_{II} = 2°$ to $l_{II} = 27°$.

Three full precession cycles were recorded during the rocket flight, and since a filter change occurred almost in phase with the precession we have essentially a complete precession cycle of data for each of the three filter conditions. The data from the precession cycle with no filter in place have been the subject of a previous paper[8]. The counting rates with background subtracted observed with the three filter conditions when the detector crossed *ScoX*-1 and crossed the region along the Galactic equator are listed in Table 1. The counting rates represent an average over the same fraction of the precession cycle for the three cases. Listed also is the attenuation, defined as the ratio of the counting rates for the two filter combinations compared with no filter.

The significance of the attenuation factor can be partially understood from the following arguments. Photons at 2·5 keV will give the observed attenuation of about 0·7 per filter. In order to obtain the same attenuation factor in the case of a distribution of energies, the number of lower energy photons present, which are absorbed more strongly, must be compensated for by high-energy photons which are absorbed less strongly. Thus, there must be comparable numbers of photons above and below 2·5 keV. The magnitude of the attenuation depends on the true spectral distribution and can be calculated from the relation:

$$\text{Attenuation} = \int\varphi(\lambda)e^{-\mu(\lambda)x}\varepsilon(\lambda)\mathrm{d}\lambda/\int\varphi(\lambda)\varepsilon(\lambda)\mathrm{d}\lambda \qquad (1)$$

where $\varphi(\lambda)$ is an assumed spectrum in terms of number of photons per unit wave-length interval, $\varepsilon(\lambda)$ is the counter efficiency, $\mu(\lambda)$ is the linear absorption coefficient of the filter and x is the thickness of the filter. We performed this calculation for three assumed spectra, namely, (1) a power law spectrum of the form:

$$\varphi(\lambda) = A\lambda^{-(\alpha+1)} \qquad (2)$$

Equation (2) is equivalent to a distribution of the form $\nu^{-\alpha}$ (ν = frequency) when the spectrum is expressed in terms of power per unit frequency interval.

(2) An exponential spectrum of the form:

$$\varphi(\lambda) = (A/\lambda)\exp(-hc/\lambda kT) \qquad (3)$$

Except for the weak energy dependence of the Gaunt factor this spectral distribution describes free-free emission by electrons having a Maxwellian distribution of energy.

(3) A thermal spectrum of the form:

$$\varphi(\lambda) = A\lambda^{-4}[\exp(hc/\lambda kT) - 1] \qquad (4)$$

The quantity A that appears in these three distribution laws is a constant that can be determined from the relation:

$$A = N/\int\varphi(\lambda)\varepsilon(\lambda)\mathrm{d}\lambda \qquad (5)$$

where N is the observed counting rate.

For each of the distribution laws and for each filter condition, equation (1) was evaluated by numerical integration for a series of values of α in the case of the power law spectrum and of T in the case of exponential and thermal spectra. The observed attenuations for *ScoX*-1 are obtained with $\alpha = -1{\cdot}1 \pm 0{\cdot}3$ for a power law spectrum, with $T = (3{\cdot}8 \pm 1{\cdot}8) \times 10^7$ °K for an exponential spectrum, and $T = (9{\cdot}1 \pm 0{\cdot}9) \times 10^6$ °K for a blackbody spectrum. The listed uncertainties result from the statistical fluctuations expected from the total accumulated counts. Within the precision of the measurement, the spectrum from the two-source regions is the same over the interval of wave-lengths to which the Geiger counter is sensitive. Furthermore, it is not possible to decide between the three spectral types from these data alone.

Additional spectral results come from the observation during flight II of the same two-source regions by an NaI(Tl) crystal with area of 38·5 cm² and a thickness of 1 mm covered by 6·9 mg/cm² of aluminium. The crystal was viewed by a 7188 CBS photomultipler and the combination had a measured resolution of 48 per cent FWHM at 22 keV. The detector field of view was limited to 5° × 25° FWHM and the detector was mounted with its axis at

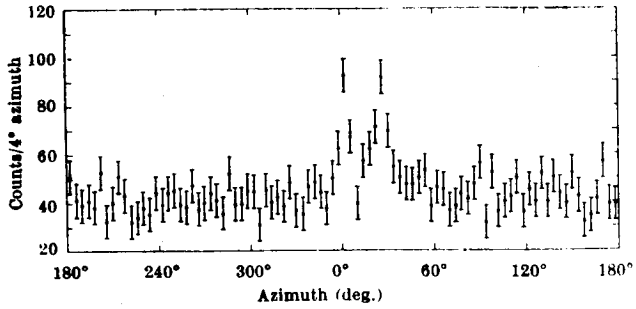


Fig. 1. Azimuthal distribution of counts observed in NaI detector

Table 2. Counting Rates and Absolute Fluxes observed for the Two-source Regions

Numbers listed for 1–10 keV are derived from Geiger counters and those listed for > 8 keV are derived from the NaI detector. The listed errors are based on the count statistics and in the case of the integrated power and flux in the 1–10 keV range include the effect of the uncertainty of the spectral index

	Counting rate counts/cm²-sec	Integrated power ergs/cm²-sec	Integrated flux photons/cm²-sec
ScoX-1			
1–10 keV	16·3 ± 0·6	(1·61 ± 0·4) × 10^{-7}	32 ± 6
> 8 keV	1·2 ± 0·3	(3·3 ± 0·8) × 10^{-4}	1·8 ± 0·4
Galactic equator			
1–10 keV	4·3 ± 0·2	(0·4 ± 0·1) × 10^{-7}	8 ± 2
> 8 keV	0·67 ± 0·15	(1·9 ± 0·4) × 10^{-4}	0·8 ± 0·2

60° from the long axis of the rocket. During the flight this detector scanned substantially the same source regions in the sky as did the Geiger counters in flight I, and the rocket motion was comparable with that of flight I.

The results from this detector consisted of those photomultiplier pulses above a threshold equivalent to about 8 keV. These were stretched to 1 ms with their pulse height preserved and telemetered in real time from the rocket. Pulses from successive spins of the rocket were summed as a function of both pulse height and rocket azimuth. The azimuthal distribution of all telemetered pulses is shown in Fig. 1. Sources are apparent at azimuths of 2° and 26° which correspond respectively to traversal of the regions containing *ScoX*-1 and the Galactic equator. We have assumed that the same X-ray sources are responsible for the radiation detected in the NaI and Geiger counter detection systems.

The differential pulse height distributions of the data within the source regions are shown with background subtracted in Fig. 2, as well as the background spectrum itself. The data below 10 keV show the cut-off resulting from the electronic threshold. Above 10 keV the distribution of pulse heights observed in the two-source region is markedly different from the background distribution. The distribution observed from *ScoX*-1 is consistent with a cut-off in the spectrum at about 15 keV, whereas the radiation from the Galactic equator region extends to higher energies and there is evidence for a possible peak at 20 keV from the same region. The observation of this peak must be regarded as only tentative because of the low statistical precision of the results; however, this feature cannot be an instrumental effect since it does not appear in either of the other two spectra.

The ambiguity in the choice of spectral distribution law that arises from the Geiger counter data alone can be partially resolved by considering the NaI data as well. The counting rates observed for the two-source regions by the two detectors are listed in Table 2. The ratio of counting rates for *ScoX*-1 is (14 ± 3) : 1, which can be

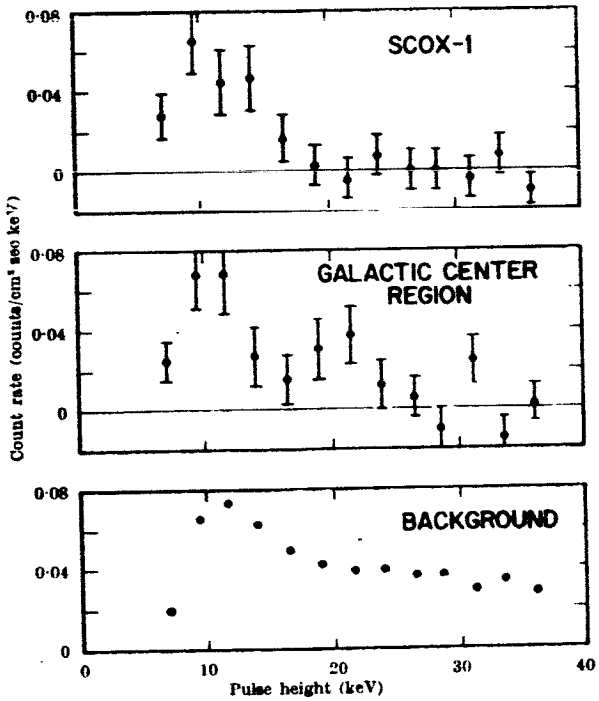


Fig. 2. Pulse height distribution of counting rates observed in NaI detector

obtained for either a power law or exponential spectral distribution with the parameters determined from the Geiger counter data. To fit a black-body distribution, however, requires a temperature of (17 ± 1) × 10^8 °K which cannot be reconciled with the Geiger counter data. The black-body temperature consistent with the Geiger counter data predicts a ratio of about 200 : 1. This analysis applied to the ratio of counting rates observed in the Galactic counter region yields the same general results; namely, that the ratio can be fitted with either an exponential or power law spectrum but that a black-body spectrum yields an insignificant flux in the NaI detector compared with what is observed. It is possible that a series of black-body sources gives rise to the observed radiation which, however, implies that one of the sources has a temperature of several times 10^7 °K.

In the case of *ScoX*-1, if one wishes to fit a thermal spectrum of the order of 10^7 °K as is consistent with the Geiger counter data alone plus a high-energy tail to account for the NaI results, the power in the tail must be the order of 25 per cent of that in the thermal portion of the spectrum and to fit a lower temperature requires an

even more substantial non-thermal tail. Thus, if a neutron star is postulated as the X-ray source, a large fraction of the observed flux cannot arise from the black-body radiation from that object.

More generally the absence of a substantial thermal contribution to the spectrum indicates that the observed X-rays are being generated in regions that are optically thin. Whether the X-rays are generated in a hot plasma or by the synchrotron process cannot be determined on the basis of these data except for noting that, in a hot plasma line, emission and edge discontinuities can arise, either of which could account for the peak at 20 keV for which there is some evidence from the NaI detector. The synchrotron process cannot give rise to such features.

Table 2 lists the counting rate, the integrated power and photon flux observed in the two source regions by the two detectors. For *ScoX*-1 the counting rates are corrected for the shadowing of the collimators and result from the fact that the detector axis comes only within 2° of the source. No such correction was made in the case of the sources near the Galactic centre. In the 1–10-keV region the integrated power and photon flux were obtained by assuming a power law distribution with the spectral index obtained from the filter attenuation of the Geiger counter results. The uncertainty in the spectral index yields the uncertainties in the integral quantity. In the > 8 keV region the integrated power and photon fluxes were obtained by summing over the NaI pulse-height distribution.

In summary, the results presented here indicate the following:

(1) The ratio of the counting rate in the Geiger counters to that in the NaI detector is not consistent with a single thermal spectrum.

(2) The NaI detector does not detect significant radiation from *ScoX*-1 beyond about 15 keV, whereas radiation is observed from the Galactic centre region to beyond 20 keV. The minimum detectable flux density at 20 keV (defined as equivalent to 1σ above background) is about 3×10^{-27} ergs cm^2-sec (c/s). Clark[7] measures a flux of $(2{\cdot}4 \pm 0{\cdot}6) \times 10^{-27}$ ergs/cm^2-sec (c/s) over the range of 20–40 keV from the Crab Nebula. The power from *ScoX*-1 at these high energies is thus considerably below what is emanating from the Crab even though at lower energies (1–10 keV) *ScoX*-1 is the brighter object as reported by Friedman[2].

(3) For both source regions the attenuation of the counting rate in the Geiger counters by the filters indicates that the X-ray flux below 2·5 keV is comparable with that above 2·5 keV. This result does not agree with that reported by Fisher[3] that little or no radiation is present below 4 keV from these sources.

The work reported here was sponsored by the U.S. National Aeronautics and Space Administration, Office of Space Sciences, under contract *NASw*-898.

[1] Clark, G., Garmire, G., Oda, M., Wada, M., Giacconi, R., Gursky, H., and Waters, J., *Nature* (this issue, p. 584). Reported also by Giacconi, R., *et al.*, at Sec. Conf. Relativistic Astrophysics, Austin, Texas (December 1964).
[2] Bowyer, S., Byram, E. T., Chubb, T. A., and Friedman, H., *Science*, **147**, 394 (1965). Reported also by Friedman, H., at Sec. Conf. Relativistic Astrophysics, Austin, Texas (December 1964).
[3] Fisher, P. C., Johnson, H. M., Jordan, W. C., Meyerott, A. J., and Acton L. W. (submitted to *Astrophys. J.*).
[4] Giacconi, R., Gursky, H., Paolini, F. R., and Rossi, B., *Phys. Rev. Letters*, **9**, 439 (1962).
[5] Giacconi, R., Gursky, H., Paolini, F. R., and Rossi, B., *Proc. Fifth Intern. Space Sci. Symp.* (to be published).
[6] Bowyer, S., Byram, E. T., Chubb, T. A., and Friedman, H., *Science*, **146**, 912 (1964).
[7] Clark, G., *Phys. Rev. Letters*, **14**, 91 (1965).
[8] Giacconi, R., and Gursky, H., *Space Sci. Rev.*, **4**, 151 (1965).
[9] Giacconi, R., Gursky, H., Waters, J., Clark, G., and Rossi, B., *Nature*, **204**, 981 (1964).
[10] Oda, M., Clark, G., Garmire, G., Wada, M., Giacconi, R., Gursky, H., and Waters, J., *Nature*, **205**, 554 (1965).

Printed in Great Britain by Fisher, Knight & Co., Ltd., St. Albans

APPENDIX F

ASE-1003B

SOME OBSERVATIONAL ASPECTS OF X-RAY ASTRONOMY

Based on Lectures delivered by
Riccardo Giacconi

at the

"High Energy Astrophysics"
Course

of the

International School of Physics

Enrico Fermi

Varenna, Italy

July 1965

SOME OBSERVATIONAL ASPECTS OF X-RAY ASTRONOMY

R. Giacconi, H. Gursky and J. R. Waters
American Science and Engineering, Inc., Cambridge, Massachusetts

B. Rossi, G. Clark, G. Garmire, M. Oda and M. Wada
Massachusetts Institute of Technology, Cambridge, Massachusetts

1.0 INTRODUCTION

The first totally unexpected result of space astronomy was the discovery of strong X-ray sources outside the solar system.

Because of atmospheric absorption, X-rays, of course, cannot be observed with land-based instruments. The altitude requirements for X-ray astronomy become clear from an examination of Fig. 1, showing the altitude where electromagnetic waves of different wavelengths arrive with different degrees of attenuation (1/2, 1/10, 1/100). One sees that X-rays with wavelength λ greater than about one A (quantum energy E smaller than 12 keV) can be observed only at altitudes greater than 50 km, which can be reached only by rockets or space vehicles. X-rays with quantum energies E greater than about 15 keV, on the other hand, penetrate to altitudes of the order of 30 km, which are within the range of balloon flights.

Even beyond the atmosphere, X-ray astronomy is limited by the absorption in interstellar space. This is shown in Fig. 2; the curves represent the density of interstellar matter (in atoms per cm^3) times the distance (in light years) corresponding to various degrees of attenuation, plotted against wavelength. Since the average density of interstellar

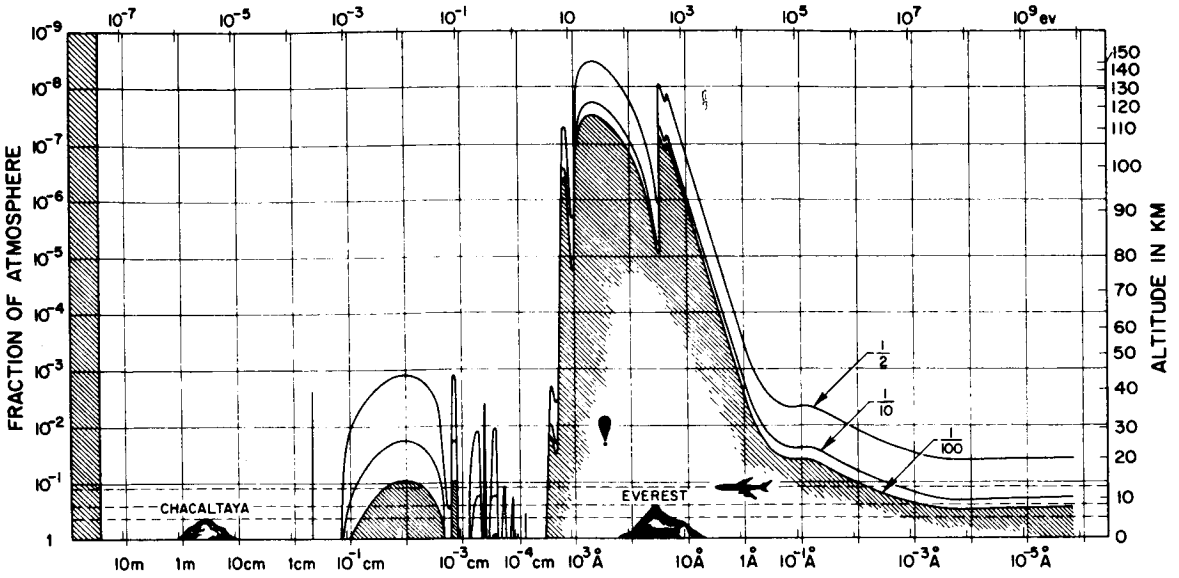


Fig. 1 Attenuation of electromagnetic radiation in the atmosphere. Solid curves indicate altitude (and corresponding pressure expressed as a fraction of one atmosphere) at which a given attenuation occurs for radiation of a given wavelength.

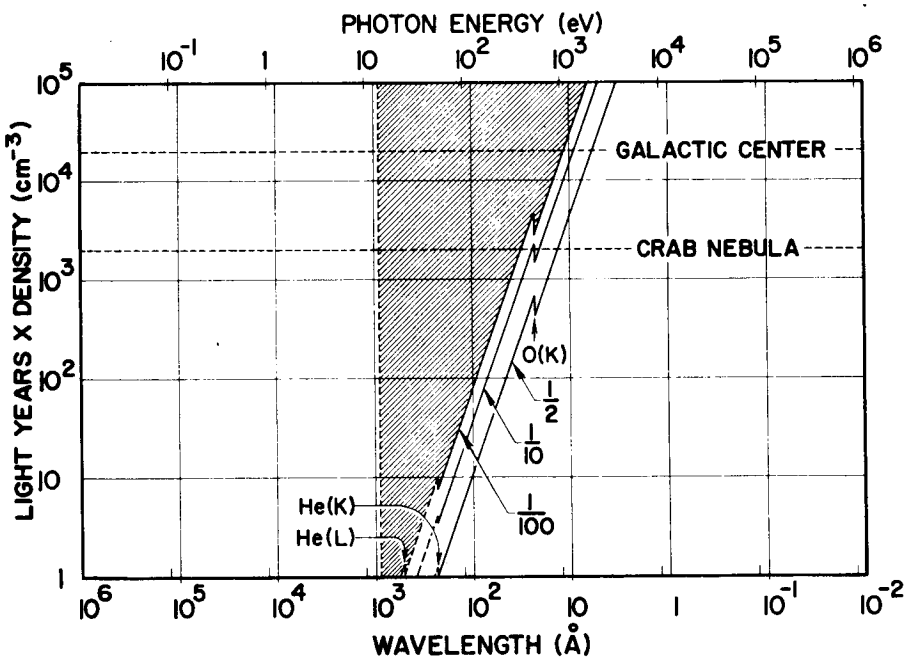


Fig. 2 Attenuation of electromagnetic radiation in interstellar space. The ordinate represents the integrated particle density in terms of light years times the number of particles per cc. The solid curves give the integrated density at which a given attenuation occurs for radiation of a given wavelength. O(K), He(K) and He(L) indicate the K absorption edges of O and He, and the L absorption edge of He. The ordinates corresponding to the Crab Nebula and the galactic center are calculated using the known distance to these objects and an assumed particle density of 0.3 atoms per cc. and one atom per cc. respectively.

matter is of the order of 0.3 atoms per cm^3, we see that, for wavelengths less than about 6A, the whole Galaxy is essentially transparent; while X-rays with wavelengths greater than about 100A can reach the earth only from sources closer than 100 light years.

Extrasolar X-rays were first detected by means of a rocket launched in June 1962 by Giacconi, Gursky, Paolini of AS&E and Rossi of MIT.[1] The detectors were Geiger counters without a collimator and, therefore, with a wide field of view. The results revealed the existence of a strong source in the constellation Scorpius not far from the galactic center, of a possible secondary source in the constellation of Cygnus and of a diffuse X-ray background, apparently also of celestial origin. Two additional rocket experiments by the same group (October 1962 and June 1963),[2] with similar instrumentation, confirmed these results and gave a slight indication of another source in the general direction of the Crab Nebula. In the meantime, (April 1963), a collimated counter, flown by a group at the Naval Research Laboratory under H. Friedman, again detected the Scorpio source.[3] The improved resolution made it possible to place an upper limit of 5° to its angular diameter and to determine its location with an accuracy of about 2°. Since the galactic center was below the horizon at the time of this flight, the X-ray source was certainly not coincident with the galactic center. The same flight provided clear evidence for another weaker source in Taurus, within about 2° of the Crab Nebula, and also confirmed the existence of the diffuse background.

In July 1964, the NRL group, using a pointing rocket, succeeded in observing the occultation of the Crab Nebula by the Moon.[4] This remarkable experiment showed that the X-ray source in Taurus was indeed

coincident with the Crab Nebula.

In addition to this flight, five other rocket flights were carried out in 1964, two by the NRL group, two by the AS&E-MIT group, and one by a group at Lockheed headed by Fisher. These flights reconfirmed the source in Scorpius. They also detected a complex of sources in the galactic plane, clustered within about 20^{o} of the galactic center, and some additional sources in the constellations of Cygnus and Serpens.

The year 1964 saw also the first successful attempt to observe X-rays from celestial objects by means of balloon-borne instruments.[5]

Figure 3 shows the region of the sky that has been explored thus far, and the approximate locations of the X-ray sources that have been detected.

2.0 INSTRUMENTATION

2.1 X-ray Detectors

A necessary requirement of the detectors for X-ray astronomy is high efficiency and large effective area because the flux of X-rays from celestial sources, although stronger than had been anticipated, is quite small.

The detectors used so far belong to three different categories.

2.1.1 Gas Counters (Geiger counters and proportional counters).

These instruments may be made in a variety of sizes and shapes. Figure 4 shows a typical design. Their operation as X-ray detectors is based primarily on the production of secondary electrons by the photoelectric

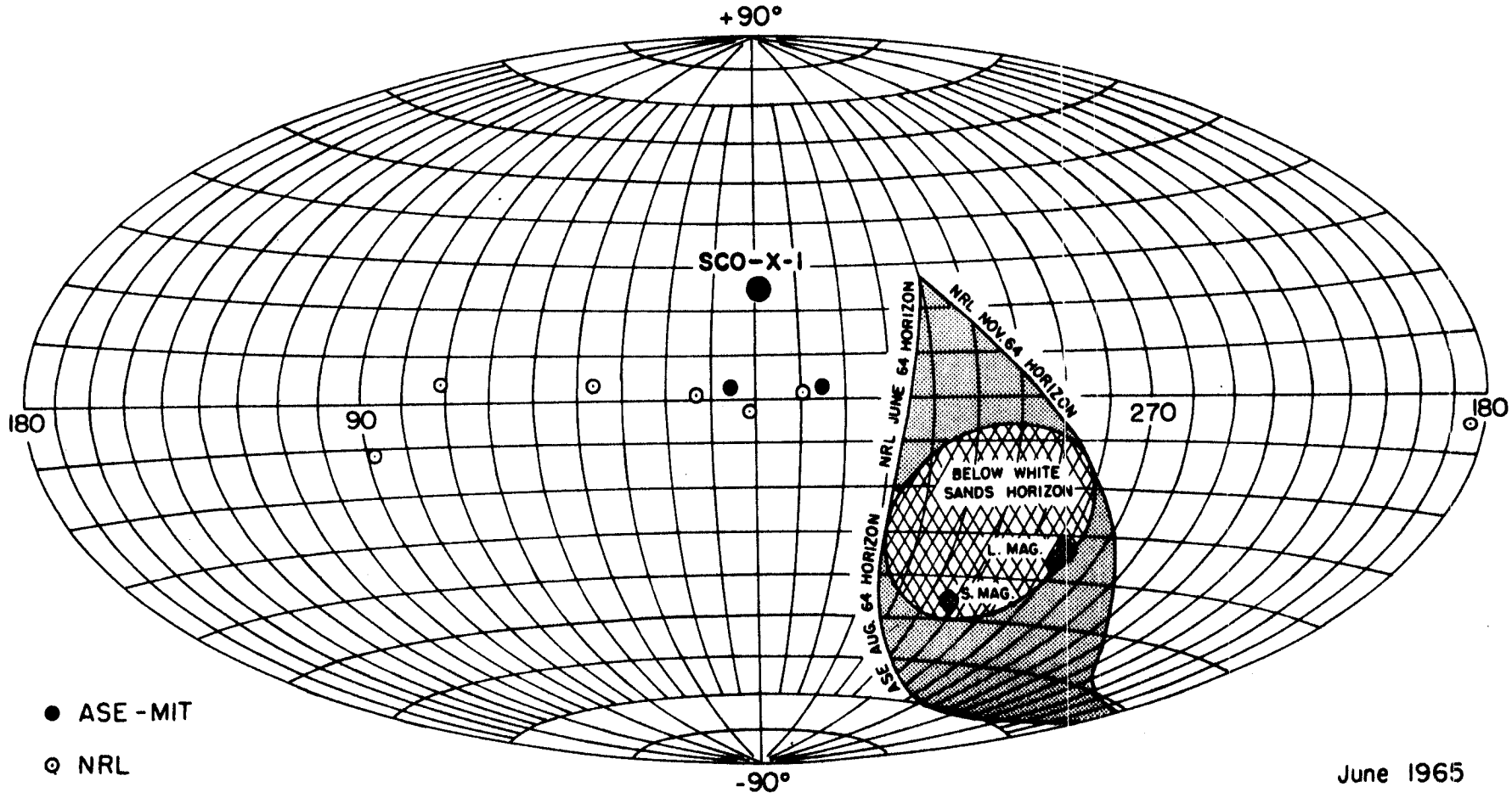


Fig. 3 X-ray source locations in the galactic coordinate system (ℓ^{II}, b^{II}). Cross-hatched region is not observable at the White Sands Missile Range. Shaded region is accessible but was not scanned in the rocket flights performed so far. This region includes the large Magellanic Cloud (L. Mag.) and the Small Magellanic Cloud (S. Mag.). The minimum detectable source intensity in the surveyed region is about 0.05 of the intensity of ScoX-1.

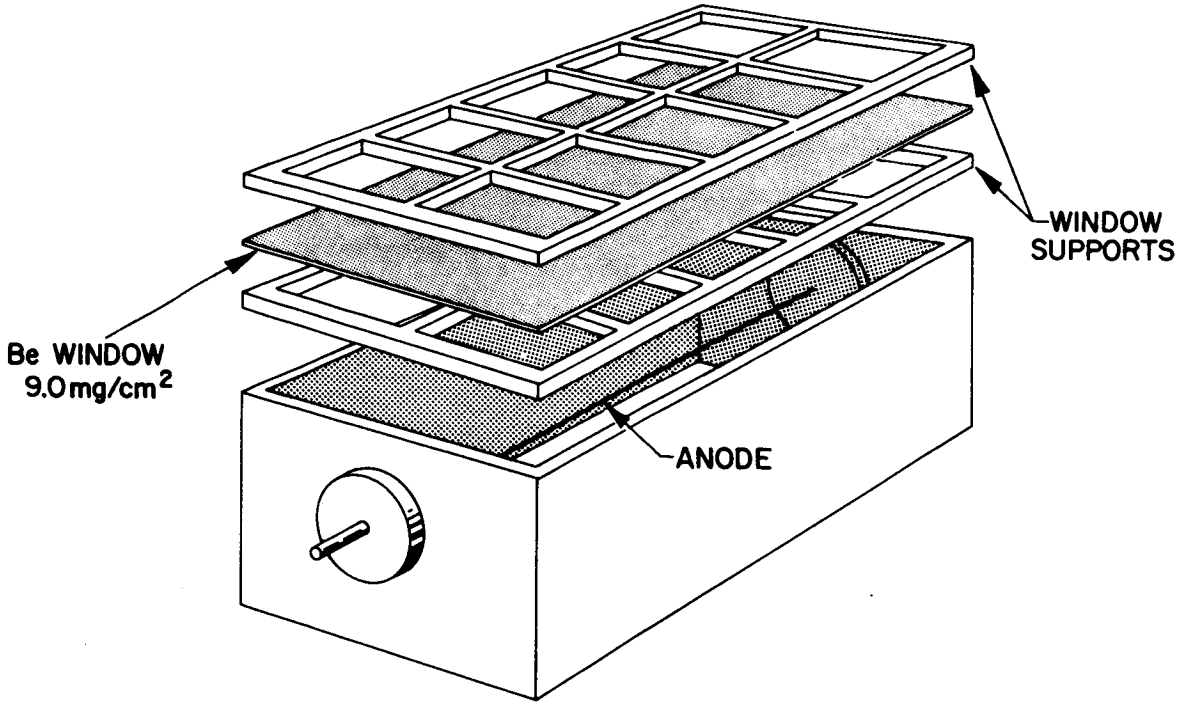


Fig. 4 Schematic drawing of a thin-window gas counter used for the detection of soft X-rays.

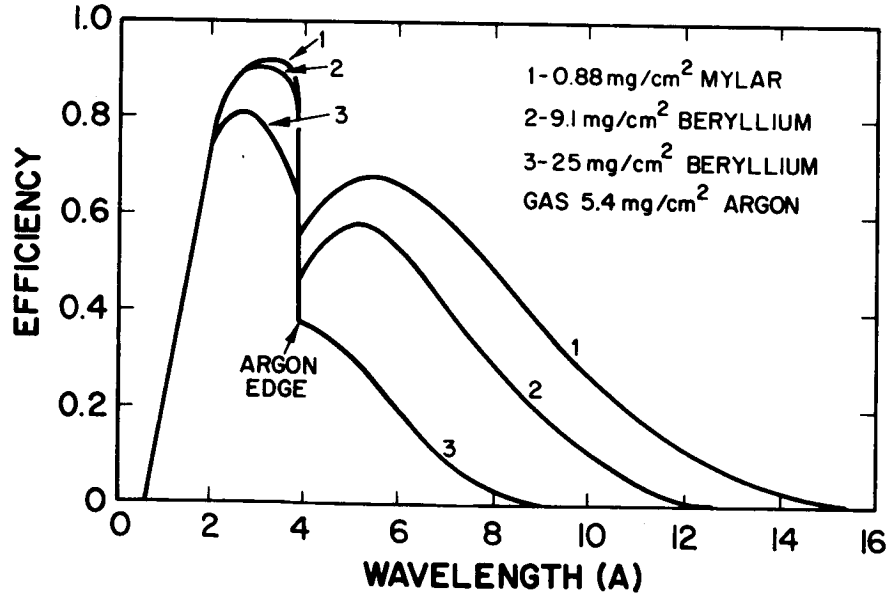


Fig. 5 Calculated efficiency of gas counters with argon filling and different windows.

effect of the photons in the gas, and on the cascade multiplication of the ions produced by these electrons. The counters must be provided with windows thin enough to let X-rays through, yet sufficiently strong to withstand the gas pressure. The efficiency of a counter, $\mathcal{E}$, is the product of the probability for an X-ray photon to traverse the window, times the probability for the photon to be absorbed in the gas. It is thus given by the equation:

$$\mathcal{E}(\lambda) = e^{-\mu_w x_w} \quad (1-e^{-\mu_g x_g}) \tag{1}$$

where μ_w and μ_g are the absorption coefficients of the window and the gas, x_w and x_g the respective thicknesses. Since μ_w and μ_g depend strongly on wavelength λ, $\mathcal{E}$ is also a function of λ; in fact, $\mathcal{E}$ is appreciably different from zero only within a certain range of wavelengths; which depends on the atomic number and on the thickness of the window and of the gas. The long wavelength limit of the sensitive region is determined by the window becoming opaque and the short wavelength limit by the gas becoming transparent. Thus, a thin, low-Z window and a low Z gas filling will tend to make the counter preferentially sensitive to long wavelengths; with a comparatively thick window and a high-Z gas filling, on the other hand, the counter will discriminate in favor of short wavelengths. Examples of efficiency functions for gas counters with argon filling and different windows appear in Fig. 5.

The lower limit on the window thickness of a gas counter is set by the practical problem of achieving a gas-tight seal. If one insists on this requirement, it is difficult to extend the upper limit of the sensitivity range beyond about 10A, although the transmission curves of certain materials

have "windows" at somewhat longer wavelengths (e.g., aluminum has a "window" from 8A to about 15A).

The long wavelength limit may be extended by relaxing the requirement that the window be gas tight. Although very thin windows (less than several hundred micrograms/cm^2) invariably leak, a gas reservoir and pressure regulator may hold the gas pressure in the counter constant within a few percent for the short period of a rocket flight. This is essential because the gas multiplication factor is very sensitive to pressure.

By a suitable choice of voltage between the case and the wires, a gas counter may be operated as a Geiger counter or as a proportional counter (the first mode of operation requiring a higher voltage than the second). As a Geiger counter, the detector gives pulses of uniform size, irrespective of the number of ion pairs N produced in the gas. In the proportional counter regime, the size of a pulse is proportional to N. The average value of N, N_{av}, is proportional to the energy dissipated in the gas. If the stopping power of the gas is sufficiently large, this energy may be taken as equal to the photon energy E[(*)] so that we can write:

$$N_{av} = E/E_o \qquad (2)$$

(*)When a photon undergoes photoelectric absorption, the photoelectron acquires a kinetic energy equal to the photon energy minus the atomic binding energy which may be a substantial fraction of the photon energy. However, most of the binding energy will appear promptly in the form of de-excitation radiation or of kinetic energy of an Auger electron. If the stopping power of the gas is sufficient to absorb all of the electrons and photons emitted subsequent to the process of photoelectric absorption, the energy dissipated in the gas will be practically equal to that of the photon.

where E_o a characteristic energy dependent on the gas (e.g., E_o = 27 eV for argon). Thus, the pulse height distribution of a proportional counter is directly related to the spectrum of the observed radiation. The counter, however, has a limited spectral resolution, for two separate reasons. In the first place, there may be cases where not all of the energy of the photon which has undergone photoelectric absorption is dissipated in the gas (this effect becomes increasingly important with increasing photon energy). In the second place, the actual value of N corresponding to a given energy dissipation undergoes statistical fluctuations around N_{av} (this effect becomes increasingly important as the photon energy decreases). Note that only if the counter is carefully designed will the multiplication factor remain essentially constant over its sensitive volume.

Examples of actual pulse height distributions obtained with a proportional counter exposed to monoenergetic X-rays of different energies appear in Fig. 6.

With detectors of the type described, ultraviolet rays, cosmic rays and other charged particles of lower energy are possible sources of background. It is easy to protect the detector against ultraviolet rays by a proper choice of the window. In order to reduce the cosmic-ray background, the counters are often set into a well-type scintillation counter whose output pulses are placed in anticoincidence with those of the X-ray counter. Low-energy charged particles, particularly electrons, whose energy is sufficient to traverse the window but not to penetrate the anticoincidence counter cannot be eliminated, and, therefore, represent a source of background that must be taken into consideration.

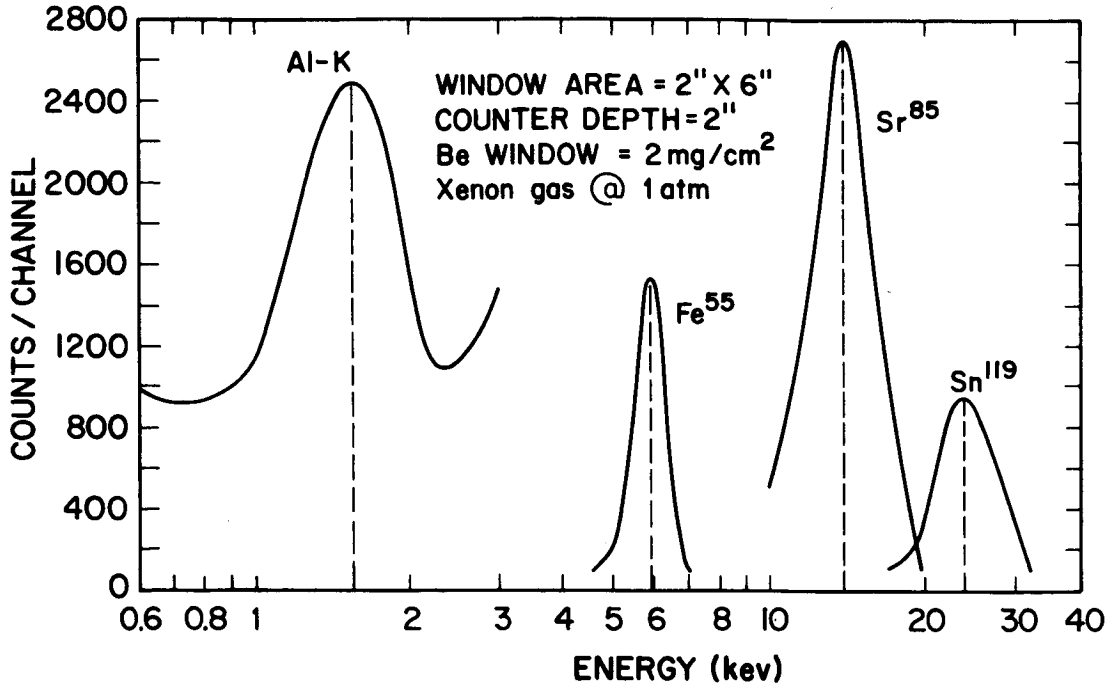


Fig. 6 Pulse-height distributions obtained with a proportional counter exposed to mono-energetic X-rays generated by K-capture (i.e., Sr^{85}), isomeric transition (Sm^{119}) and K-X-rays induced by electron bombardment. (Al).

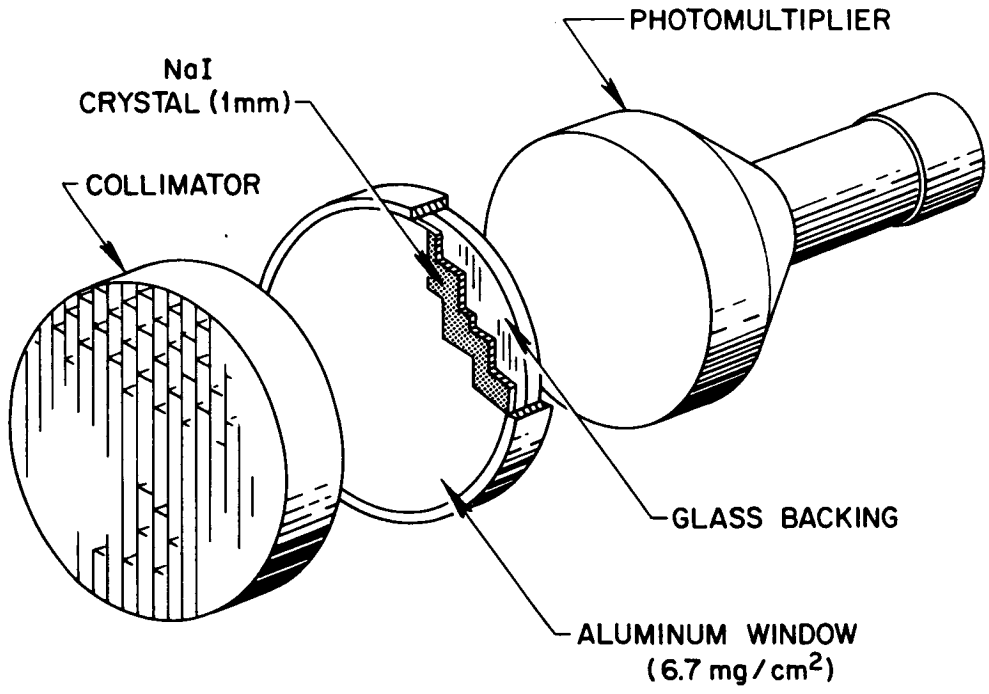


Fig. 7 Schematic drawing of a scintillation counter used for the detection of soft X-rays.

2.1.2 Scintillation Counters

Figure 7 shows, as an example, the design of a scintillation counter used in several rocket experiments. X-ray quanta, incident on the thin slab of scintillating material (e.g. NaI crystal) produce secondary electrons by photoelectric effect. Practically all of these come to rest in the scintillator, giving light pulses proportional to their energy. Some of the photons thus produced reach the photocathode of the photomultiplier, releasing a certain number N of photoelectrons. The photomultiplier output is closely proportional to N.

The efficiency of the detector is the product of two terms. The first is the probability for the X-ray photon to produce a photoelectron in the scintillating material; this probability depends on the thickness and on the atomic number of the scintillator, being high for a high-Z scintillator (such as NaI), and low for a low-Z scintillator (such as anthracene). The second term is the probability that at least one photoelectron be released from the photocathode by the light pulse ($N > 1$). The average pulse height is proportional to the average value of N. It is therefore a linear function of the energy of the X-ray photon, and may be represented by an equation of the type of Eq. (2). In typical situations, the average energy per photoelectron E_o is of the order of 1000 eV. Comparing this number with the average energy for the production of an ion pair in a gas counter we see that, for a given E, N is smaller for a scintillation counter than for a gas counter. Thus, the smallest detectable photon energy is higher for a scintillation counter than for a gas counter.

The spectral resolution is limited by the fluctuations in the pulse-height corresponding to a given photon energy, which is a decreasing function of N. Therefore, for small values of E, a scintillation counter will not yield as good an energy resolution as may be obtained with a proportional gas counter. For sufficiently high photon energies, on the other hand, scintillation counters have both better efficiency and higher energy resolution than gas counters because of the relatively higher stopping power of the sensitive medium.

A further limitation to the efficiency of scintillation counters for low-energy photons arises from photomultiplier noise. Under optimum conditions, scintillation counters can detect photons down to about 1 keV energy. Because of additional difficulties arising from the requirement of a large sensitive area, until now scintillation counters have been used in X-ray astronomy only in the energy region above 10 keV.

Scintillation counters must be covered with thin films of opaque material to protect the photomultipliers from visible or ultraviolet light. Cosmic-rays and other high-energy particles produce pulses of greater size than X-ray photons, and, therefore, can be easily distinguished from them. Low-energy particles, in particular electrons, cannot be distinguished from X-ray photons on the same basis. However, it is possible to separate these particles from X-rays by comparing the counting rates of two detectors with scintillation crystals of the same mass per cm^2 but different Z (e.g., NaI and anthracene). Such counters have nearly the same response for electrons, but the low-Z counter is practically insensitive to photons.

2.1.3 Photoelectric Detectors

Gas counters cannot be operated in a vacuum without a window and each window places a low-energy limit to the observable portion of the X-ray spectrum. The photoelectric detector does not need a window

and can, therefore, be used to extend the measurements to lower photon energies than are accessible to gas counters.

The possibility of building a photoelectric detector for X-rays rests on the fact, discovered by a group of Russian scientists in 1960,[6] that several alkali halides have an anomalously high photoelectric yield for X-rays. The design of a photoelectric detector for X-ray astronomy built by the AS&E group is shown in Fig. 8. The photocathode is an evaporated layer of KCl or CsI deposited on a spherical surface. The electrons ejected from the photocathode are focused on the first dynode of an electron multiplier, whose output pulse is proportional to the number of these electrons. The sensitive area of this particular instrument is 40 cm^2. Its measured efficiency ranges from about 8% for 5 keV photons to about 25% for 0.8 keV photons. Although the instrument may be operated without a window in the high vacuum found at the altitudes where the measurements are made, a filter may be necessary to absorb ultraviolet light. Furthermore, such a window is needed to exclude ambient ionospheric electrons. Several hundred angstroms of aluminum evaporated on a thin organic film will achieve these purposes while allowing the transmission of X-rays well beyond the K-edge of carbon at 44A. Rejection of visible light does not present a serious problem because of the high work function of KCl or of CsI.

Detectors of this kind have already been flown. Although the results obtained so far are only of a preliminary character, they show that photoelectric detectors hold great promise for the future of X-ray astronomy.

2.2 Collimators

2.2.1 Cellular Collimators

In order to obtain accurate information on the location of the X-ray sources and on their angular sizes, it is necessary to limit the

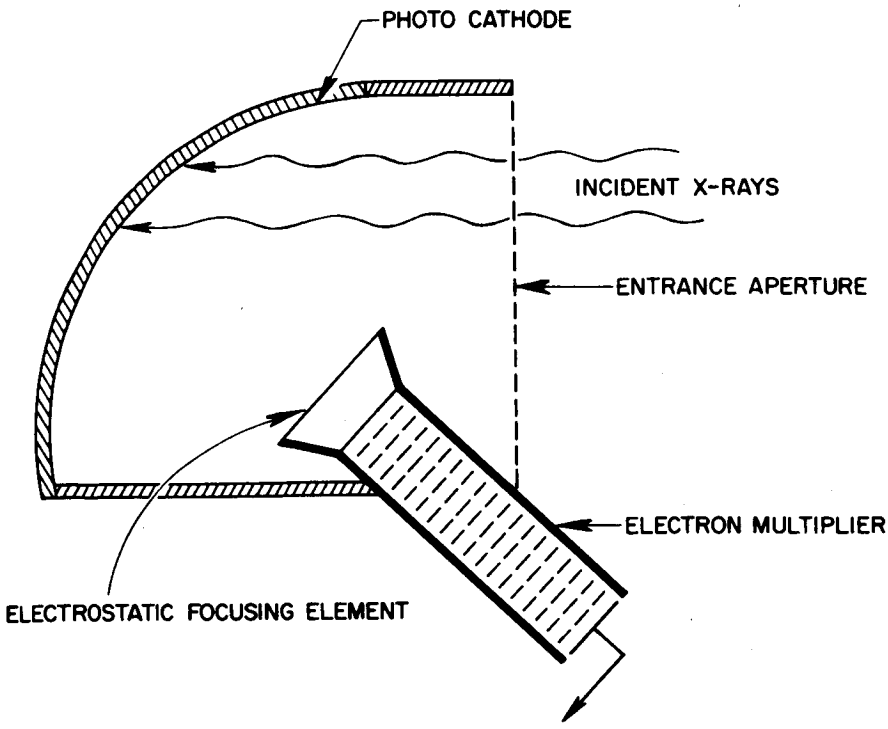


Fig. 8 Schematic diagram of a photoelectric detector for soft X-rays.

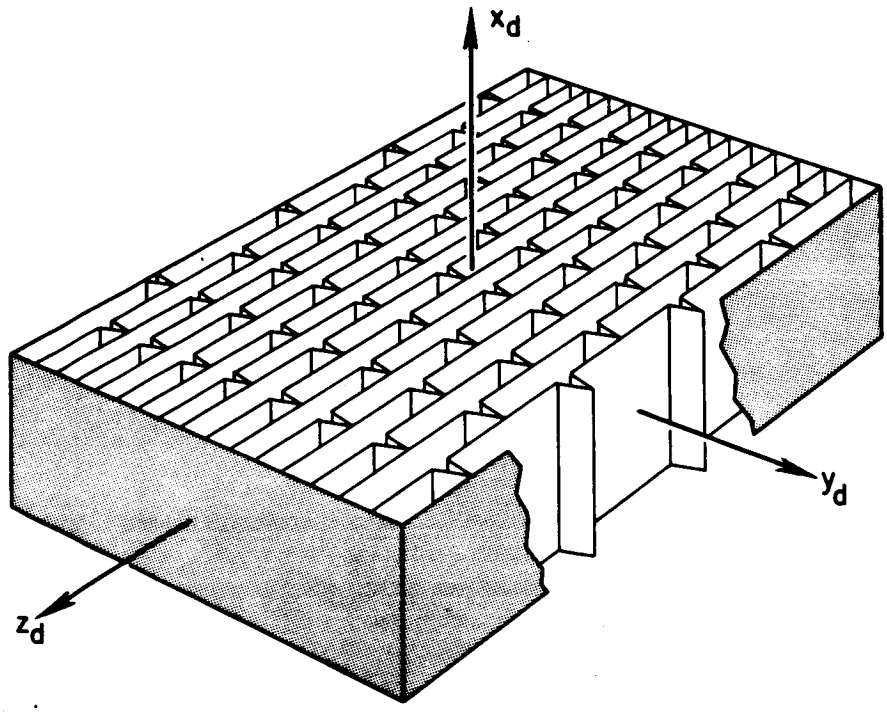


Fig. 9 Schematic drawing of a cellular collimator.

field of view of the detectors by means of suitable collimators. Because of the large area of the detectors and of the limited space available, cellular type collimators have been used such as that shown in Fig. 9. With these collimators one can obtain fields of view of different shapes and different angular widths down to about two degrees. The transmission, of course, is a maximum for a beam parallel to the axis of the collimator (i.e., the normal x_d to its plane; see Fig. 9). The response curves (i.e. the curves giving transmission as a function of angle of incidence in planes containing the collimator axis) have typically nearly triangular shapes. As an example, Fig. 10 shows the computed and the experimental response curves in the plane $x_d y_d$ of a collimator of the type shown in Fig. 9.

2.2.2 Modulation Collimators

In order to improve the angular resolution of a cellular collimator, it is necessary to decrease its field of view. In this manner, however, one also decreases the number of counts recorded when the X-ray source passes across the field of view, and therefore one reduces the statistical accuracy of the data. There is thus a practical limit to the resolution that may be obtained with these devices when used on spinning rockets.

A collimator of a different type, which combines high resolution with wide field of view was conceived by M. Oda[7] and has been developed by the ASE-MIT group. Known as the "modulation collimator", it consists essentially of two plane grids of parallel wires placed one in front of the other at a suitable distance (Fig. 11). The diameter of the wires, d, is nearly equal to the spacing between adjacent wires, s. In a parallel beam

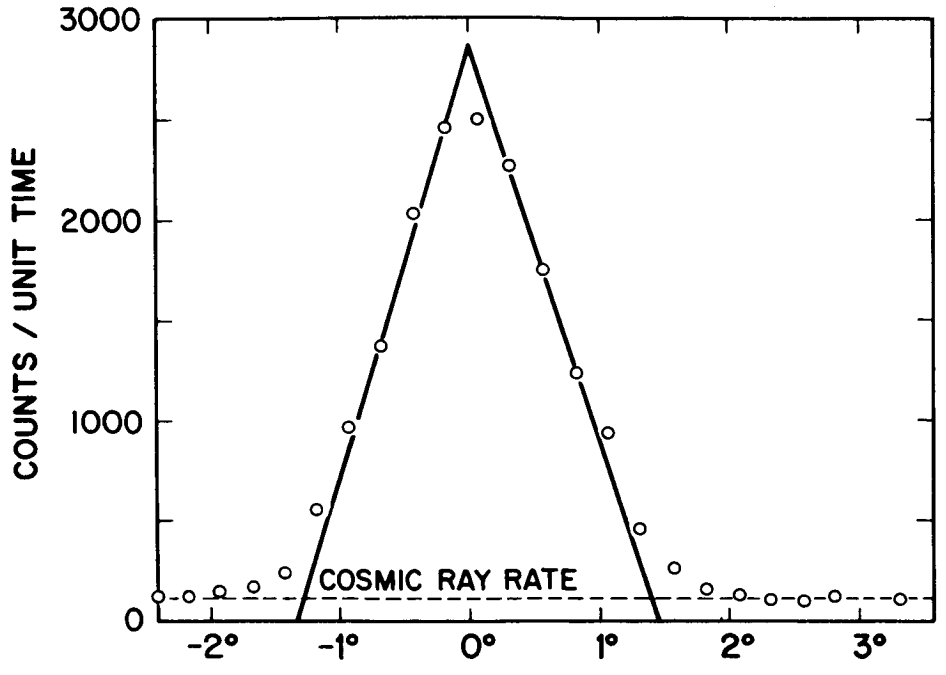


Fig. 10 Experimental response curve of a cellular collimator to X-rays (circles) compared with its computed response function (solid line). The angular divergence of the X-ray beam was less than $1/2^{\circ}$. The X-ray beam was in the $(\hat{x}_d, \hat{y}_d)$ plane (Fig. 9) and the abscissa represents the angle formed by this beam with the normal to the collimator $(\hat{x}_d)$.

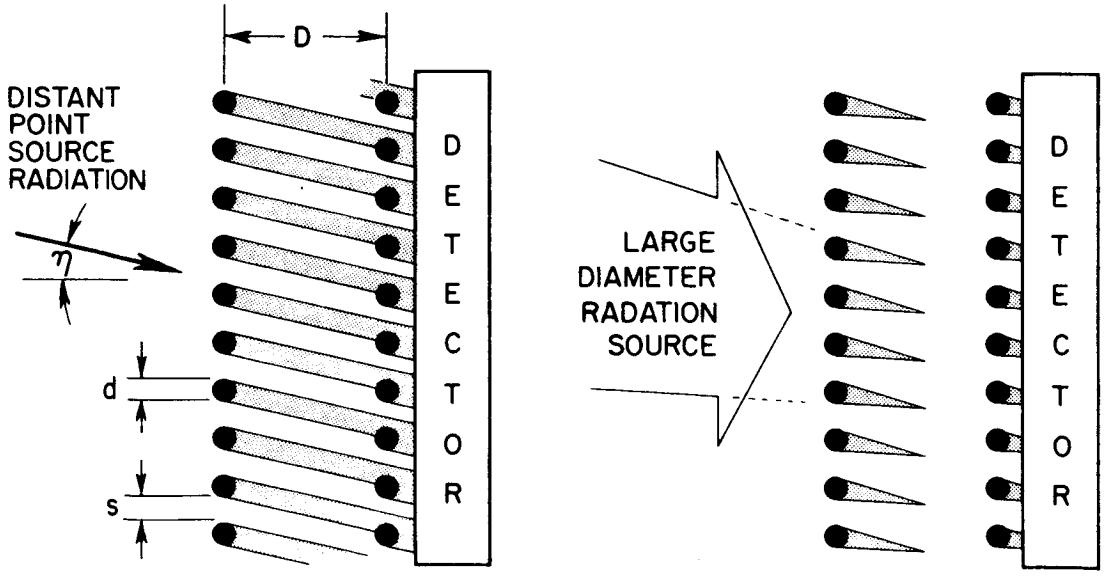


Fig. 11 Illustrating the principle of operation of the modulation collimator. The drawing on the left indicates the shadowing that obtains with parallel radiation.

of rays, the front grid casts a shadow on the rear grid. The shadow shifts as the orientation of the collimator relative to that of the incident beam changes, and the transmission of the collimator changes correspondingly, being a maximum when the shadow of the front wires falls exactly on the back wires, and a minimum when it is centered between adjacent wires.

Figure 12 shows the computed response curve of a modulation collimator in a plane perpendicular to the wires in the case of a parallel beam coming from a distant point source. The abscissa is the angle η between the beam and the collimator's axis (i.e. the normal to the planes of the grids; see Fig. 11). The ordinate is the transmission. The distance D between the grids is large compared with the distance d + s between the axes of adjacent wires. For small values of η the angular distance between maxima is:

$$\Delta \eta = (d + s)/D$$

It is clear that a distant source with angular dimensions δ small compared with $\Delta \eta$ will produce practically the same pattern of maxima and minima as a point source. If, on the other hand, the source has angular dimensions large compared with $\Delta \eta$ no "modulation" of the transmitted intensity will occur as the angle of incidence varies. With a source of angular dimensions comparable to $\Delta \eta$, a variation of the angle of incidence will produce a partial modulation, from which it may be possible to estimate the actual angular size of the source in the direction perpendicular to the wires. The minimum angular size of a source that can be distinguished from a point source depends on the mechanical precision achieved in the construction of the collimator, on the statistical accuracy of the data and on the contribution

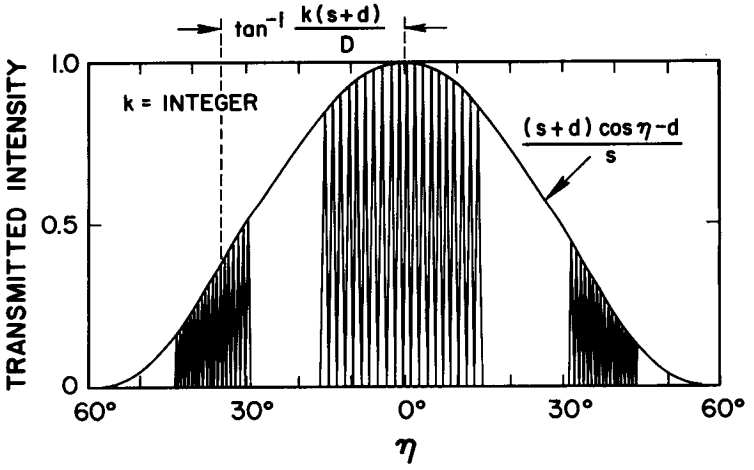


Fig. 12 Calculated angular response of a modulation collimator. The X-ray beam lies in the plane perpendicular to the grids ($\hat{x}_d$, $\hat{y}_d$ plane), the abscissa is the angle η formed by the beam with the normal to the grids.

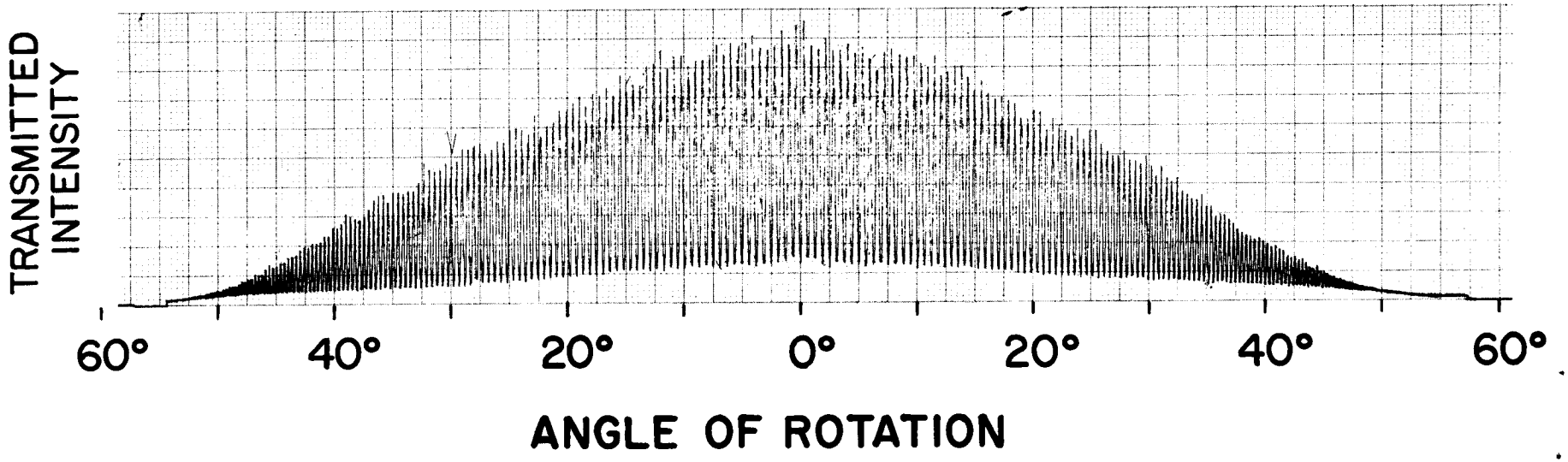


Fig. 13 Angular response of modulation collimator measured with visible light. The abscissa is the angle η (Fig. 11). Dimensions of the collimator are shown.

of the diffuse background radiation to the measured fluxes. The experience with the collimators that have been used has shown that this minimum size is about a quarter of $\Delta \eta$.

Modulation collimators with $\Delta \eta$ as small as 8 arc minutes have been used. Figure 13 shows the response curve of a modulation collimator with $\Delta \eta$ of about 32 arc minutes, measured with visible light; Fig. 14 shows a similar curve for a modulation collimator having a $\Delta \eta$ of 2 degrees, measured with X-rays.

2.3 Image Forming Telescopes

It seems difficult to obtain resolving powers substantially better than several arc seconds by means of modulation collimators such as those described above. Moreover, these devices give ambiguous results when several sources are within their field of view. In order to improve the resolution further and to investigate the actual structure of an extended source, instruments of a different type are needed. The ideal instrument is an image-forming telescope. It is actually possible to build telescopes for X-rays using the phenomenon of total external reflection of X-rays under grazing incidence.[8, 9] It can be shown that two reflections are needed to obtain an image. The two reflecting surfaces may be a paraboloid and an hyperboloid with its external focal point at the focal point of the paraboloid, such as shown schematically in Fig. 15. Other combinations of surfaces, however, are possible.

Image forming telescopes have been used so far only for solar X-ray astronomy. Figure 16 is the photograph of one such instrument. In Fig. 17 a picture of the Sun in X-rays obtained with this telescope from a rocket[10] is compared with a picture of the Sun in Hα obtained almost simultaneously

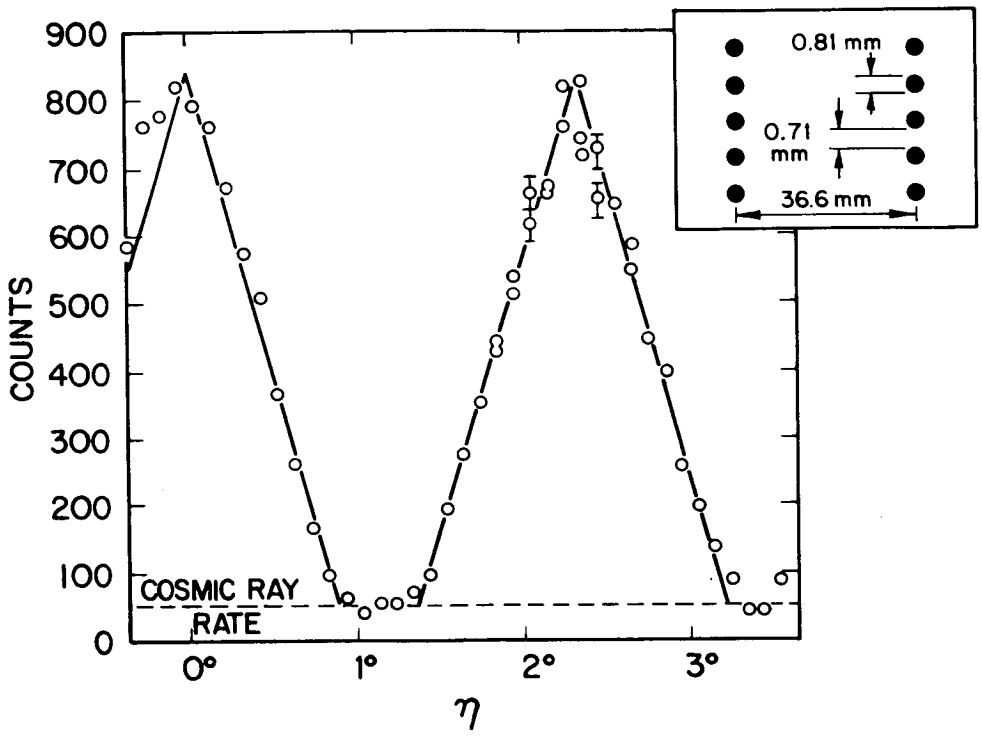


Fig. 14 Angular response of modulation collimator measured with X-rays. The abscissa is the angle η (Fig. 11).

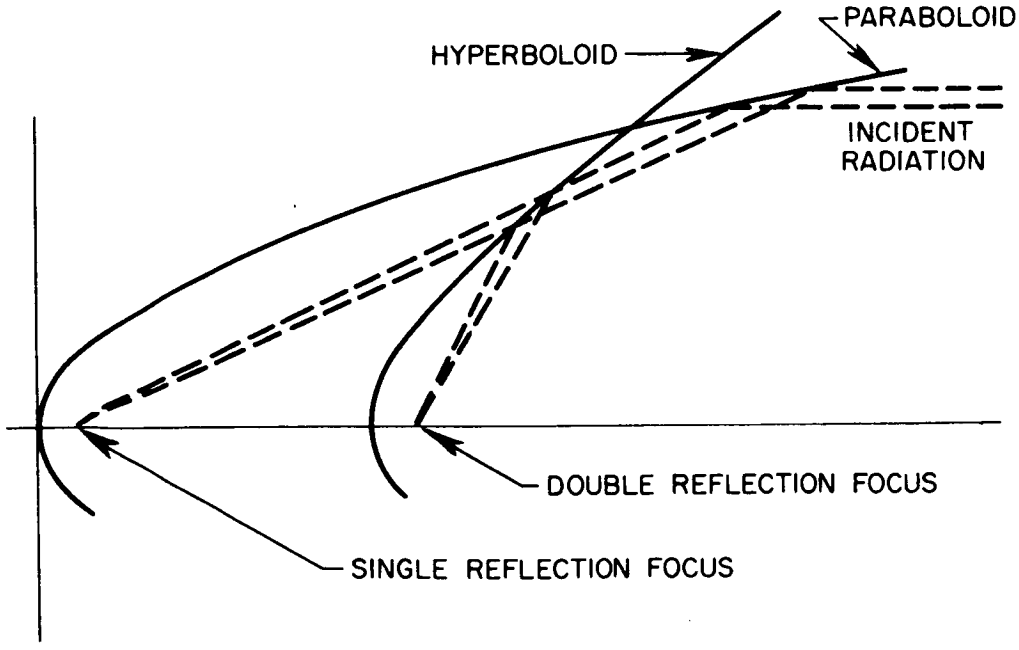


Fig. 15 Ray tracing in a grazing-incidence X-ray telescope. The focus of the paraboloid coincides with the external focus of the hyperboloid.

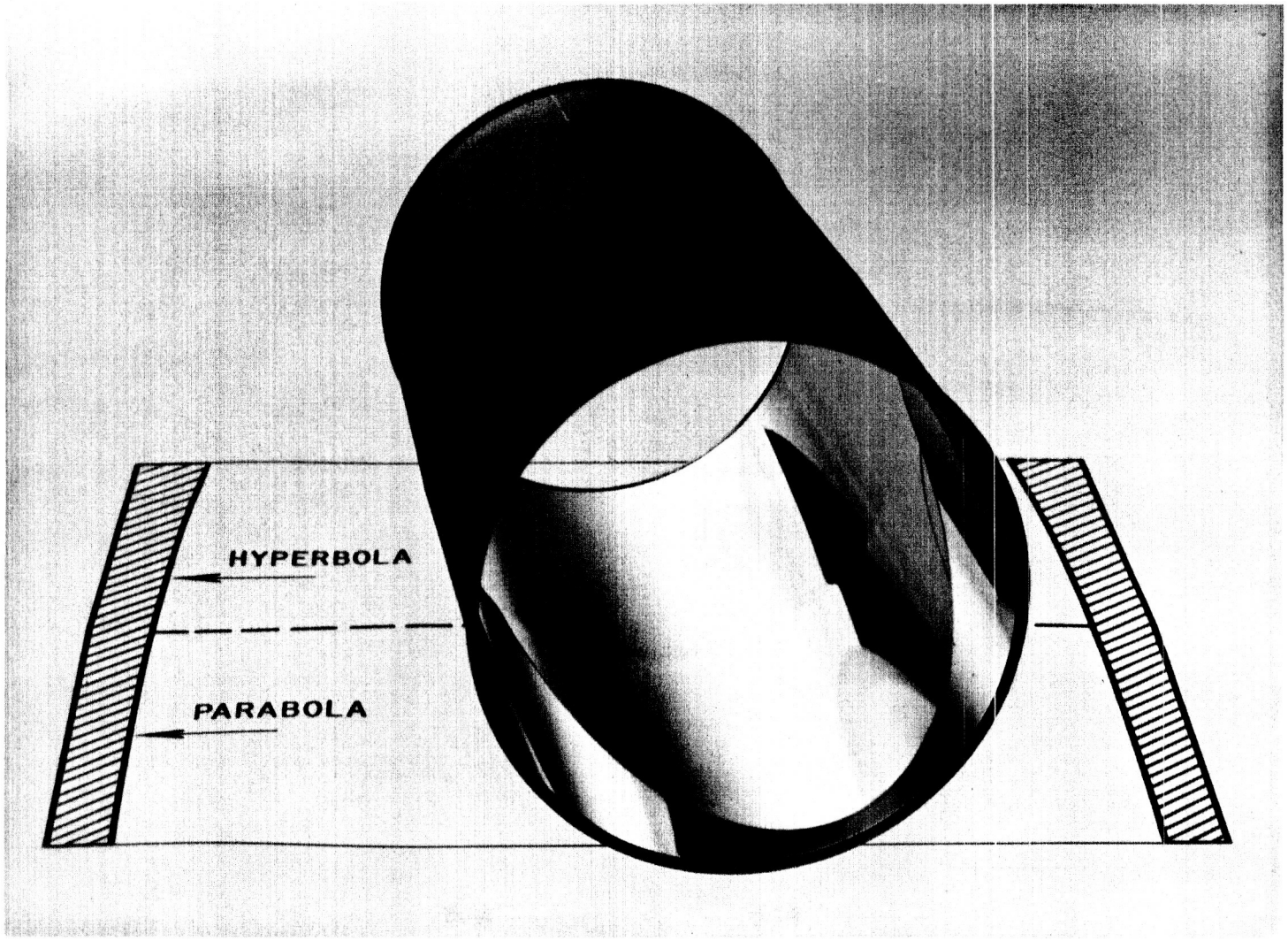
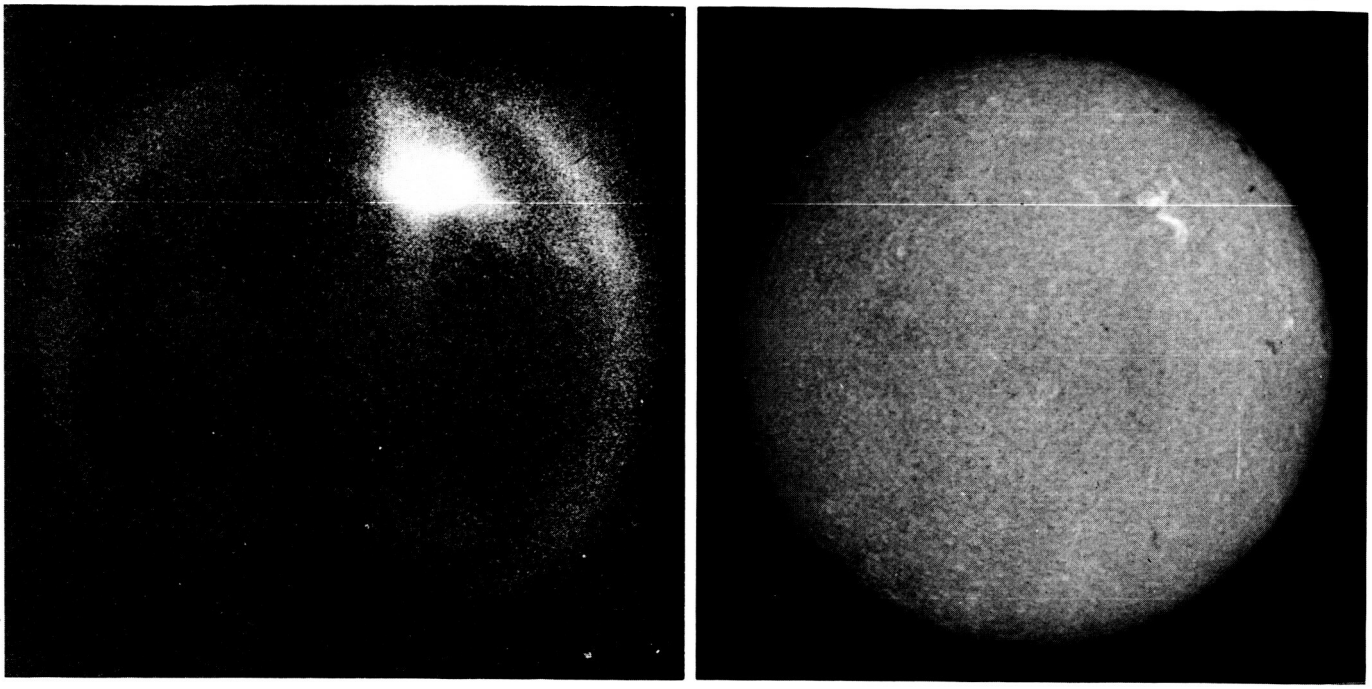


Fig. 16 Photograph of a focusing X-ray telescope superimposed on the drawing of a section of the interior surfaces.



X-Ray photograph of Sun
17 March 1965, 1510-1515 hrs. U. T. WSMR
100 sec exposure
0.15 mil mylar filter (2200 Å Al)
Ilford Industrial G film

Hα
17 March 1965, 1520 hrs. U.T.
(by courtesy of Sacramento Peak Observatory,
Air Force Cambridge Research Laboratory)

Fig. 17 Photographs of the Sun in X-rays and in Hα. X-ray photograph at left was taken during rocket flight, using the focusing telescope shown in Figure 16.

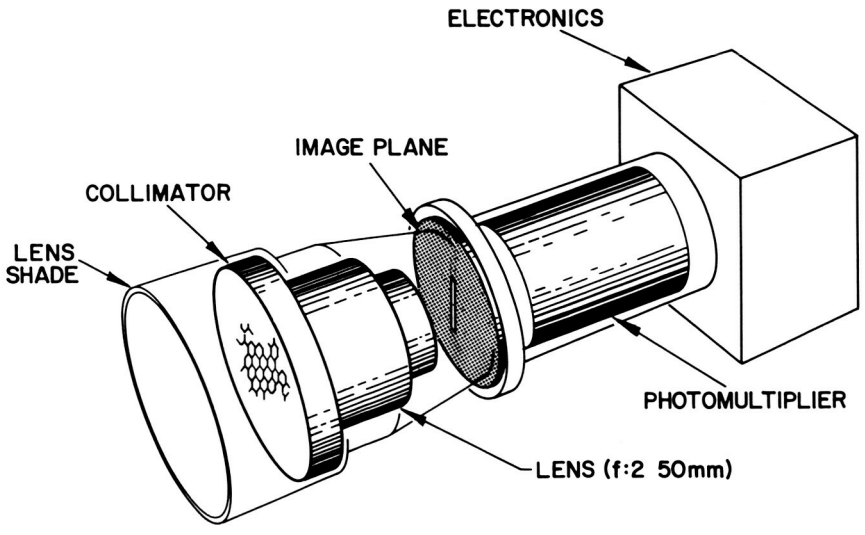


Fig. 18 Schematic drawing of an optical aspect sensor.

with an ordinary telescope from the ground. The use of image forming telescopes for the study of extra solar sources shows great promise.

2.4 Optical Sensors

In order to determine the parameters of the vehicle's rotational motion during the period of observation, one generally uses optical sensors, capable of detecting celestial objects such as the Sun, the Moon and the stars. An example of such an instrument is shown in Fig. 18. It consists essentially of an objective lens with a rectangular slit in its focal plane and a photocell behind it. This arrangement provides a "rectangular" response function as defined by the slit in the focal plane.

3.0 ANALYSIS PROBLEMS RELATIVE TO ROCKET OBSERVATIONS

Both freely spinning rockets and attitude controlled rockets have been used for X-ray observations. In the first instance, if the rocket behaves like a rigid body and external torques are negligible, its rotational motion consists of a spin (with constant angular velocity ω_s) around the minor axis of inertia, accompanied by a precession (with constant angular velocity ω_p) of the spin axis around an axis fixed in space and parallel to the total angular momentum (precession axis). The minor axis of inertia is practically coincident with the longitudinal axis of the rocket whose momental ellipsoid may be regarded as a surface of revolution around this axis. The half-apex angle of the precession cone, α, is related to ω_s and ω_p by the equation:

$$\cos \alpha = \frac{\omega_s}{\omega_p} \sqrt{\frac{I_1}{I_2 - I_1}} \qquad (3)$$

where I_1 and I_2 are the moments of inertia relative to the spin axis and to a direction perpendicular to it. In the most accurate observations, it becomes necessary to take into account the possibility that the actual rotational motion of the rocket may differ slighly from that described above. The deviations occur mainly not because of the presence of external torques, but because the rocket does not behave exactly like a rigid body. Therefore, the direction of the precession axis remains fixed in space, but ω_s, ω_p and α may undergo small and gradual changes during the time of observation.

Useful X-ray observations may be made only above 80 km. The rockets that have been used (Aerobee) usually reach a maximum altitude somewhat in excess of 200 km, which gives an observation time of about 5 minutes. During boost the rocket is spun up to two revolutions per second for the purpose of stabilization. If it is not purposely despun, the rocket will maintain approximately this spin frequency until it re-enters the atmosphere (atmospheric friction during the ascent does not reduce the spin frequency substantially). With such high spin frequency, the apex angle of the precession cone is small and $\omega_p << \omega_s$.

In some experiments, the spin angular velocity of the rocket is reduced by means of gas jets or a yo-yo despin mechanism after the rocket has traversed the denser part of the atmosphere. The decrease of ω_s results in a widening of the precession cone and, in the extreme case, α may approach 90°.

Actively controlled rockets offer the possibility of exploring selectively predetermined regions of the sky. On the other hand, one cannot use rigid-body dynamics to predict the character of their motion. In the experiments carried out thus far, an attitude control system (or ACS), based on gyroscopes

as sensing devices, is used to control the rocket orientation. By means of gas jets, it is possible to point the axis of any given detector to within several degrees of any given direction in the sky, or to sweep it at a prescribed speed over a prescribed angular interval.

3.1 Frames of Reference

In the analysis of the data and in the presentation of the results obtained with freely spinning rockets, it is convenient to consider a number of different frames of reference. Each shall be defined by a Cartesian coordinate system, specified by three mutually perpendicular unit vectors $\hat{x}$, $\hat{y}$, $\hat{z}$. We shall call x, y, z the three coordinates of the unit vector $\hat{r}$ specifying a given direction. To each Cartesian system, we shall associate a polar system of coordinates ϕ, λ, where ϕ is the azimuth and λ is the elevation. We take the polar axis in the direction of $\hat{z}$ and the plane $\phi = 0$ coincident with the $(\hat{x}, \hat{z})$ plane.

Thus:
$$x = \cos\phi \cos\lambda$$
$$y = \sin\phi \cos\lambda$$
$$z = \sin\lambda$$

A list of the various frame of reference appears below.

(a) Celestial Frame of Reference $\hat{x}_c$, $\hat{y}_c$, $\hat{z}_c$; the $(\hat{x}_c, \hat{y}_c)$ plane coincides with the celestial equator (which coincides with the Earth's equator); $\hat{z}_c$ points toward the north pole and $\hat{x}_c$ toward the ascending node of the ecliptic. Thus ϕ_c is the right ascension and λ_c is the declination.

(b) Precession Frame of Reference $\hat{x}_p$, $\hat{y}_p$, $\hat{z}_p$; $\hat{z}_p$ is parallel to $\vec{\omega}_p$, i.e. to the axis of the precession cone; $\hat{x}_p$ is parallel to the vector product $\hat{z}_c \times \hat{z}_p$; i.e. it lies in the $(\hat{x}_c, \hat{y}_c)$ plane, and points in the direction of the "ascending node of the precession equator". With respect to

the celestial frame of reference, the precession frame of reference is defined by the right ascension $\phi_c^{(p)}$ and by the declination $\lambda_c^{(p)}$ of the precession axis $\hat{z}_p$. If angular momentum is conserved, the precession frame of reference is fixed with respect to the celestial frame of reference.

(c) The Spin Frame of Reference $\hat{x}_s$, $\hat{y}_s$, $\hat{z}_s$; $\hat{z}_s$ is parallel to $\vec{\omega}_s$, i.e. to the spin axis of the rocket; $\hat{x}_s$ lies in the direction of $\hat{z}_p \times \hat{z}_s$. With respect to the precession frame of reference, the spin frame of reference is defined by the angles $\lambda_p^{(s)}$ and $\phi_p^{(s)}$, which are the elevation and the azimuth of $\hat{z}_s$ as measured in the precession frame of reference, as shown in Fig. 19. If momentum and energy are conserved, $\lambda_p^{(s)}$ is a constant and $\alpha = \frac{\pi}{2} - \lambda_p^{(s)}$ represents the semi-aperture of the precession cone, while $\phi_p^{(s)}$ varies uniformly from 0 to 2π during one precession period.

(d) The Rocket Frame of Reference $\hat{x}_r$, $\hat{y}_r$, $\hat{z}_r$; $\hat{z}_r$ coincides with the figure axis of the rocket and $\hat{x}_r$ is fixed with respect to the rocket. If the figure axis coincides with the spin axis then $\hat{z}_r$ coincides with $\hat{z}_s$. $\hat{x}_r$ rotates relative to $\hat{x}_s$ with angular velocity ω_s, and if ω_s is constant, the azimuth of $\hat{x}_r$ in the spin frame of reference is $\phi_s^{(r)} = \omega_s (t - t_o)$ where t_o is the time when $\hat{x}_r$ and $\hat{x}_s$ are coincident. In the ASE-MIT experiments so far it has not proven necessary to allow for the possible small discrepancy between the spin and figure axes.

In what follows we shall have occasion to use the equation relating the elevation λ_r of a unit vector $\vec{r}$ in the rocket frame to the elevation λ_p of the same vector in the precession frame and to the relative azimuth, $\phi_p - \phi_p^{(s)}$, of the vector and of the spin axis in the precession frame. This equation may be derived from the vector identity $(\hat{z}_p \times \hat{z}_s) \cdot (\hat{z}_p \times \vec{r}) = \hat{z}_s \cdot \vec{r} - (\hat{z}_s \cdot \hat{z}_p)(\vec{r} \cdot \hat{z}_p)$ and reads:

$$\sin \lambda_r = \sin \lambda_p \cos \alpha + \cos \lambda_p \sin \alpha \cos (\Phi_p - \Phi_p^{(s)}) \qquad (4$$

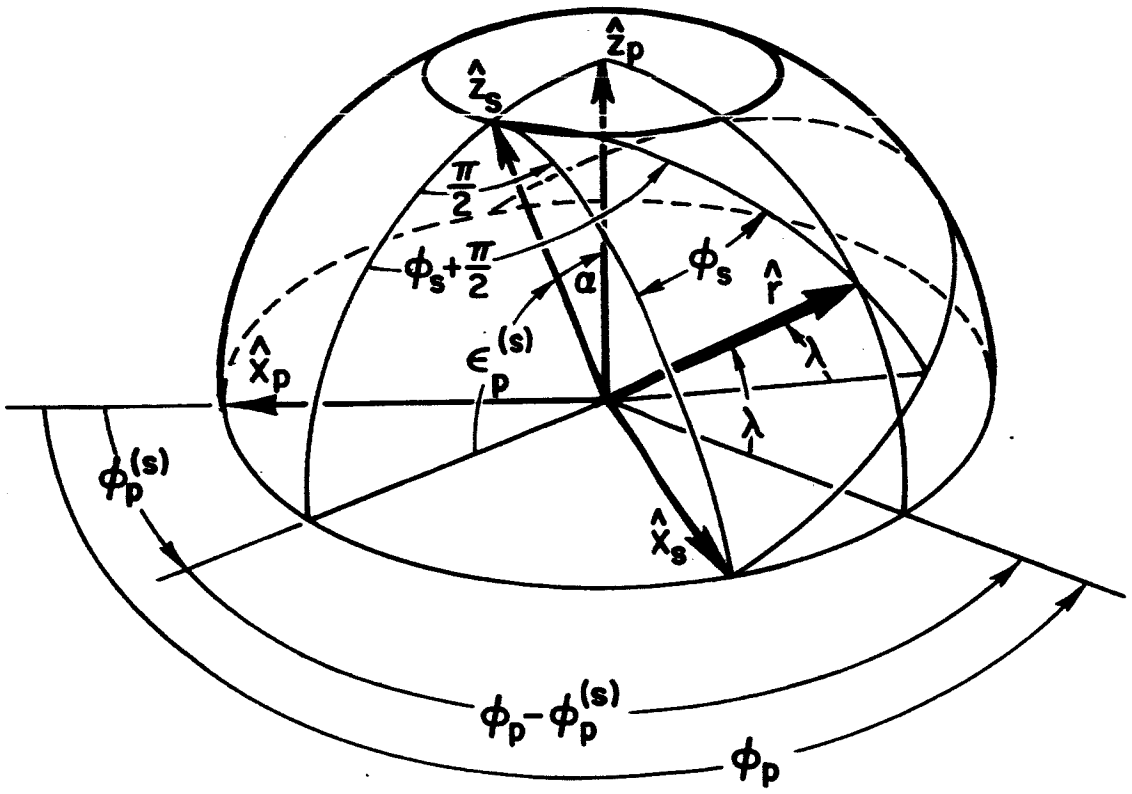


Fig. 19 Precession and spin coordinate systems.

The above equation shows that if $\vec{r}$ is fixed in the precession frame, λ_r varies from $\lambda_p + \alpha$ to $\lambda_p - \alpha$ during a precession cycle. Note that if λ_p and α are small angles, Eq. (4) may be approximated by:

$$\lambda_r = \lambda_p + \alpha \cos (\Phi_p - \Phi_p^{(s)}) \tag{5}$$

3.2 Freely Spinning Rockets

Consider now a freely spinning rocket carrying a detector (X-ray counter or optical sensor). Suppose that the detector's axis forms an angle $\lambda_r^{(d)} = \lambda_s^{(d)}$ with the equatorial plane of the rocket. Then its elevation in the precession frame will oscillate between $\lambda_r^{(d)} - \alpha$ and $\lambda_r^{(d)} + \alpha$ during each spin. On a rectangular grid (plate Carree projection) its representative point will describe a nearly sinusoidal curve with an amplitude equal to α and a phase that changes gradually from one spin to the next (see Fig. 20). Thus the region of the sky explored by the detector becomes wider as the apex angle of the precession axis increases.

In the rocket's frame of reference, on the other hand, the detector's axis is fixed, while the vector pointing to a celestial object moves in azimuth with slightly varying angular velocity, while changing its elevation between $\lambda_p^{(o)} - \alpha$ and $\lambda_p^{(o)} + \alpha$ during the precession cycle. On a rectangular grid, the representative point of the celestial object moves along a nearly horizontal line, which oscillates up and down filling the band between $\lambda_p^{(o)} - \alpha$ and $\lambda_p^{(o)} + \alpha$ (see Fig. 21). The object will be seen by a given detector if the latter's field of view overlaps this band.

(a) Despun rockets with long spin periods (~ 5 sec), long precession periods (~ 300 sec), and large precession cone angles

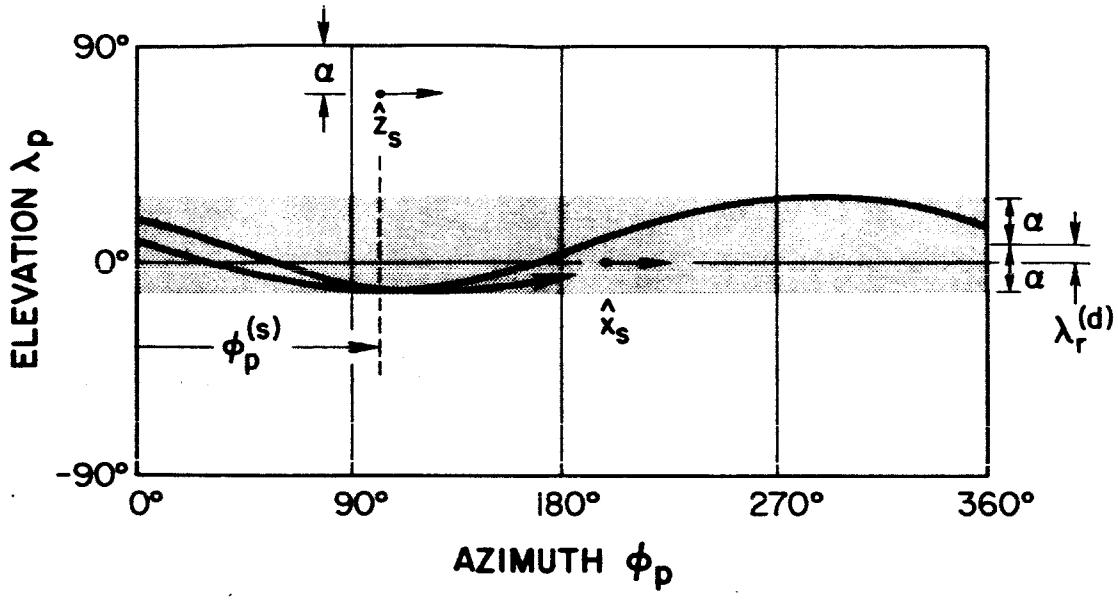


Fig. 20 Motion of detector axis in the precession frame of reference. Shaded region represents the band covered by the detector axis during an entire precession cycle. The solid curve within the shaded region is the path of the detector axis during about 1.5 spin periods. The short arrow at z indicates the motion of the rocket axis during the same time. $\lambda_r^{(d)}$ is the elevation angle of the detector axis in the rocket frame of reference.

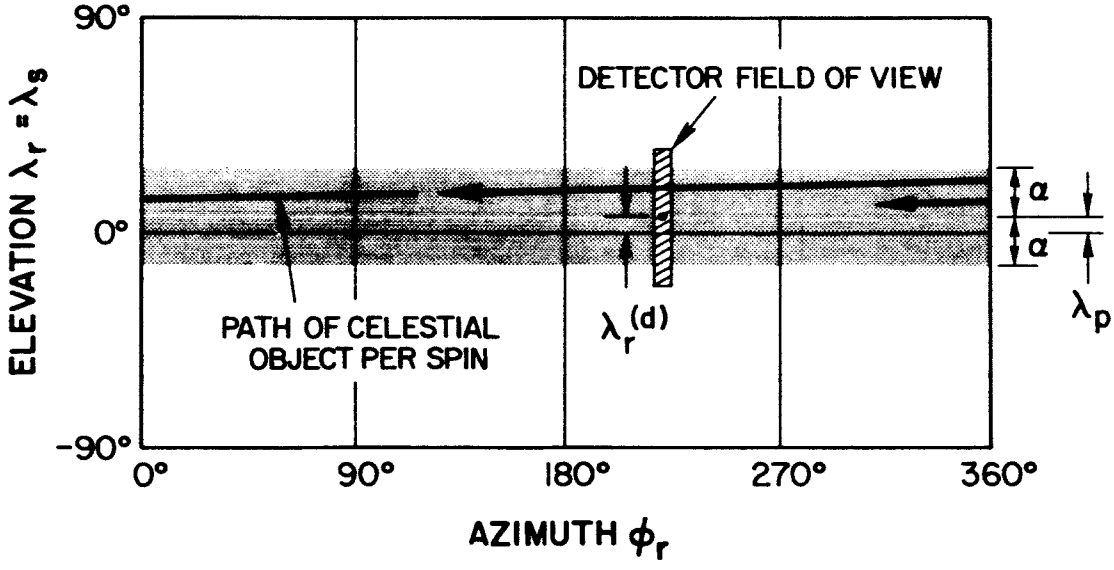


Fig. 21 Motion of a celestial object in the rocket frame of reference. Shaded portion is the region traversed by a given celestial object during the precession cycle and the solid line is the motion of the object during slightly more than one spin period.

($\alpha \gtrsim 60^{\circ}$) have been employed in the NRL experiments. The nearly sinusoidal curve traced out by the representative point of the axis of a detector carried on such a flight changes in phase by a substantial amount during each spin. Thus any source within the large region of explored sky is detected on only a few successive spins out of the entire flight. In analyzing the X-ray data from such an experiment, one searches for evidence of significant variations in the counting rate. These may show periodicities extending over several spins if the detector's field of view is large enough so that the regions swept out in successive spins overlap one another. The celestial orientations of the detector's axis when the maximum rates are recorded is, of course, established by reference to the data obtained by optical and magnetic sensors. If the field of view has a nearly circular shape, then it is possible to estimate a source's position making use of the fact that the number of counts produced by the source during one spin is a decreasing function of the minimum angular distance between the detector's axis and the source during that spin. By plotting the numbers of counts as a function of this distance, and comparing the curve thus obtained with the known angular response of the collimator, one can also evaluate the angular diameter of the source, or place an upper limit to it. Obviously the accuracy of both the position and size determinations will depend on the statistical accuracy of the data (and, therefore, on the area of the detector) as well as on the angular aperture of the collimator.

(b) A situation of a somewhat different character occurs in experiments like those of the ASE-MIT group, which have employed rockets that retain their relatively high initial spin rates ($\sim 2\ \mathrm{sec}^{-1}$), have small precession cone angles ($\alpha \lesssim 10^{\circ}$), and have precession periods that are

sufficiently short so that several complete precession cycles occur during the period of observation. In these experiments a source within the relatively small region of sky scanned by a given detector is detected on many successive spins during those portions of the several precession cycles when the elevation of the source lies within the sensitive range of the detector. In order to exploit the information about a source which is potentially available in the data it is necessary to combine the data from many spins, taking proper account of the effect of the precession motion on the periodicity. A source too weak to have a statistically significant effect on the counting rate during one spin may be detected in the combined data from many spins. From such data it is possible to obtain precise information on the sizes and locations of sources.

In order to deal with the complications caused by precession motion in the analysis of data obtained from fast and freely spinning rockets, we have found it convenient to introduce a special angular variable ψ which we call the bearing. This angle is defined by the equation

$$\psi = \phi_s + \phi_p^{(s)} + \pi/2$$

where ϕ_s is the azimuth of a given direction in the spin frame, and $\phi_p^{(s)}$ is the azimuth of the spin axis in the precession frame. If the given direction is fixed in the rocket frame, as are the directions of the axes of the various detectors, then we have $\dot{\phi}_s + \dot{\phi}_p^{(s)} = \omega_s + \omega_p$. Thus the bearing angle $\psi^{(d)}$ of a detector's axis at any given instant may be expressed as a function of time by the equation

$$\psi^{(d)} = \int_o^t (\omega_s + \omega_p)\, dt + \psi_o^{(d)}$$

where $\psi_o^{(d)}$ is the bearing angle at $t = 0$. If the given direction is that of

a celestial object (which is, of course, fixed in the precession frame) then during each precession cycle $\phi_p^{(s)}$ increases uniformly by 2π while $\phi_s^{(o)}$, the spin azimuth of the object, decreases non-uniformly by 2π. Thus the bearing angle of the object $\psi^{(o)}$ varies about an average value which is, in fact, the precession azimuth of the object, i.e.

$$\psi_{av}^{(o)} = \phi_p^{(o)}$$

This is obviously true in the limit $\alpha = 0$ where $\phi_p^{(o)} = \phi_p^{(s)} + \pi/2 + \phi_s^{(o)}$ as can be seen in Figure 19. In this case we have

$$\psi^{(o)} = \phi_p^{(o)}$$

In the general case when $\alpha \neq 0$, one can show that the difference $\psi^{(o)} - \phi_p^{(o)}$ is an antisymmetric function of the difference $\phi_p^{(o)} - \phi_p^{(s)}$. Since $\psi^{(o)} = \phi_p^{(o)}$ when this difference is zero (or π), the average value must be equal to $\phi_p^{(o)}$ as previously stated.

Under the assumption of a rigid, freely-spinning rocket, $(\omega_s + \omega_p)$ is a constant so that the bearing angle of a detector's axis, $\psi^{(d)}$, increases linearly by 2π during a time interval equal to $2\pi/(\omega_s + \omega_p)$. The transit times of a celestial object through the meridian plane of a detector are determined by the intersections of the heavy solid curve, representing the time dependence of the bearing angle $\psi^{(o)}$ of a celestial object, with the saw-tooth solid line representing the time variation of the bearing angle $\psi^{(d)}$ of the detector's axis (see Fig. 22).

The explicit expression for the bearing angle of a given unit vector $\vec{r}$ fixed in the precession frame in terms of α and $\phi_p^{(s)}$ is rather cumbersome. It may be expressed implicitly, however, in the following way which is particularly well suited to computer calculations. The components r_{si} in

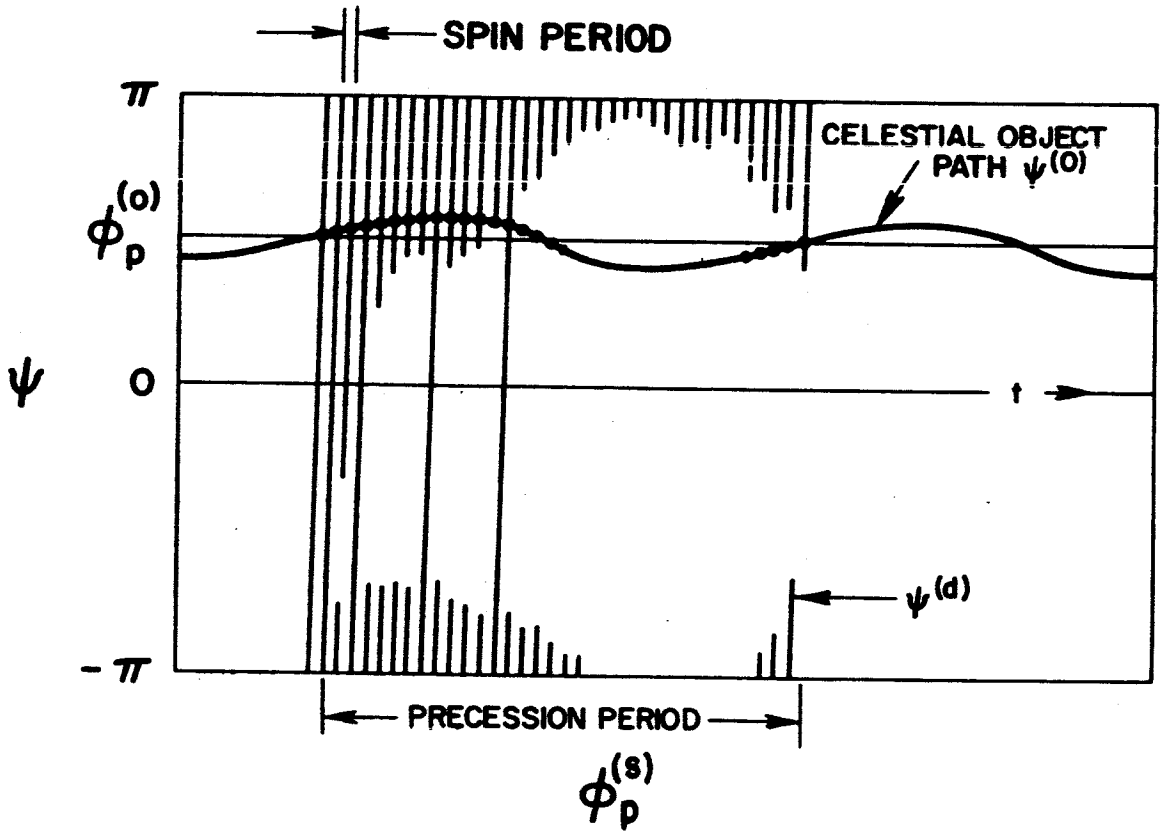


Fig. 22 Time variation of the bearing angle of a celestial object (heavy solid line) and of the X-ray detector axis (light solid line) during several precession cycles. Average bearing angle of the object is its precession azimuth $\phi_p^{(o)}$.

the spin frame are related to the components r_{pk} in the precession frame by the matrix equation

$$r_{si} = T_{ij}^{(2)} \; T_{jk}^{(1)} \; r_{pk} \; -$$

where

$$r_{pk} = \begin{Vmatrix} (\cos \lambda_p & \cos \phi_p) \\ (\cos \lambda_p & \sin \phi_p) \\ (\sin \lambda_p & \end{Vmatrix}$$

$$T_{jk}^{(1)} = \begin{Vmatrix} [\cos (\phi_p^{(s)} + \pi/2)] & [\sin (\phi_p^{(s)} + \pi/2)] & 0 \\ [-\sin (\phi_p^{(s)} + \pi/2)] & [\cos (\phi_p^{(s)} + \pi/2)] & 0 \\ 0 & 0 & 1 \end{Vmatrix}$$

$$T_{ij}^{(2)} = \begin{Vmatrix} 1 & 0 & 0 \\ 0 & \cos \alpha & \sin \alpha \\ 0 & -\sin \alpha & \cos \alpha \end{Vmatrix}$$

The orthogonal transformation matrices $T_{jk}^{(1)}$ and $T_{ij}^{(2)}$ correspond to the two rotations required to bring the precession frame into coincidence with the spin frame, namely, a positive rotation by the angle $\phi_p + \pi/2$ about the $\hat{z}_p$ axis, followed by a positive rotation by the angle α about the $\hat{x}_s$ axis. The bearing angle can be expressed in terms of the transformed components of $\vec{r}$ by the equation

$$\psi^{(o)} = \frac{r_{s2}}{|r_{s2}|} \arccos \left(r_{s1} / \sqrt{r_{si}^2 + r_{s2}^2}\right) + \phi_p^{(s)} + \pi/2.$$

Turning now to the actual analysis of the data, the first step is to find an approximate value for $\omega_p + \omega_s$, the bearing angular velocity of the detector axes. To do this we search for a sequence of nearly periodic signals from one of the sensors (optical, X-ray or magnetic). The average value of the interval between successive signals in a sequence divided into 2π is then used as the first approximation to $\omega_p + \omega_s$.

The second step is the computation of the values of the bearing $\psi^{(d)}$ relative to the bearing $\psi_o^{(d)}$ at some given arbitrary time of the detector axis at the instants when signals were observed. This is done using the formula

$$\psi^{(d)} - \psi_o^{(d)} = \int_{t_o}^{t} (\omega_s + \omega_p)\, dt$$

with $\omega_s + \omega_p$ initially taken as constant and equal to the approximate value of this quantity determined as described above. In order to obtain a second approximation to $\omega_p + \omega_s$ we construct a plot in which each signal is indicated by a mark with the coordinates $(\psi^{(d)} - \psi_o^{(d)}, t)$. Recurrent signals from a celestial object give rise to a trail of marks advancing in t, and drifting gradually one way or another in $\psi^{(d)} - \psi_o^{(d)}$, depending on the error in $\omega_s + \omega_p$. From the trends revealed by this plot we determine an improved value of $\omega_s + \omega_p$ which reduces the long term drift in the relative bearing. It turns out, however, that sounding rockets with liquid fuels are not perfectly rigid bodies after cutoff. Thus $\omega_s + \omega_p$ generally varies significantly during an experiment. To allow for this we express $\omega_s + \omega_p$ as a power series in t in the form

$$\omega_s + \omega_p = \omega_o + At + Bt^2 + \ldots$$

In practice we have found it necessary to use only the first order term in t in order to eliminate nearly all long term drift.

Of course, even after correcting the computation of the relative bearing for the long term drift of $\omega_s + \omega_p$, there remain the periodic variations in the relative bearing of a fixed source due to the precession motion. This motion, as we have seen, causes the bearing of the source to vary around its average value (which is its precession azimuth). A plot of the frequency of signals versus the relative bearing of the detector's axis will therefore show a peak whose width is greater than the spread due to the azimuthal angular resolution of the detector and the angular width of the source itself. At this point the periodic precession variation of $\psi^{(o)}$ as well as any residual long term drift in $\omega_s + \omega_p$ can be compensated by adding an empirically determined and smoothly varying quantity to the calculated values of $\psi^{(d)}$. A plot of this compensated quantity, which is essentially $\psi^{(d)} - \psi^{(o)}$, will now show a peak whose width is as narrow as the limit set by the resolution of the detector and the angular width of the object. When this method, which we call "self-synchronization", was applied to the ScoX-1 peak in Figure 29, the width of the modified peak was found to be consistent with the assumption that the angular width of ScoX-1 is less than 20 arc minutes.

It is worth noting that the average over an integral number of precession cycles of the bearing of the signals in a peak is a correct measure of the precession azimuth of the corresponding celestial object even if the object passes in and out of the detector's elevation range. This is true because the deviation of $\psi^{(o)}$ from $\phi_p^{(o)}$ when the object crosses a given rocket elevation in one direction is just the negative of the deviation when it crosses in the other direction. Thus the average relative bearing of the object during the time when it is within the detector's elevation range, plus the phase $\psi_o^{(d)}$, which is yet to be determined, is, in fact, the precession azimuth of the object.

The third step in the analysis is the determination of the precession motion and the orientation of the precession axis in the celestial frame of reference. The celestial orientation of the precession frame of reference is determined from the star sensor data. These data consist of the transit times of various stars whose identity is initially unknown. Selecting data from portions of the precession cycle when signals from several stars are observed in each rocket rotation, we determine the relative bearings of the unknown stars. With the aid of a star catalogue and an appropriate computer program we then search for a spin axis direction in the celestial frame which would cause the star sensor to sweep over a combination of stars with relative bearings that match the ones observed. In this way the stars which caused the observed signals are unambiguously identified, and first approximations to the spin orientations at several points around the precession cycle are obtained.

As the spin axis precesses, the rocket elevation of a given star varies so that the amplitude of its signal is modulated according to the response function of the star sensor. This modulation may be a prolonged appearance or disappearance of a periodic signal as the star crosses one boundary or the other of the elevation range of the sensor. It may be a momentary disappearance as it crosses a masked interval in the middle of the sensitive elevation range. In any event, the sequence of times at which significant modulation events occur in the amplitudes of the star signals is determined by the response function of the sensor and by the parameters of the precession motion: i.e. the celestial orientation of the precession axis, defined by $\alpha_c^{(p)}$ and $\delta_c^{(p)}$, the precession angular velocity ω_p, and the opening angle α of the precession cone. Only a particular combination of the precession parameters will lead to a predicted sequence of times of modulation events that matches the one observed. In practice we search for this combination with the aid of a computer. By successive approximations we obtain a set of parameters which minimizes

the sum of the squared deviations between the predicted and observed times, and in this way we establish the celestial orientation of the precession frame and the precession cone angle. Any object whose precession azimuth and elevation is known can now be located in the celestial frame by a simple transformation.

The fourth step is the determination of the precession azimuths of the X-ray sources. Already, by comparing the bearing distribution plots for the X-ray detector and star sensor data described earlier, the relative average bearings (i.e. relative precession azimuths) of the X-ray sources and the various stars can be established. Now that the stars are identified, the absolute average bearings of the X-ray sources can be determined, and these are the precession azimuths.

The fifth step is the determination of the precession elevations of the sources. This can be accomplished, in principle, by measuring the variation of a source's bearing during the precession cycle, since, as previously noted, the amplitude of this variation depends on α and $\lambda_p^{(o)}$. This method amounts to a kind of "triangulation" of the source with a base line equal to twice the opening angle α of the precession cone. For the small values of α that occurred in the ASE-MIT experiments, the accuracy of this method is not very high.

A more accurate method for the determination of $\lambda_p^{(o)}$ is based on an analysis of the variation in the counting rate from a source which is caused by the periodic change in the elevation of the source in the rocket frame. By inspection of the bearing distribution we select an interval of bearing within which essentially all of the counts from the source occur. For each count recorded in this interval we compute the quantity $\ell = \lambda_r^{(d)} - \alpha \cos (\phi_p^{(s)} - \phi_p^{(o)})$ where $\phi_p^{(o)}$ is the precession azimuth of the source as previously determined, and $\lambda_r^{(d)}$ is the rocket elevation of the

detector axis. If α and $\lambda_p^{(d)}$ is sufficiently small, then to a good approximation $\ell = \lambda_p^{(d)}$ when $\phi_p^{(d)} = \phi_p^{(o)}$; i.e. at the moment when the source transits the meridian plane of the detector in the precession frame (see Eq. 5). Moreover, if $\lambda_p^{(o)}$ lies with range from $\lambda_r^{(d)} - \alpha$ to $\lambda_r^{(d)} + \alpha$, then at some time during the precession cycle the detector axis sweeps across the source. At this time $\lambda_r^{(o)} = \lambda_r^{(d)}$, $\ell = \lambda_p^{(o)}$ (see Eq. 5), and therefore the counting rate plotted against ℓ shows a maximum for a value of ℓ equal to the precession elevation of the source. An example of such a distribution is shown in Fig. 30. When λ_p does not lie in the range from $\lambda_r^{(d)} - \alpha$ to $\lambda_r^{(d)} + \alpha$, one can still calculate the expected variation of the counting rate as a function of ℓ from the known response function of the detector, and for any assumed value of $\lambda_p^{(o)}$. One can then adjust $\lambda_p^{(o)}$ to obtain the best fit of the computed variation to the observed one, and in this manner one can obtain an estimate of the precession elevation of the source.

In the case of a detector with a modulation collimator whose response maxima are separated by an angle smaller than 2α, the plot of counting versus ℓ will show several maxima at values of ℓ given approximately by the equation

$$\ell_n = \lambda_p^{(o)} \pm \arctan(na).$$

where a is determined by the dimensions of the collimator. An example of such a distribution is shown in Fig. 31.

4.0 OBSERVATIONAL RESULTS

4.1 The Crab Nebula

The source whose coordinates and angular dimensions are best known is that coincident with the Crab Nebula. As already mentioned, the information concerning this source comes mainly from the observation of the occultation of the Crab Nebula by the Moon performed by the NRL group (which named the source Tau XR-1).[4] The rocket was attitude -

controlled and carried two X-ray detectors which acquired the X-ray source 150 sec. after launch and observed it for 240 sec. thereafter, during which time the edge of the Moon swept across the Crab Nebula in the manner shown in Fig. 23. The counting rates of the two detectors, and their sum are plotted as functions of time in Fig. 24. Shown in the same figure is the time derivative of the total counting rate, which represents the distribution of the X-ray source in the direction perpendicular to the advancing edge of the Moon. From these results, the authors concluded that the angular diameter of the X-ray source was about 1 arc minute, and that its center was close to the center of the visible nebula.

4.2 The Sources Near the Galactic Center

Let us consider next the complex of sources within 25° of the galactic center which includes the source in Scorpio, named ScoX-1 by the ASE-MIT group, the first X-ray source to be discovered and the strongest detected thus far.

Figure 25 illustrates the determination of the position of ScoX-1 performed by the NRL group by means of a slowly-spinning rocket in April 1963.[3] The detector had a field of view about 10° full width at half maximum. The lines with arrows are traces of the detector's axis on the sky map during different spins; the numbers along these lines are counting rates. The circles are lines of equal counting rates, whose common center represents the source position.

Figure 26 shows the results of another flight carried out by the NRL group, with similar instrumentation, in June 1964.[11] Shaded segments indicate portions of scan where the X-ray counting rate was clearly above background. Circles are positions assigned by the authors to the X-ray sources held responsible for these increases in counting rate. Of the sources near the galactic center, only ScoX-1 (indicated as I) gave a clearly separate peak. The other five were unresolved and, therefore, the results concerning these sources were somewhat tentative.

In addition to the sources near the galactic center, the instruments aboard the NRL rocket detected also two clearly resolved sources in Cygnus

From Bowyer et al, Science 146 912 (1964)

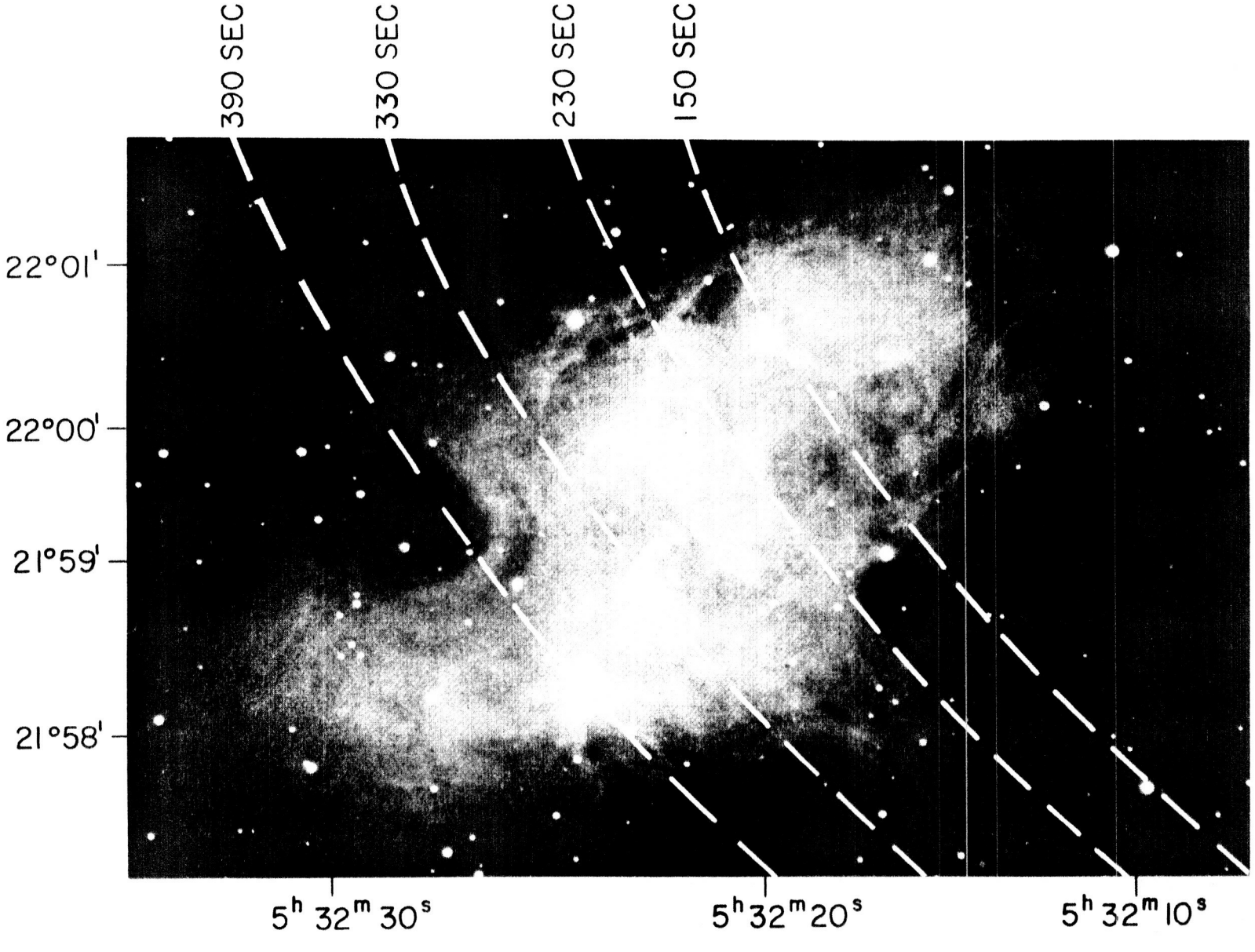


Fig. 23 Position of the edge of the Moon superimposed on a photograph of the Crab Nebula during NRL rocket flight. The maximum rate of change of the observed counting rate from the X-ray detector occurred at 230 sec; thus the centroid of the X-ray source distribution lies along the dashed line marked 230 sec.

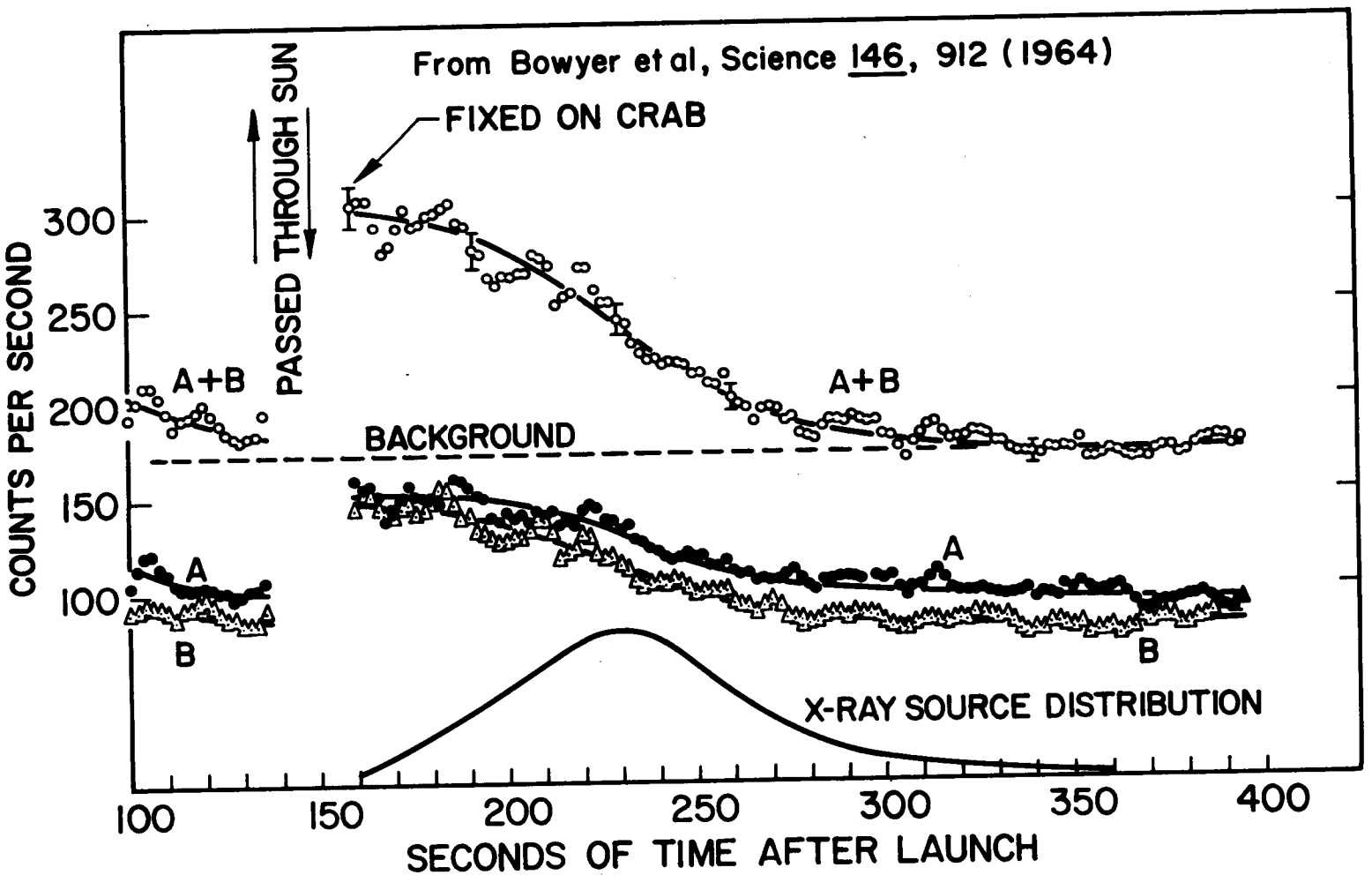


Fig. 24 Counting rates of the X-ray detectors A and B during the NRL rocket flight observing the occultation of the Crab Nebula by the Moon. The solid curve at the bottom is minus the time derivative of the A and B counting rate.

From Bowyer et al, Nature 201, 1307 (1964)

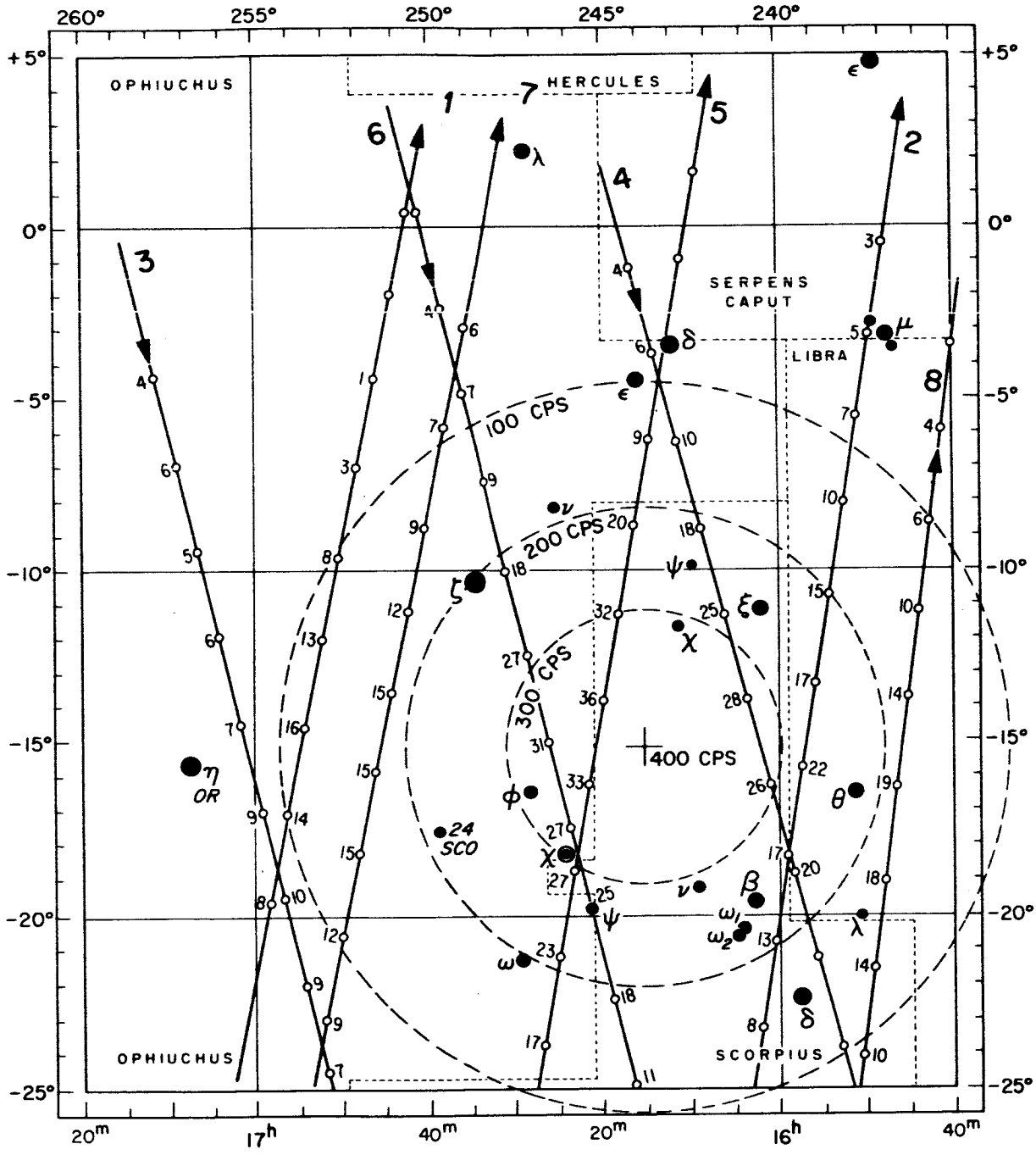


Fig. 25 Observation of the X-ray source in Scorpio by the NRL group. Solid curves show motion of the detector axis during successive passes over the region of the sky containing the source. Dashed circles are contour of equal counting rates consistent with observed counting rates. The centroid of these contours gives the best location of the source.

From Bowyer et al, Science 147 394 (1965)

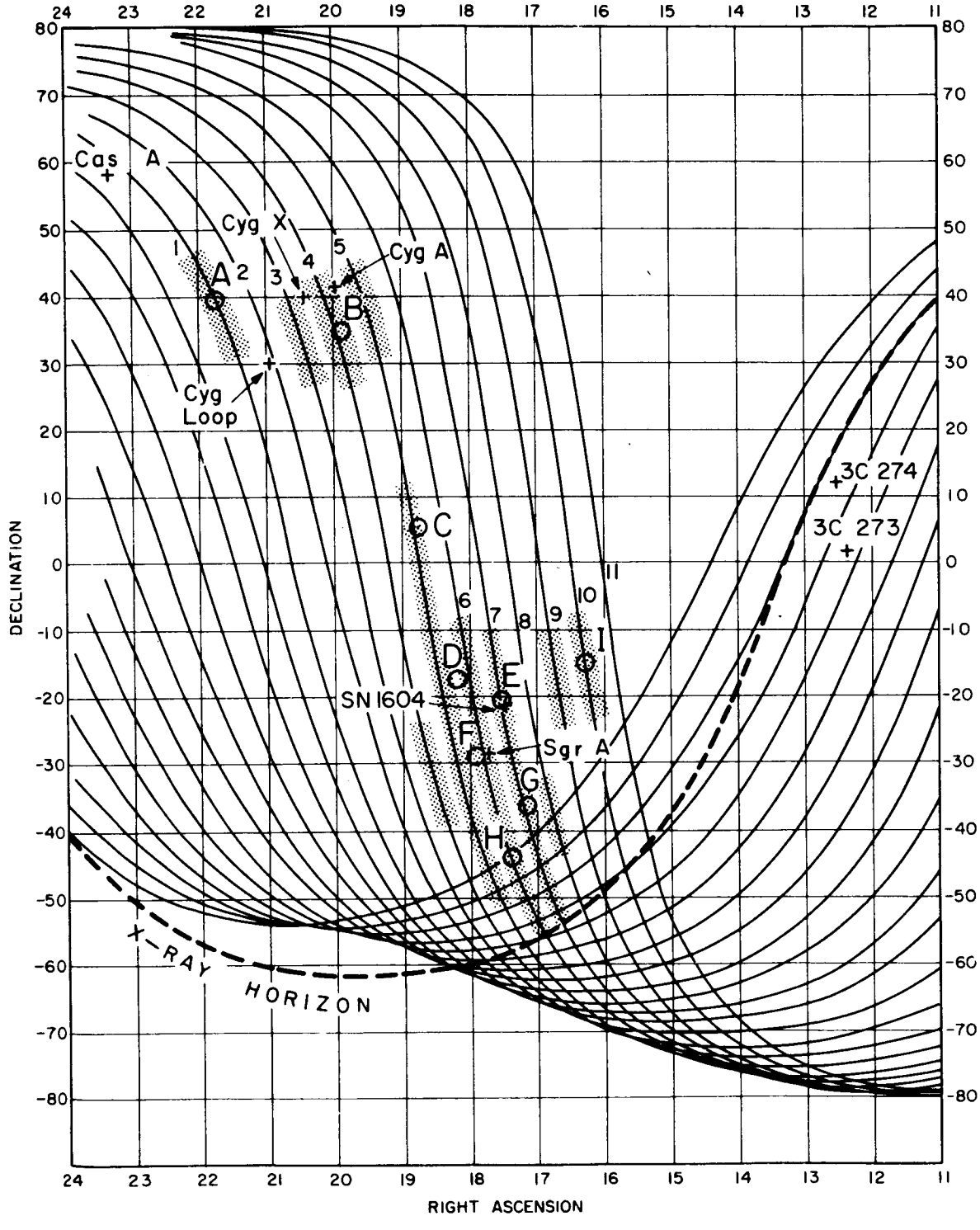


Fig. 26 Locations of X-ray sources observed during an NRL rocket flight. Solid curves represent the path of the detector axis during the flight. Shaded regions indicate times when excess counting rates were observed and circles indicate estimates of source locations.

(A and B in Fig. 26), and one unresolved source in Serpens. We shall return to these observations later.

Accurate data for some of the X-ray sources appearing in the region of the sky near the galactic center were obtained by the ASE-MIT group with a rapidly spinning rocket flown in October 1964.[12] The rocket carried three banks of Geiger counters provided with collimators having fields of view in the shape of narrow slits (GV10, GH0, GH20) and one bank of Geiger counters provided with a modulation collimator. Figure 27 shows the fields of view of these detectors and of the star sensors in the frame of reference of the spinning rocket. Figure 28 shows the regions of the sky explored by the three detectors with narrow-slit collimators, and the positions of three sources, clearly identified by these observations. One is ScoX-1; the second lies also in the constellation Scorpius and is denoted as ScoX-2; the third lies in Sagittarius and is denoted as Sgr X-1.

Let us discuss in more detail the observational evidence obtained in these experiments. Consider first the results of counter GV10, whose direction of scan was perpendicular to the long side of the collimator's slit. Figure 29 shows the bearing angle distribution of the counts with respect to β-Ceti. The sharp maximum at A is due to ScoX-1; it affords an accurate determination of the azimuth of this source in the precession frame of reference placing it on the arc A in Fig. 28. Moreover, the variation of the counting rate due to ScoX-1 during the precession cycle shows that the detector's axis came closest to ScoX-1 when its elevation in the precession frame was a maximum. This observation places a lower bound to the elevation of ScoX-1, as indicated by the dotted line in Fig. 28. The smaller and broader maximum between B and C in Fig. 29 is due to a number of unresolved sources, including Sgr X-1, ScoX-2 and probably other sources near the galactic plane. These sources must lie in the cross-hatched region between the arcs of great circles marked B and C in Fig. 28.

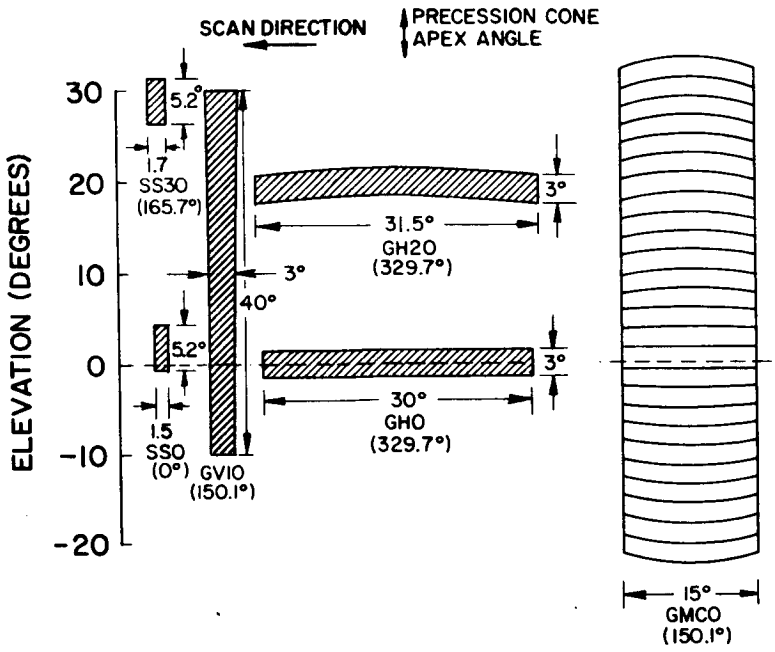


Fig. 27 Fields of view of the detectors used by the ASE-MIT group in the October 1964 rocket flight, shown on a rectangular grid plot of the rocket frame of reference. The number in parantheses below the instrument designation is the rocket azimuth of the detector axis.

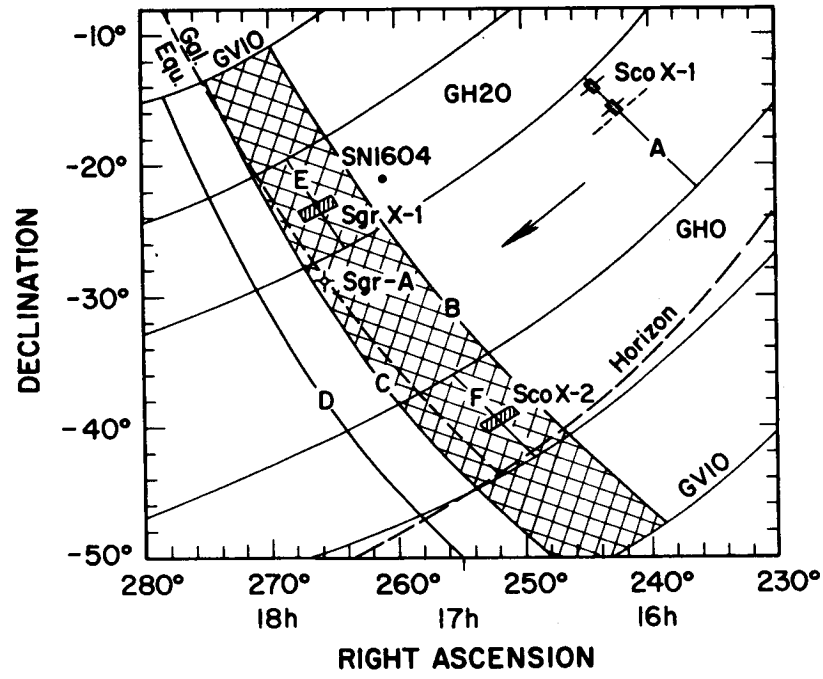


Fig. 28 X-ray source locations determined during ASE-MIT rocket flight of October 1964. The region bounded by the arcs marked by GV10 has been scanned. Sources are found to lie along the solid curves marked A, D, E, and F. The region between the curves marked B and C contains an unknown number of unresolved sources.

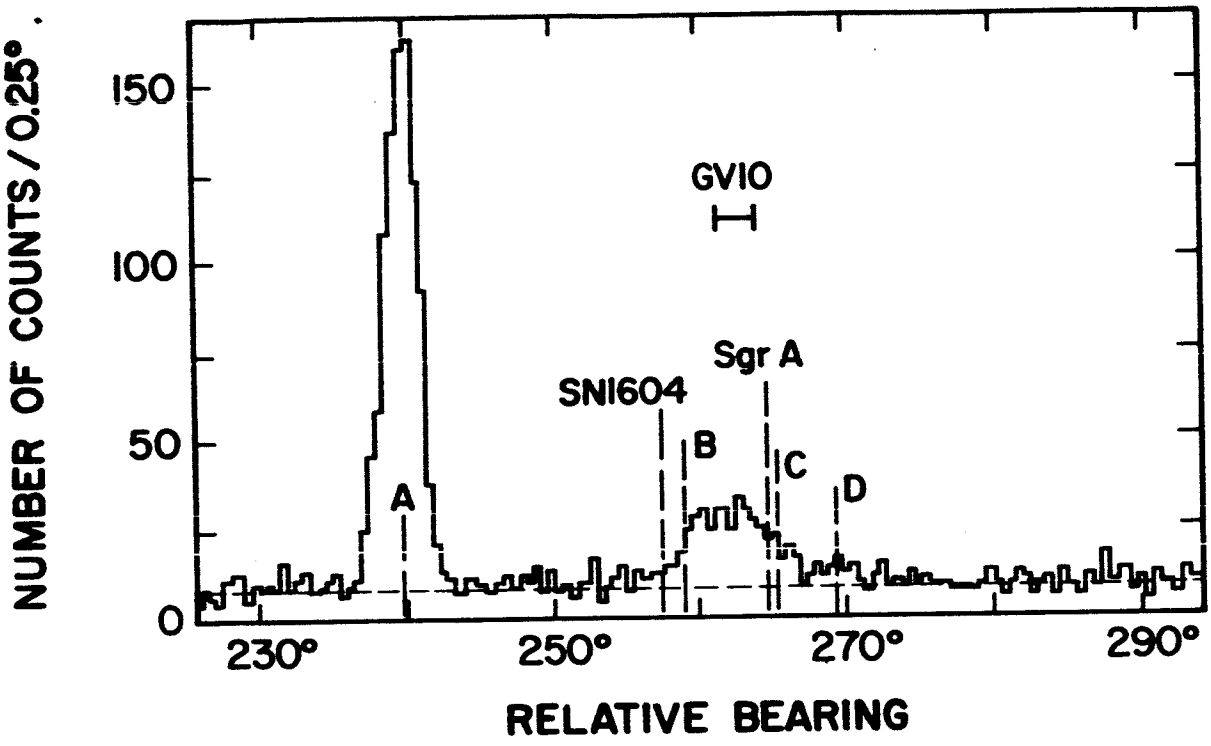


Fig. 29 Bearing angle distribution of counts observed with detector GV10 during October 1964 rocket flight. The abscissa represents the bearing angle of the detector axis with respect to complete the average bearing angle of β-Ceti. Full width of half maximum of detector response is indicated.

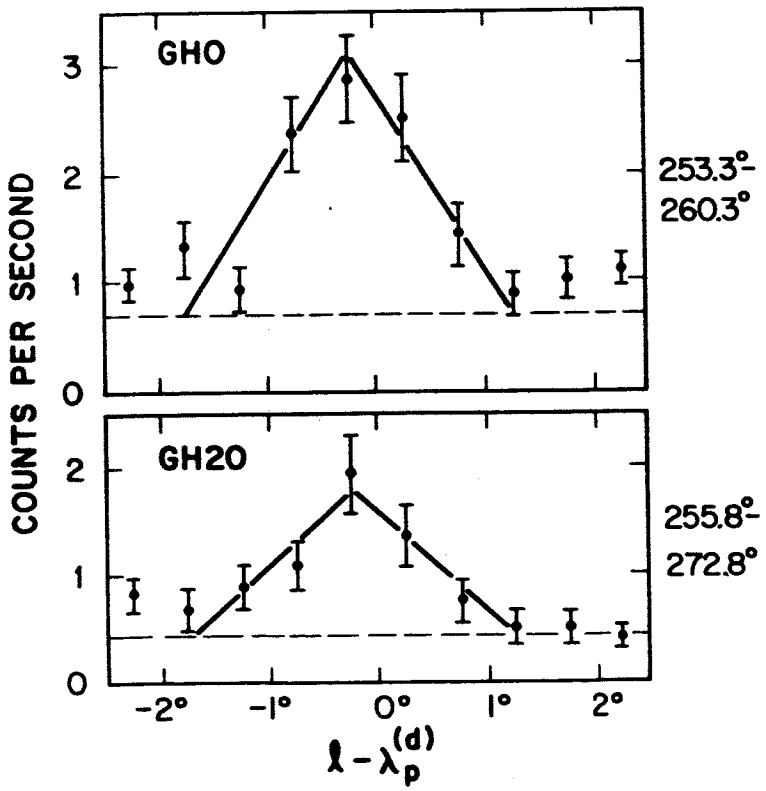


Fig. 30 The distribution in relative elevation of counting rates observed with detectors GH0 and GH20 during October 1964 rocket flight. Superimposed on the observational points are the theoretical angular responses of the detectors. The abscissa is the elevation of the detector axis in the precession frame at the moment of closest approach to the source minus the (fixed) elevation of the detector axis in the rocket frame. The bearing angle range with respect to β-Ceti is indicated at the right side of each curve.

Still another small maximum in the bearing distribution suggests the existence of a weak source along the arc marked D, although it is not clear that D is separate from the source region between B and C.

Consider next the results of counter banks GH0 and GH20. Neither of these counters saw ScoX-1. The fact that this source never entered the field of view of GH20 further restricts the possible range of elevation angles for ScoX-1, placing it below the region explored by the detector (see Fig. 28).

The curves giving the bearing angle distributions of counts recorded by both GH0 and GH20 had maxima, indicating the presence of sources lying within the bands scanned by the two detectors, and belonging to the source complex between the great circles B and C detected by GV10. The positions of the maxima determine the azimuthal angles of the sources in the precession frame, placing the sources along the arcs of great circle marked E and F in Fig. 28. Because the long dimensions of the slits representing the fields of view are in the direction of the scan, the maxima are rather flat and the azimuth determinations provided by counters GH0 and GH20 are not as precise as those provided by counter GV10. On the other hand, the narrow dimensions of the slits in the direction perpendicular to the scan affords an accurate determination of the elevation angles of the two sources in the precession frame. To obtain this information, appropriate "windows" were chosen around the azimuths of the sources, and the counts recorded within these windows, at various phases of the precession cycle, were plotted against the quantity $\ell - \lambda_r^{(d)}$ (see Section 3.2) which is approximately the relative elevation of the detector's axis at the center of the window. The results for counters GH0 and GH20 are shown by the graphs in Fig. 30. In both graphs, the counting rate is a maximum near the middle of the precession cycle, i.e., when the elevation of the detector's axis in the precession frame is nearly equal to its elevation in the rocket's frame. Thus, Sgr X-1 lies

near the center of the band scanned by GH20 and ScoX-2 lies near the center of the band scanned by GH0.

Consider, finally, the results of counter bank GMC0 provided with a modulation collimator of about 30 arc minutes resolution. Figure 31 shows the variation of its counting rate due to ScoX-1 during the precession cycle. A previous experiment with a modulation collimator of higher resolution had shown that the angular dimension of ScoX-1 was less than 7 arc minutes.[13] The completeness of the modulation observed with the present detector is entirely consistent with this result. Moreover, the position of the maxima makes it possible to place ScoX-1 on one of the circles of constant elevation corresponding to the transmission maxima of the modulation collimator at the time when a maximum of the counting rate is observed. Two of these circles fall between the limits of elevation previously determined, thus giving for ScoX-1 the two possible locations shown in Fig. 28.

Table I lists the most likely positions of ScoX-1, ScoX-2 and Sgr X-1, as obtained from the observations just described.

Data relative to the same region of the sky were also obtained by the Lockheed group, by means of an attitude controlled rocket flown in October 1964.[14] The rocket carried three detectors with collimators having fields of view in the shape of narrow slits, whose long dimensions were arranged at different angles to the rocket's axis. Thus, from the relative delay between the transit times of a given source through these fields of view, it was possible to obtain information concerning the elevation of the source in the rocket's frame of reference. The rocket was programmed to execute four different scans during its flight. Figure 32 shows the arcs traced on the sky by the normals to the detectors during these scans; the rectangles at the beginning of scan 1 show the fields of view of the three detectors, denoted as T(top), C (center), B(bottom).

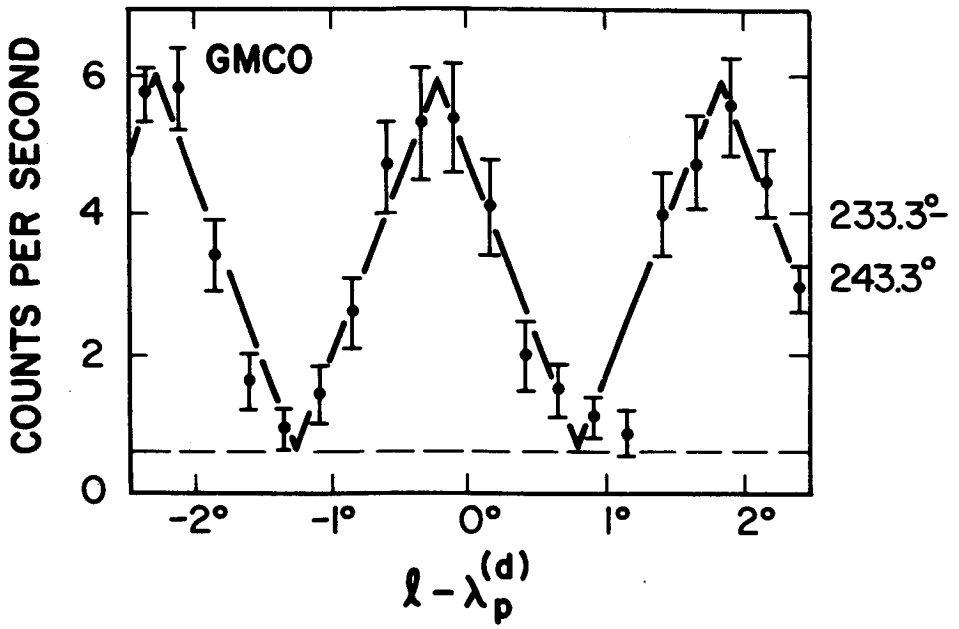


Fig. 31 Distribution in relative elevation of the counting rates from ScoX-1 observed with detector GMCO which was provided with a modulation collimator. Superimposed on the observational points is the theoretical angular response of the collimator.

SOURCE	RIGHT ASCENSION	DECLINATION
Sco X-1	$16^h 12^m \pm 2^m$ $16^h 19^m \pm 2^m$	$-15.6° \pm 0.5°$ $-14.0° \pm 0.5°$
Sco X-2	$16^h 50^m \pm 7^m$	$-39.6° \pm 0.9°$
Sgr X-1	$17^h 44^m \pm 7^m$	$-23.2° \pm 0.9°$

Table I X-ray Source Locations Determined During October 1964 Rocket Flight.

From Fisher et al, Preprint (1965)

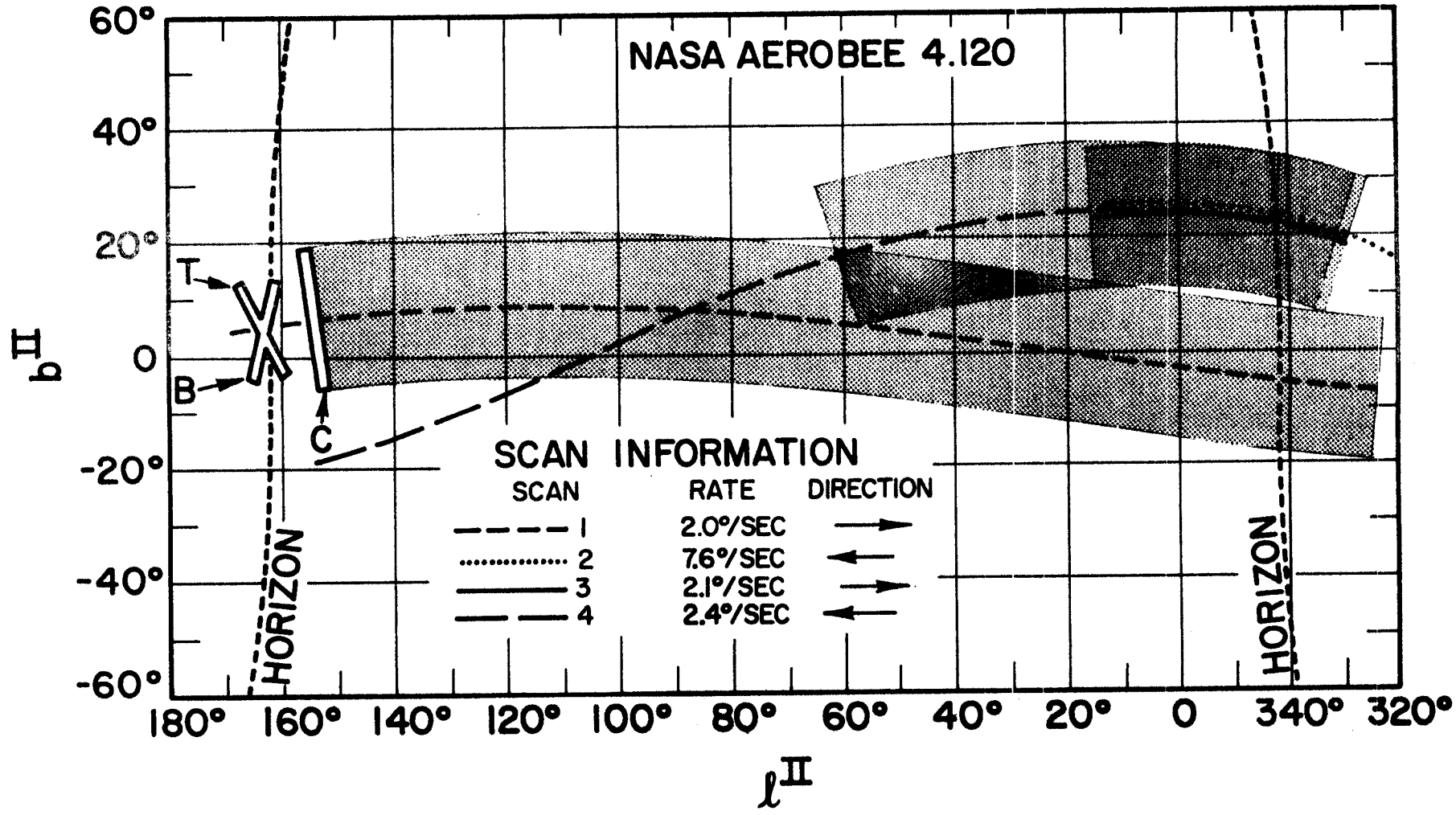


Fig. 32 Traces of detector axes during Lockheed rocket flight. Rocket was provided with attitude control.

The shaded areas indicate the bands scanned by detector C.

ScoX-1 was detected during scans #2, 3, 4. All three counters T, C, and B gave useful data during the two slower scans (#3 and 4). They provided the following determination for the position of this source:

right ascension:	$16^h 14^m \pm 1^m$
declination:	$-15^\circ\ 36' \pm 15'$

Only counter C provided useful data during scan #1, which ran along the galactic equator. The counting rate went through several maxima, indicating the existence of a number of sources. However, only the azimuthal angles of these sources in the rocket's frame of reference could be determined. The arcs of great circle corresponding to the sources near the galactic center are shown in Fig. 33 as narrow bands having a width equal to the experimental uncertainty in the angular measurement.

In Fig. 34 the results of the NRL group, the ASE-MIT group and the Lockheed group are summarized and compared. Concerning the sources near the Galactic center, we note the following:

(a) Both alternate positions for ScoX-1 found by the ASE-MIT group fall within the circle of uncertainty of the determination made by the NRL group. One of them is consistent with the position given by the Lockheed group. As already noted, we know from the results of the ASE-MIT group that the angular size of ScoX-1 is less than 7 arc minutes.

(b) The position for Sgr X-1, as determined by the ASE-MIT group, is about 1° from the arc of the great circle corresponding to one of the sources found by the Lockheed group. This discrepancy may be accounted for by experimental errors; thus, the sources observed by the two groups may be the same. However, Sgr X-1 does not lie within the circle of uncertainty of any of the sources found by the NRL group. The closest NRL source is OphXR-1, whose center

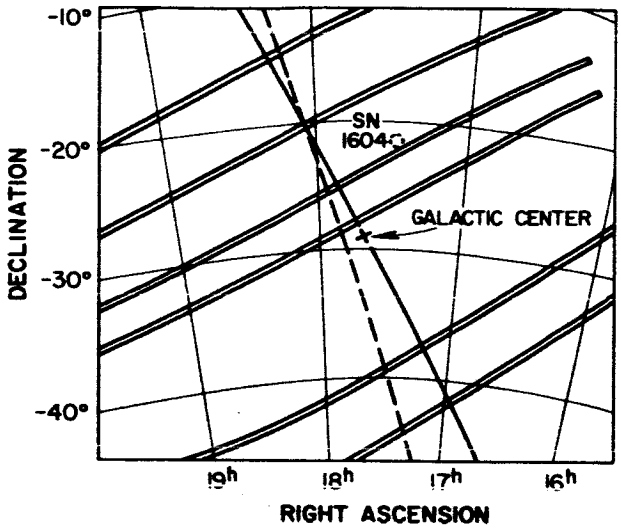


Fig. 33 X-ray source locations in the vicinity of the galactic center determined during Lockheed rocket flight. Dashed line is the path of the detector axis and the narrow bands normal to this line represent regions of the sky containing X-ray sources.

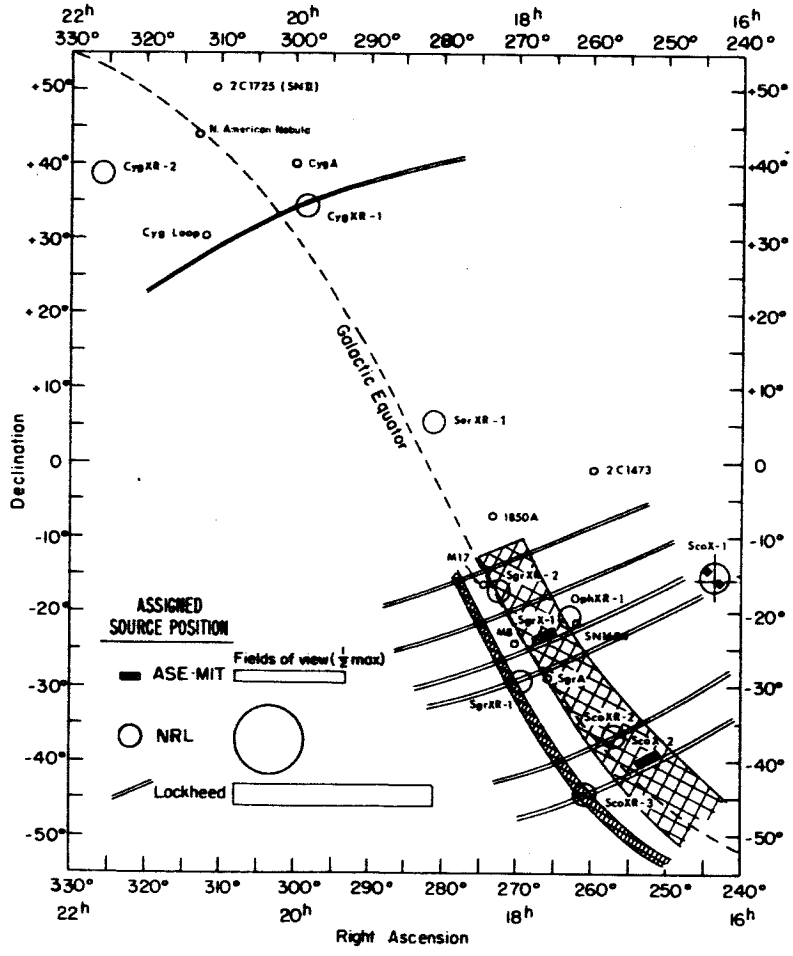


Fig. 34 X-ray source locations as determined during three 1964 rocket flights. ASE-MIT locations have been given in Figure 29: NRL locations have been given in Figure 23, and Lockheed locations have been given in Figure 34.

lies 5^{o} from the ASE-MIT position of Sgr X-1. The existence of a source in this position is not consistent with the ASE-MIT data.

(c) SgrX-1 is 5^{o} from the Kepler supernova remnant SN 1604. Thus, the ASE-MIT observation rules out the existence of a detectable X-ray source in this position, and the tentative identification by the NRL group of their OphXR-1 source with SN 1604 [11] does not seem to be correct.

(d) The position for ScoX-2, as determined by the ASE-MIT group, is about 1^{o} from the arc of great circle corresponding to one of the sources seen by the Lockheed group. Again, the discrepancy may be due to experimental errors, and the sources seen by the two groups may be the same. On the other hand, ScoX-2 lies about 5^{o} from the nearest source reported by the NRL group (ScoXR-2); the ASE-MIT results are consistent with the existence of this nearest source ScoXR-2, since the region containing it was not scanned. However, the region containing the other nearby NRL source ScoXR-3 was scanned by the same detectors which observed ScoX-2. The NRL and ASE-MIT results can be reconciled only if ScoXR-3 and ScoX-2 are two separate sources lying within the same 4^{o} band of galactic longitude and ScoXR-3 is substantially weaker than ScoX-2. But, then the question remains as to why no evidence of a source at the position of ScoX-2 was found in the NRL data.

(e) The NRL source SgrXR-2 lies half way between the arcs of great circle about 12^{o} apart, on which the Lockheed group located two separate sources. Possibly the peak of counting rate in the NRL observations resulted from the combined effects of these two sources.

(f) In addition to these two sources and to the ASE-MIT sources SgrX-1 and ScoX-2, the Lockheed results indicate the existence of at least two other sources near the galactic center. One of them may coincide with NRL source SgrXR-1. It appears difficult to identify the other with any of the NRL sources, unless there is a sizeable error in the position of ScoXR-2, quoted by NRL.

(g) SgrA, the radio center of the Galaxy, is at most a weak X-ray source compared with the other sources nearby.

4.3 Other Sources

Early observations by the ASE-MIT group suggested the presence of X-ray sources in the general region of Cygnus.[1, 2] As noted previously, the NRL group detected two sources, Cyg XR-1 and Cyg XR-2 in this region (see Fig. 34). One of them (Cyg XR-2) lies near the arc of great circle where also the Lockheed group located an X-ray source. Cyg XR-2 was not scanned by the Lockheed group. Neither Cyg XR-1 nor Cyg XR-2 coincides with the Cygnus loop or with Cyg A.

Lastly, the NRL observations indicate the existence of a source in Serpens; a small maximum in the counting rate observed by the Lockheed group in scan #1 may be due to the same source.

4.4 Spectral Information and Flux Estimates

Some information on the spectra of the X-ray sources has been obtained from absorption measurements as well as from the pulse-height distributions observed with proportional counters and with scintillation counters. Partly because of the nature of the measurements, partly because of the limited statistical accuracy, none of the available results affords a direct determination of the spectral distribution, i.e., of the function $j(E)\,dE$ giving the energy flux of X-rays with photon energy between E and $E + dE$. Rather certain a priori assumptions had to be made on the form of the spectral function $j(E)$; the experimental results

could then be used to compute the free parameters entering in the expressions for j (E), and, in some cases, to rule out certain types of spectral functions.

The spectral functions usually considered are:

Power Law:

$$j(E)\,dE = \text{const.}\ \frac{dE}{E^{\alpha}} \tag{9}$$

Synchrotron radiation and inverse Compton effect are likely to produce spectra of this kind.

Exponential Law:

$$j(E)\,dE = \text{const} \times \exp(-E/kT)\,dE \tag{10}$$

Spectra of this kind are characteristic of low-Z, fully ionized, optically thin, clouds containing electrons with a Maxwellian velocity distribution corresponding to a temperature T. In this case, the process responsible for the X-ray emission is bremsstrahlung. (In the presence of incompletely ionized matter with Z greater than about ten, there would be a substantial contribution from free-bound transitions, giving rise to characteristic discontinuities in the spectrum).

Planck's Law:

$$j(E)\,dE = \text{const}\ \frac{E^3\,dE}{e^{E/kT} - 1} \tag{11}$$

This law, characterizes the radiation from a black body at a surface temperature T.

4.4.1 The Crab Nebula

The NRL group in their Nov. 1964 flight observed the Crab Nebula with two X-ray counters provided with mylar windows 1/4 mil

and 1/2 mil thick respectively. The measured counting rates (2.7 and 1.6 per cm^2 sec) were consistent with a power-law spectrum of the type

$$j(E)\,dE = \text{const}\,\frac{dE}{E^{1.1}}$$

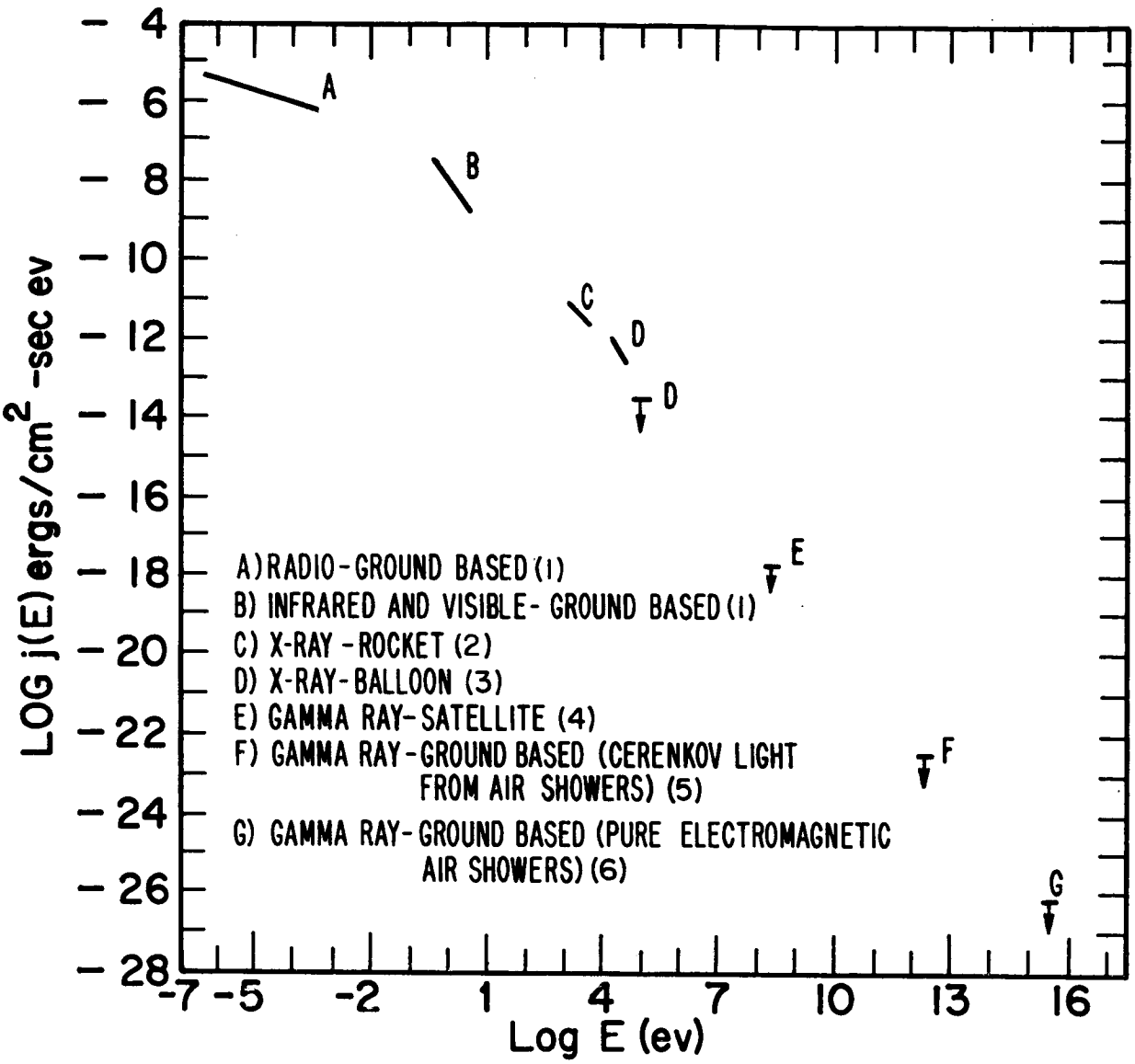
The energy range to which this result applies extends from 1.2 to 4.0 keV.

The Crab Nebula was also observed by G. Clark by means of a scintillation counter flown with a balloon in July 1964.[5] The pulses were analyzed in four channels corresponding to (nominal) energies from 15 to 28, from 28 to 42, from 42 to 62 and greater than 62 keV. The counting rates in the three lower channels (after subtraction of background and correction for atmospheric absorption) were consistent with a power-law spectrum of the type:

$$j(E)\,dE = \frac{\text{const}}{E^2}\,dE$$

The higher channel did not contain any statistically significant signal, thus placing an upper limit to the flux. This upper limit indicated an increase in the logarithmic slope of the spectrum beyond 62 keV.

The experiments described above provided information not only on the shapes of the spectrum but also on the absolute values of the flux in the two regions explored. It is thus possible to combine their results into a single spectrum extending from about 1 to about 60 keV. It is also possible to compare the results relative to this range of energy with the flux measurements in the visible and in the radio regions of the electromagnetic spectrum, and with upper limits that have been obtained by various experimenters for the flux in the γ-ray region, from about 10^8 eV to about 10^{15} eV. The results of this comparison are summarized in Fig. 35. It



(1) C. R. O'Dell, Ap. J. 136, 809 (1962)
(2) H. Friedman (unpublished)
(3) G. Clark, Phys. Rev. Letters 14, 91 (1965)
(4) W. Kraushaar, G. Clark, G. Garmire, H. Helmken, P. Higbie and M. Agogino, Ap. J. 141, 845 (1965)
(5) A. E. Chudakov, V. I. Zatespin, N. M. Nesterova and D. L. Dadiken, Proc. of Fifth Interamerican Seminar on Cosmic Rays, Vol V, pXLIV-1 (La Paz 1962)
(6) K. Suga, I. Escobar, K. Murakami, V. Domingo, Y. Toyoda, G. Clark and M. LaPointe, Proceedings of the International Conference on Cosmic Rays, Jaipur (1963)

Fig. 35 Summary of experimental data on the spectrum of electromagnetic radiation from the Crab Nebula.

appears that the spectrum of the Crab Nebula may be approximated by a single power law with exponent of about 1 from a few eV to a few 10 keV. For higher energies, however, the spectrum becomes considerably steeper. Moreover, interstellar absorption must produce a "gap" in the spectrum which has not yet been observed, but whose detailed experimental investigation promises to afford important information on the composition of interstellar gases.

4.4.2 The Sources Near the Galactic Center

Early results of the ASE-MIT group on the atmospheric attenuation of X-rays from these sources (as observed with Geiger counters) were found to be consistent with a black-body radiation corresponding to a temperature of about 10^7 ^{o}K, without, however, providing any evidence for or against the assumption that the shape of the spectrum was of this particular form. Later results for ScoX-1 by the NRL group (based again on atmospheric absorption) gave an effective temperature between 2 and 3 x 10^6 under the assumption of a black-body spectrum.[11]

Additional data were obtained in 1964-1965 by the Lockheed group, the ASE-MIT groups and the NRL group. The results of the Lockheed group refer to ScoX-1 alone. They are based on observations made with the same three proportional counters that also provided the data on the location of this source[14] (T, C, and B in Fig. 32). Counters T and C had 5-mil thick Be windows, counter B had a 0.5 mil thick Al window. All counters were 4.0 cm deep and were filled to a pressure of 83 cm Hg with a mixture of 90 percent argon and 10 percent methane. From the computed efficiency curves, the estimated energy resolution of the counters and the associated circuitry, and the observed pulse height distributions, they obtained the

energy spectrum shown in Fig. 36. No significant signal was observed in the lowest channel so that only an upper limit could be placed to the flux in the 2-4 keV interval. This upper limit appears to indicate a sharp drop-off of the spectrum below 4 keV; however, it has been reported privately that the interpretation of the measurements in the 2-4 keV channel is affected by considerable uncertainty.

The ASE group obtained spectral data in a rocket flight carried out in August 1964, as well as in the rocket flight of October 1964, mentioned previously.[15] The instrumentation of the August flight included a bank of Geiger counters with Be windows of 9.0 mg/cm^2 thickness, filled with argon to a gas thickness of 5.4 mg/cm^2. The computed efficiency curve of this counter was checked by means of the beam from a tungsten target, windowless X-ray tube operated at different voltages from 1.8 to 10 keV. The counter bank was provided with a collimator which made it possible to separate the signals received from ScoX-1 and from the sources near the galactic equator.

At launch two filters, one of 7.0 mg/cm^2 Be (F-1) and one of 1.72 mg/cm^2 Mylar (F-2) were placed in front of the counters. During the flight, first one then the other filter was removed so that the counting rates with F-1 and F-2, with F-1 alone and with no filter could be measured. Data relative to essentially a full precession cycle are available for each of the three situations; therefore, no correction is needed for a change in the average angle of incidence of the radiation during the three measurements.

The results are summarized in Table II. Note, in the first place, that the spectral information obtainable from these data refers to the energy region for about 1 to about 10 keV. Note also that there is no

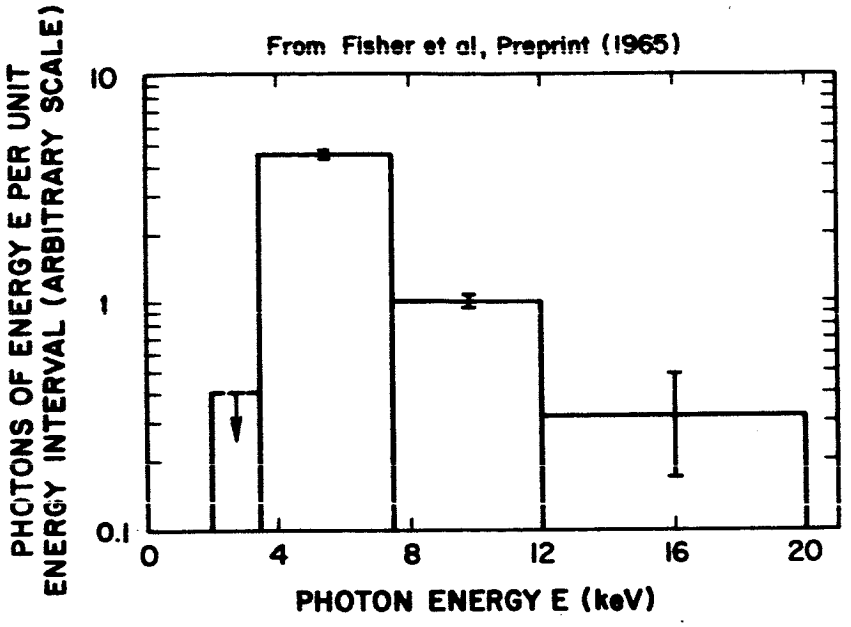


Fig. 36 Spectral distribution of X-rays from ScoX-1 as obtained from pulse height distribution of a proportional counter.

FILTER CONDITION	SOURCE REGION	COUNTING RATE MEASURED cts/sec	ATTENUATION RELATIVE TO NO FILTER
NO FILTER	SCOX-1	620 ± 20	1
F1	SCOX-1	440 ± 18	0.71 ± .04
F1 + F2	SCOX-1	350 ± 17	0.56 ± .03
NO FILTER	GAL CEN	350 ± 18	1
F1	GAL CEN	240 ± 18	0.70 ± .06
F1 + F2	GAL CEN	210 ± 15	0.62 ± .05
TYPICAL BACKGROUND RATE		30 cts/sec	

Table II Filter Absorption Data on X-ray Sources .

statistically significant difference between the attenuations observed from ScoX-1 and for the sources near the galactic plane. It turns out that the experimental results do not permit a distinction between the three types of spectra represented by Eqs. 6, 7, and 8. For each assumed type of spectrum, however, they provide a determination of the characteristic parameter, to wit:

$$\text{Power Law:} \quad \alpha = 1.1 \pm 0.3$$

$$\text{Exponential Law:} \quad T = (3.8 \pm 1.8) \times 10^{7} \ ^{\circ}K$$

$$\text{Planck's Law:} \quad T = (9.1 \pm 0.9) \times 10^{6} \ ^{\circ}K$$

The data are not consistent with the sharp dropoff of the spectrum below 4 keV tentatively indicated by the Lockheed results.

The instrumentation of the October flight included a NaI scintillation counter, provided with a suitable collimator. The pulse-height distributions observed in the two source regions, with background subtracted, are shown in Fig. 37. The cut-off below 10 keV results from the electronic threshold. Above 10 keV, the three pulse-height distributions are significantly different. The distribution observed from ScoX-1 falls below the minimum detectable level at about 18 keV (a result consistent with a cut-off of the spectrum at about 15 keV). On the other hand, the combined spectrum of the sources near the galactic plane extends to higher energies.

If we now compare the Geiger counter data obtained in the August flight with the scintillation counter data obtained in the October flight, we reach the following conclusions.

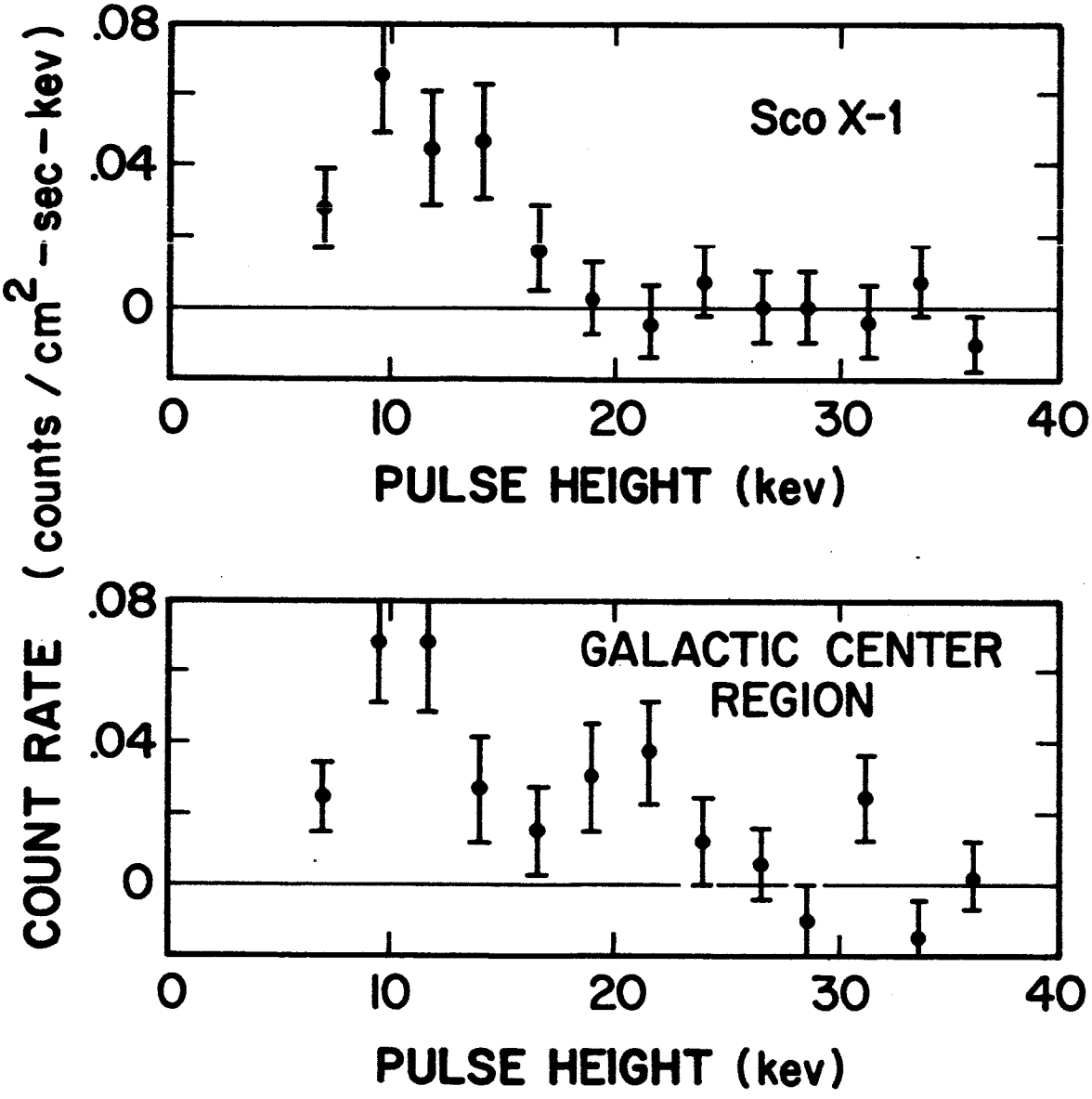


Fig. 37 Pulse height distributions of a Sodium iodide (NaI) scintillation detector, due to X-rays from ScoX-1 and from the galactic center region.

A black-body spectrum cannot fit both sets of data for either ScoX-1 or the sources near the galactic equator since such a spectrum falls off with increasing energy much more rapidly than the experimental results indicate. On the other hand, both a power law and an exponential law, with the appropriate values of the parameters mentioned previously, can account for the data obtained with the scintillation counter as well as with the Geiger counters. There is, however, evidence that the combined spectrum of the sources near the galactic equator is somewhat harder than that of ScoX-1.

The NRL group obtained spectral information on celestial X-ray sources both during the June 1964 flight,mentioned previously, and during a flight carried out in April 1965, whose results, so far, have been described only in a preliminary report.

In the June 1964 flight, ScoX-1 was observed at different altitudes during the descent of the rocket. From the measured atmospheric attenuation, it was concluded that of the flux detected at the highest altitude about 1/3 was accounted for by photons with energies above 2 keV and 2/3 by photons with energies between 1.2 and 2 keV.

In the April 1965 flight, the NRL group used four counters with the following characteristics: (1) argon filling, 1 mil mylar window; (2) argon filling, 1/4 mil mylar window; (3) neon filling, 1/4 mil mylar window; (4) helium filling, 1/4 mil mylar window. The relative counting rates of these detectors, which had very different spectral response curves, were found to be significantly different for different X-ray sources. These differences indicate differences in the spectra, ScoX-1 being one of the

sources which appeared to have the softest spectrum. The results concerning ScoX-1 could not be accounted for by a black-body spectrum. They also provided evidence for a strong increment of flux at long wavelengths, in marked disagreement with the tentative results of the Lockheed group.

To conclude this section, we summarize in Table III some estimates for the X-ray fluxes in two different spectral regions from the Crab Nebula, from ScoX-1 and from the source complex along the galactic equator, within 20° of the galactic center. Note that these estimates depend, among other things, on the assumed shapes of the spectra which are still quite uncertain.

4.4.5 Background Radiation

Since the earliest observations by the ASE-MIT group, the existence of an isotropic X-ray background has been indicated. Information on the background flux is summarized in Fig. 38. The ratios η, of the counting rate of the isotropic component to the peak Λ counting rate from ScoX-1 for various experiments are plotted versus the solid angle or corresponding to the field of view of the respective measurements. This ratio is insensitive to the experimental conditions provided the spectra of ScoX-1 and the background are essentially similar. The ratio is: $\phi_B \cdot \Lambda / \phi_{Sco}$ where ϕ_B is the background flux per unit solid angle and ϕ_{Sco} is the flux density from ScoX-1. Results of the ASE-MIT measurements show that η is roughly proportional to Λ as is expected if the background consists of X-rays distributed isotropically, except for one result which is suspected to be in error because of a partial failure of the anticoincidence counter which rejected cosmic ray particles. All other

TABLE III

INTEGRATED ENERGY FLUX FOR VARIOUS X-RAY SOURCES AND TWO DIFFERENT RANGES OF PHOTON ENERGY

Source	Spectral Range (keV)	Energy Flux $(ergs)/cm^2 sec$	Remarks
Crab	1 to 10	2×10^{-8}	NRL Data
	20 to 30	$(6 \pm 2) \times 10^{-9}$	G. Clark Balloon Data
ScoX-1	1 to 10	$(1.6 \pm 0.4) \times 10^{-7}$	ASE Geiger Counter ** Data
	20 to 30	$< 6 \times 10^{-9}$*	ASE Scintillation Counter Data
Galactic equator (including Sgr X-1 ScoX-1 and probably several additional sources.)	1 to 10	$(0.4 \pm .1) \times 10^{-7}$	ASE Geiger Counter ** Data
	20 to 30	$(16 \pm 5) \times 10^{-9}$	ASE Scintillation Counter Data

* Represents 2 σ deviation above background; no significant excess was observed.

** Assuming E^{-1} power spectrum.

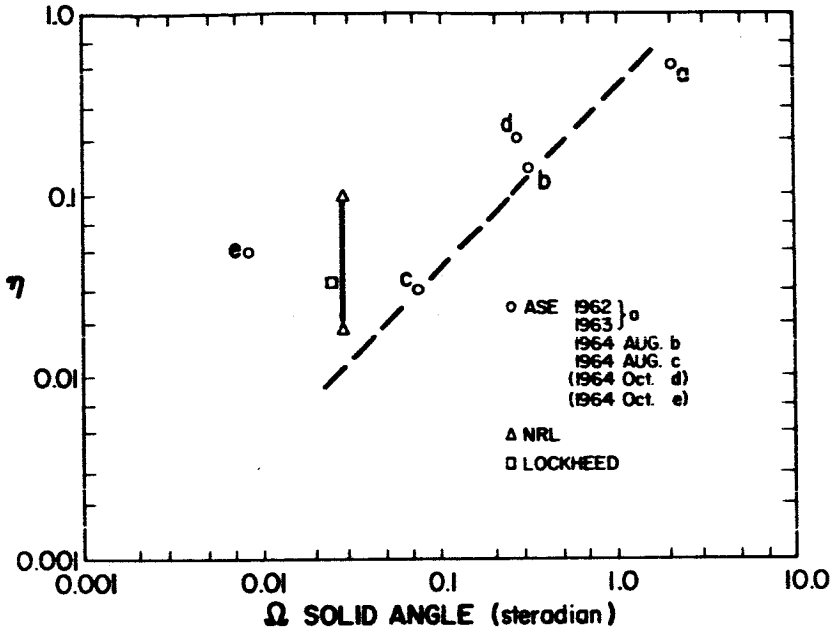


Fig. 38 Comparison of observations of the X-ray background made by various experimenters. The quantity η is the ratio of the counting rate of the background to peak counting rate of ScoX-I as observed in a given experiment.

data were obtained without an anticoincidence counter and, hence, it is understandable that they show slightly higher background fluxes. The estimate of the flux by NRL is based on the difference of the counting rate when the detector was looking upwards and downwards. The lower limit of NRL values of η is consistent with ASE-MIT results. Thus, the background component, which is proportional to the field of view of the detector, is estimated as about 6 count/(cm^2 sec ster) in the 2 ~ 8A band. If we consider the spectral response of the detector and the energy spectrum, the flux may be as much as 10 quanta/(cm^2 sec ster).

There is no evidence for anisotropy for any specific direction of galactic coordinate: e.g. say the direction of the Milky Way. Also, there is no positive indication to show a bright atmospheric horizon or any preferential local azimuth. All information indicates that a background flux of extraterrestrial X-rays truly exists; however, it cannot yet be excluded that a portion of this background originates from the Earth's magnetosphere.

ACKNOWLEDGMENTS

This work was supported in part by National Aeronautics and Space Administration under Grant NsG-386 and Contract NAS w-898, and by the United States Atomic Energy Commission under Contract AT(30-1) 2098.

REFERENCES

1. Giacconi, R., Gursky, H., Paolini, F. and Rossi, B. : 1962 Phys. Rev. Letters 9, 439.

2. Gursky, H., Giacconi, R., Paolini, F. and Rossi, B. : 1963 Phys. Rev. Letters 11, 530.

3. Bowyer, S., Byram, E. T., Chubb, T.A. and Friedman, H. : 1964 Nature 201, 1307.

4. Bowyer, S., Byram, E.T., Chubb, T.A., and Friedman, H. : 1964 Science 146, 912.

5. Clark, G.W. 1965 Phys. Rev. Letters, 14, 91.

6. Lukirskij, A.P., Rumsh, M.A., and Smirnov, L.A. : 1960 Opt. i Spekroskopija 9 , 265, 353

7. Oda, M. : 1965 Applied Optics 4, 143

8. Giacconi, R. and Rossi, B. : 1960 J.G.R. 65, 773.

9. Giacconi, R., Harmon, N., Lacey, R. F. and Szilagyi, Z.: 1965 J. Opt. Soc. Am. 55, 345

10. Giacconi, R., Reidy, W. P., Zehnpfennig, T., Lindsay, J.C. and Muney, W.A. : 1965 Astrophys. J. 142, 1274

11. Bowyer, S., Byram, E.T., Chubb, T.A. and Friedman, H. : 1965 Science 147, 394.

12. Clark, G. W., Garmire, G., Oda, M., Wada, M., Giacconi, R., Gursky, H. and Waters, J. : 1965 Nature 207, 584.

13. Oda, M., Clark, G.W., Garmire, G., Wada, M., Giacconi, R., Gursky, H. and Waters, J. : 1965 Nature 205, 554.

14. Fisher, P.C., Johnson, H.M., Jordan, W.C., Meyerott, A.J., and Acton, L.W. : submitted for publication to Astrophy. J. (1965)

15. Giacconi, R., Gursky, H. and Waters, J.R. : 1965 Nature 207, 572

APPENDIX G

ASE-1145

FREE-FREE EMISSION AS A SOURCE OF GALACTIC X-RAYS

Oscar P. Manley

American Science and Engineering, Inc.
Cambridge, Massachusetts 02142

Accepted for publication in Astrophysical Journal, to appear May, 1966

ABSTRACT

We have examined the assumptions underlying a simple model for discrete galactic X-ray sources, viz. free-free emission from a hot, fully-ionized, hydrogenic plasma. We have found that, for internal consistency, some combinations of the model parameters must be constrained, i. e. the parameters cannot be prescribed arbitrarily. The interpretation of the currently available data relevant to Sco X-1 in terms of our simple model yields significant lower bounds on the distance, size, and mass of that X-ray source. In fact, we have shown that, on using a self consistent model, it is possible to interpret the data relevant to Sco X-1 in terms of free-free emission from a tenuous cloud of hot hydrogenic plasma. Our calculation indicates that Sco X-1 may be as close as 1 light-year.

FREE-FREE EMISSION AS A SOURCE OF GALACTIC X-RAYS

INTRODUCTION

The observation of extra solar X-ray sources by Giacconi et al (1962) was soon followed by other observations (Gursky 1963; Bowyer 1964) confirming the initial discovery, as well as determining the approximate location of the dozen or so X-ray sources, apparently within our galaxy. The radiation flux from these sources has been measured at 10^{-7} to 10^{-8} ergs/cm^2-sec in the interval ~1 to ~10 Å.

Since these sources may be as distant as 1-10 kpc, the observed irradiance implies power emitted by the source to be of the order of 10^{36} to 10^{38} ergs/sec in the X-ray region. On the other hand, there is a possibility that at least one of the sources, viz. Sco X-1, may be relatively nearby. Furthermore, the several sources, having been by now observed over a period of several years, must have reasonably long lifetimes. No known stellar structures can account for these observations. Since the initial discovery, various theoretical models have been proposed to account for the galactic X-ray sources. They have been briefly reviewed by Giacconi and Gursky (1965).

One of the possible mechanisms suggested is free-free emission from a hot plasma (Rossi 1964; Burbidge 1965). In this paper we follow this suggestion and investigate its consequence in a model of a free-free emission X-ray source. Specifically we address ourselves to the requirement that the kinetic energy of the emitting plasma is given by the Maxwell-Boltzmann distribution. We find that this, in addition to the requirement of internal consistency, leads to various combinations of significant parameters -

e.g. size, density and temperature - which are suitably constrained. Having determined these constraints, we combine the results of our simple model with the currently available data for a specific X-ray source, viz. Sco X-1, and deduce from it some information concerning distance, size, and mass consistent with our initial assumptions. Note that with the meager data available concerning X-ray sources other than Sco X-1 the applicability of our model to those sources is as yet not excluded.

ASSUMPTIONS AND THEIR CONSEQUENCES

For our model, we make the following assumptions about the precise physical state of the hot plasma. (We shall use the cgs - ^{o}K system except where specific statement to the contrary is made).

1) We consider a pure hydrogen plasma whose electrons and ions have a Maxwellian (non-degenerate) distribution characterized by a temperature $T = 10^{7}$ to $10^{8}{}^{o}$K. The number density, n_e, is between 10 and 10^{5} particles/cm^{3}.

2) There are no internal energy sources and cooling by expansion is negligible.

It can be shown that, consistent with these assumptions, in our model the following physical conditions prevail:

1) The atoms are nearly fully ionized and hence line excitation and emission is negligible.

2) Recombination rates are negligible.

3) The only significant cooling mechanism is by free-free emission and this is sufficiently slow to allow the source to radiate X-rays over hundreds or thousands of years.

The requirement of Maxwellian energy distribution imposes some limitations on the possible extent of the X-ray source. This follows from the hypothesis that the required distribution is maintained by sufficiently frequent energy sharing electron-electron collisions (Spitzer 1956). The relevant "self-collision time", t_c, is assumed here to be given by

$$t_c \sim 10^{-2} T^{3/2}/n_e \text{ sec} \tag{1}$$

Thus, the distance ℓ_c between "self-collisions" is approximately

$$\ell_c \sim \bar{v} t_c \sim 4 \times 10^3 T^2/n_e \text{ cm} \tag{2}$$

Here $\bar{v}$ is the thermal average speed of the electrons. Obviously, to maintain an equilibrium distribution, the characteristic dimension of the source, say radius r, must exceed ℓ_c, i. e.

$$r n_e \gtrsim 4 \times 10^3 T^2 \text{ cm}^{-2} \tag{3}$$

This requirement on r can be relaxed if one takes into account that the hot plasma may be contained by an irregular magnetic field. In fact, as shown in the Appendix, in the presence of a magnetic field the requirement of a Maxwellian distribution may be satisfied almost independently of the source size.

Equation (3) yields a lower bound on the mass M of the source: thus, on assuming a roughly spherical volume we have

$$M/M_\odot \gtrsim 10^{-2} (T_7 r_p)^2 \tag{4}$$

where

$M_\odot$ is the solar mass

T_7 is the electron temperature in units of 10^7 °K, and

r_p is the radius of the source in pc.

Of course, in the presence of an irregular magnetic field this bound on the mass M may be relaxed considerably.

FREE-FREE EMISSION

We now turn to a brief discussion of some aspects of free-free emission. We use here the results of Karzas and Latter (1961). Since their computations are not amenable to exact analytic representation, we restrict ourselves to presenting the pertinent numerical results in graphical form.

As is seen from Figure 1, from temperatures between 10^6 and 10^{8o}K, ($10^{-1} \leq \gamma^2 \equiv 1.6 \times 10^5/T \leq 10^{-3}$) the quantity $e^{-u} \langle g_{ff}(u, \gamma^2) \rangle$, which is proportional to the spectral intensity F_ν ergs/sec-c/s, is very weakly dependent on temperature, (i.e. on γ), but it is by no means slowly varying near $u \equiv h\nu/kT = 1$ which is the region of interest. Note that neglecting the departure of the gaunt factor $\langle g_{ff} \rangle$ from constancy leads to the wrong spectral shape. On the other hand, setting g equal to a constant makes little measurable difference in the total flux. In Figure 2 we show the flux of continuum radiation in the interval 1 to 10 Kev, W(1-10) ergs-cm^3/sec as a function of the electron temperature. The total energy loss rate, $W_{bs}(T)/n_e^2$ ergs-cm^3/sec by free-free emission, is shown in the same figure. For comparison, we have plotted in this figure the ratio η of the power flux between 1 and 10 Kev to the total flux W(T). It is seen that at $T \sim 5 \times 10^{7o}$K, η is maximum, and there about 70% of the energy loss by free-free emission is in the 1 to 10 Kev range.

Apart from the free-free emission of electrons in the Coulomb field of protons, a possible additional source of bremsstrahlung results from radiative electron-electron collisions. However, as shown by Kvasnica (1960), the contribution of electron-electron bremsstrahlung relative to that due to electron-proton bremsstrahlung is of the order of $kT/m_o c^2$ and hence,

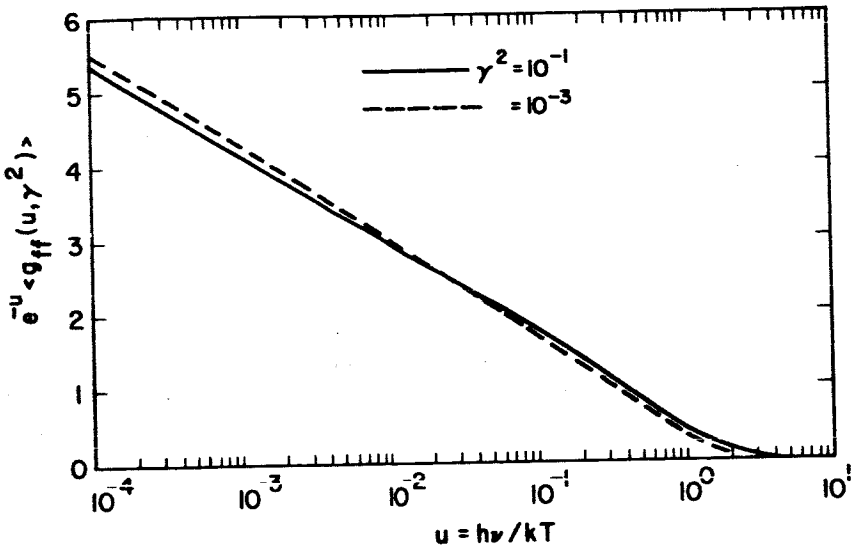


Fig. 1 Relative spectrum of free-free emission from a hot hydrogenic plasma

$$u = h\nu/kT;\ \gamma^2 = Z^2\alpha^2 m_o c^2/2kT$$

(from Karzas and Latter, 1961).

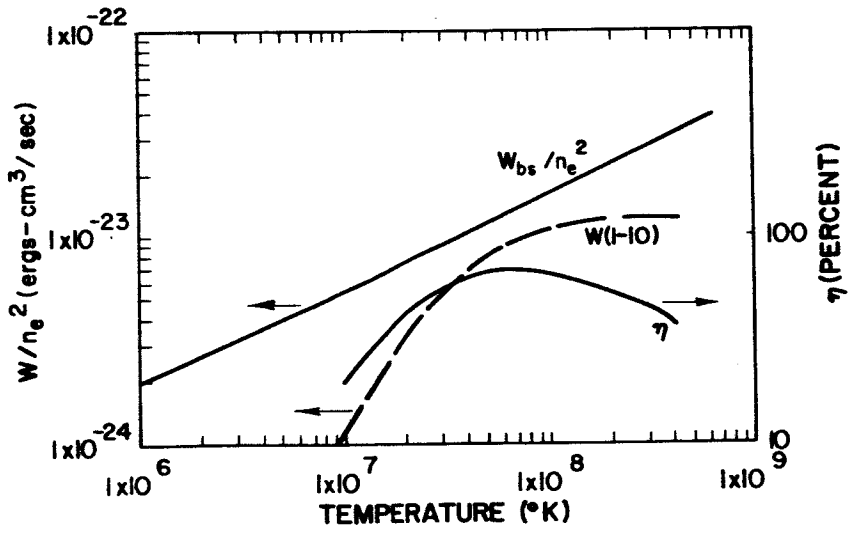


Fig. 2 Specific free-free emission from a hot hydrogenic plasma. W_{bs} - total emission; W(1-10) - specific emission between 1 and 10 Kev; $\eta = W(1\text{-}10)/W_{bs}$.

in the present context is negligible. This is in accord with classical considerations which show that electron-electron bremsstrahlung should give vanishing intensity in the dipole approximation (Landau 1959; Malkov 1961). The quadrupole contribution which does not vanish, is of the order $(v/c)^2$. It should be noted here (cf. Stabler 1965) that due to a confusion in the definition of the cross section of Joseph and Rohrlich (1958), Koch and Motz (1959) have reported erroneously the electron-electron bremsstrahlung cross-sections originally obtained by Garibyan (1953) as being of the same order as the electron-positron (electron-proton) cross-section. According to Rohrlich (1965) apart from other minor corrections, Equation 58 in his and Joseph's paper should be multiplied by $\beta^2/2$ in order to be consistent with their Equation 56.

COMPARISON OF MODEL WITH OBSERVATIONS OF SCO X-1)

We shall now use the free-free emission model in conjunction with the available experimental data and deduce therefrom some information concerning the X-ray source identified as Sco X-1. The pertinent observations are enumerated in Table I.

The observed X-ray irradiance, J_x, on the basis of our hypotheses is

$$J_x = VW_x/4\pi R^2 = W_x r^3/3R^2 \ \text{ergs/cm}^2\text{-sec} \qquad (5)$$

where V is the volume of the source (assumed to be spherical) and W_x is $n_e^2 W(1\text{-}10)$ where $W(1\text{-}10)$ is the X-ray emission given in Figure 2. R is the distance to the source.

Defining now the angular diameter of the source δ as

$$\delta = 2r/R$$

then

$$J_x = (1/12)\pi n_e^2 \delta^2 W(1\text{-}10) \geq 1.6 \times 10^7 T^4 \delta^2 W(1\text{-}10)/12r \qquad (6)$$

where we have used the constraint of Equation (3). Hence, the radius of the source, consistent with our assumptions as well as the measurable quantities δ and J is

$$r \geq 4 \times 10^{6} T^{4} \delta^{2} W(1-10)/(3J_{x}) \tag{7}$$

Similarly, the distance to the source is

$$R \geq 8 \times 10^{6} T^{4} \delta^{2} W(1-10)/(3J_{x}) \tag{8}$$

and the mass is

$$M/M_{\odot} \geq 2.5 \times 10^{-41} T^{10} \delta^{4} W^{2} (1-10)/J_{x}^{2} \tag{9}$$

Note that expressions (7) to (9) depend only on directly measurable quantities; for, within our model, even the temperature T is uniquely determined by the spectrum of the emission.

Thus to fix the temperature of Sco X-1, we have on the high energy end of the spectrum some relatively meager data above about 10 Kev (Giacconi et al 1965). These data are proportional to $e^{-u} \langle g_{ff}(u, \gamma^{2}) \rangle / u$, (F_{ν}/ν) the constant of proportionality being independent of u, i.e. of $h\nu$. In Figure 3, we show a comparison between the data and the theoretical fit for $T = 5 \times 10^{7}$ °K. I.e., the temperature is in the region where η is maximum (cf. Figure 2). Note that we have not used the experimental points obtained with the scintillator as given by Giacconi et al for energies below 10 Kev ($u \leq 2.5$), because they may be affected by the instrument cut-off at that energy. It is found that our model is satisfied provided that the condition

$$r n_{e}^{2} \delta^{2} \sim 10^{16} \tag{10}$$

is satisfied. While the agreement shown in Figure 3 is rather tenuous (based as it is on only three data points) it cannot be dismissed out of hand.

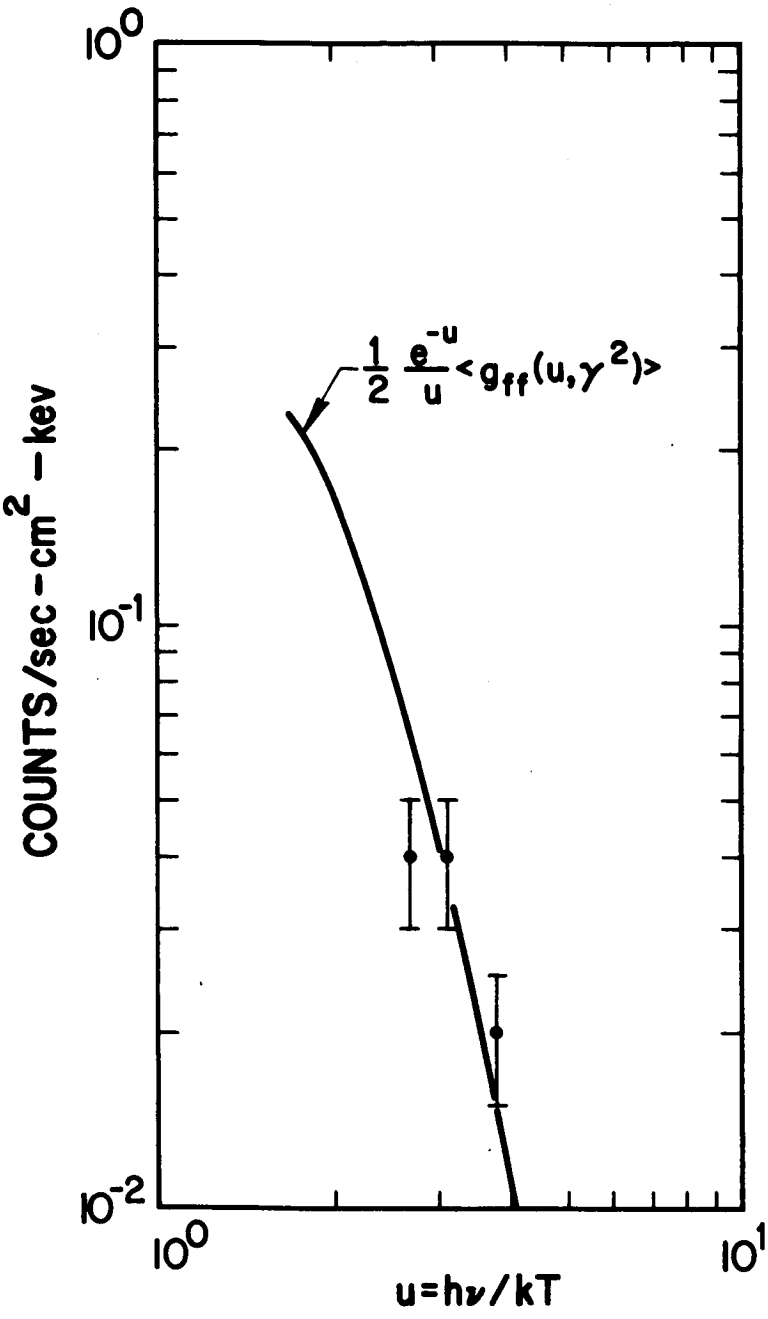


Fig. 3 Comparison of high energy X-ray data (Giacconi et al, 1965) with the free-free emission model.

Insofar as the angular extent of Sco X-1 is concerned, we find that Oda et al (1965) have put on it an upper bound of 7' of arc. Because of the current lack of precise position of Sco X-1, any of the stars within the circle of uncertainty may very well turn out to be identical with Sco X-1. On the other hand, the absence of visible radiation identifiable with it may be due to its relatively large angular size. For, if Sco X-1 is indeed a plasma cloud at $T \sim 5 \times 10^{7o}K$, its irradiance in the visible is three orders of magnitude smaller than that in the X-ray region. This would make its apparent visual magnitude greater than 13. But nebulosities subtending 2' of arc or more and fainter than 13 magnitude cannot be observed with current equipment.

For $\delta \geq 2'$, $T \sim 5 \times 10^{7o}K$, and $J_x \sim 10^{-7}$ erg/cm^2-sec there results from eqs. (7) to (9)

$$r \geq 10^{-4} \text{ pc} \qquad R \geq 1/3 \text{ pc}$$
$$M/M_\odot \geq 1.3 \times 10^{-9} \tag{11}$$

It should be recalled that the bounds derived here rest on the assumption of no magnetic scattering.

It can be verified that, the absence of an observable emission in the radio spectrum is consistent with our model.

It is to be noted that Condition (10) is compatible with the set of lower bounds established in Equation (11). One can infer from it that for consistency $n_e < 10^4/\text{cm}^3$.

CONCLUSIONS

We have shown that using a self consistent model it is possible to interpret the data relevant to Sco X-1 in terms of free-free emission from a tenuous cloud of hot hydrogenic plasma. A remarkable result of the argument presented here is that with our current knowledge of Sco X-1, it is possible

to account for it by placing the source of X-rays as close as one light-year from the solar system.

There are two critical experimental tests of the mechanism proposed here: First, a detailed and accurate measurement of the emission spectrum, in particular near the high-energy cut-off. This is necessary to confirm or reject the exponential drop in intensity predicted by our model. Second, it is necessary to measure precisely the angular size of the source, since only a large-sized source permits the absence of visible radiation in the presence of the measured X-ray flux according to our model.

N. B. Since this paper was written in its original form, extensive data gathered by Chodil et al (1965) indicate that the high energy tail of the spectrum associated with Sco X-1 can indeed by best fitted by assuming for the source a hydrogenic plasma at $T \sim 5.8 \times 10^{7o}$K.

APPENDIX

The constraint given by Equation (3) may be relaxed in the presence of a containing magnetic field. In order for such a containment to be effective, the magnetic energy density must be at least comparable with the particle kinetic energy density

$$B^2/8\pi \sim n_e kT \quad \text{ergs/cm}^3 \qquad \text{A1}$$

where B is the r.m.s. magnetic field in Gauss.

The existence of such a field is very likely because of the turbulence almost certainly present in the plasma (Batchelor 1950; Olbert 1965). The average B field under such conditions may be small, but large fluctuations are probable. Therefore, it is possible to deflect strongly the electrons by nearly perfectly elastic collisions, extend the path length within the source, and thus increase the probability of "self-collision" within a given volume.

In the presence of magnetic field, the restriction imposed on the size of the object and its kinetic temperature corresponding to Equation (3) may be estimated from very general considerations which are independent of the particular model discussed here, viz. the random walk concept (Chandrasekhar 1943). Consider a region with linear dimension L in which a particle with the speed v is scattered. In the random walk, the mean distance L traversed by the particle after n collisions is proportional to $\sqrt{n}$, i.e.

$$L \sim \lambda_s \sqrt{n} \qquad \text{A2}$$

where λ_s is the scattering mean free path. On the other hand, the mean time t_{esc} required by the particle to escape the region L, is by definition

$$t_{esc} = n t_s \qquad \text{A3}$$

where $t_s = \lambda_s/v$ is the scattering time. Upon elimination of n between Equations A2 and A3 we find that

$$L/v \sim \sqrt{t_s t_{esc}}$$

or

$$L \sim \sqrt{\lambda_s r_{esc}}$$

where

$$r_{esc} = v t_{esc}$$

is interpreted as the true path length traversed by the colliding particle before it escapes the confines of the radiating object. It is obvious that in order for the electron to be confined long enough so that an energy sharing collision with another electron can occur, it is necessary that

$$r_{esc} \gtrsim \ell_c = 4 \times 10^3 T^2/n_e$$

(cf. Equation (2).) Thus

$$L/\ell_c \sim \sqrt{\lambda_s/\ell_c}$$

That is, in order for the magnetic confinement to effect a decrease in the size of the radiating source under the present assumptions, it is required that

$$\lambda_s < \ell_c \qquad \text{A4}$$

where λ_s is assumed to be the mean free path for scattering from magnetic irregularities. To proceed further we assume that

$$\lambda_s > R_L = pc/eB$$

where R_L is the Larmor radius and p is the momentum. Thus, on using Equation A1 it is found that Inequality A4 holds whenever

$$n_e/T^4 \lesssim 10^{-4}$$

which is satisfied for a variety of situations of astrophysical interest. The constraint on the dimensions of the object, when confinement by magnetic scattering is effective, reduces to

$$L \gtrsim 4 \times 10^4 T/n_e^{3/4} \qquad \text{A5}$$

It can be verified that this constraint is so easily satisfied that under the assumptions stated at the beginning of this paper it imposes no significant bounds on the distance and mass of the X-ray source, Sco X-1. To put it another way, in the presence of magnetic scattering, as described here, the plasma is in a kinetic equilibrium, practically irrespective of the dimensions of the source.

It should be noted that in the present case cooling by synchrotron emission is negligible in spite of the large magnetic field ($\sim 10^{-3}$ to 10^{-2} gauss). This is so because this emission is strongly self absorbed in the plasma. It can be shown that for our model the absorbtion coefficient is about 1 cm^{-1} (Riesenfeld, 1963).

TABLE I

SUMMARY OF MEASUREMENTS ON Sco X-1

X-ray flux (J_x) ~ 10^{-7} ergs/cm^2-sec.

Effective wavelength (λ_{eff}) ~ 3Å.

Angular diameter (δ) $\lesssim 2 \times 10^{-3}$ radians.

Effective temperature (T_{eff}) @ 10^4 Mc/s < 0.1°K (a).

Apparent magnitude (M) @ $\delta \sim 10^{-3}$ radians $\gtrsim +13$ (b).

(a) Based on private communication from A. Barrett.

(b) Based on lack of visible radiation identifiable with Sco X-1. Note the reported absence of significant amount of interstellar dust in the vicinity of Sco X-1. (Private communication from H. Johnson).

ACKNOWLEDGEMENT

The author wishes to thank Professor B. Rossi and Professor M. Oda for introducing him to the model discussed here. Thanks are also due to Drs. J. W. Carpenter, R. Giacconi, H. Gursky and M. Annis who helped to clarify some ideas contained herein. This work has been supported in part by NASA Contract #NASw-1284.

REFERENCES

Batchelor, G. K., 1950, Proc. Roy. Soc. (London) A 201, 405.

Bowyer, S., et al, 1964, Proc. IV Inter. Space Sci. Symp. Space Res. IV, 966; North Holland Publishing Co., Amsterdam.

Burbidge, G. R., et al, 1965, Phys. Rev. Letters 14, 289.

Chandrasekhar, S., 1943, Revs. Mod. Phys. 15, 1.

Chodil, G., et al, 1965, Phys. Rev. Letters 15, 605.

Garibyan, J. M., 1953, Zhur. Eksp, Teoret. Fiz. 24, 617.

Giacconi, R., et al, 1962, Phys. Rev. Letters 9, 439.

Giacconi, R., et al, 1965, Nature, 207, 572.

Giacconi, R., and Gursky, H., 1965, Space Science Rev. 4, 151.

Gursky, H., et al, 1963, Phys. Rev. Letters 11, 530.

Joseph, J., and Rohrlich, F., 1958, Revs. Mod. Phys. 30, 354.

Karzas, W. J., and Latter, R., 1961, Ap. J. Suppl. 6, 167.

Koch, H. W., and Motz, J. W., 1959, Revs. Mod. Phys. 31, 920.

Kvasnica, J., 1960, Check. J. Phys. B10, 14.

Landau, L., and Lifshitz, E., 1959, The Classical Theory of Fields, A-W Publ. Co., Reading, Mass.

Malkov, E. I., and Shmushkevich, I. M., 1961, Sov. Phys. JETP 12, 1282.

Oda, M., et al, 1965, Nature 205, 554.

Olbert, S., 1965, private communication.

Riesenfeld, W. B., 1963, Plasma Physics and Thermonuclear Research, Vol. 2 C. L. Longmire, et al, Ed., New York.

Rohrlich, F., 1965, personal communication.

Rossi, B., 1964, quoted by Burbidge, et al (1965).

Spitzer, L., 1956, Physics of Fully Ionized Gases, Interscience, New York.

Stabler, R. C., 1965, Nature, 206, 922.

APPENDIX H

THE POSITION OF TAU XR-1 RELATIVE TO THE OPTICAL CENTER AND THE CENTRAL STAR OF THE CRAB NEBULA

R. Finn, O. Manley and G. Ouellette

American Science and Engineering, Inc.
Cambridge, Massachusetts 02142

INTRODUCTION

Recently, Bowyer et al (Reference 1) reported in some detail their observation of the lunar occultation of X-ray emission from the Crab nebula. They indicated that "... the maximum of the X-ray flux distribution was observed at about 230 seconds (after launch), when the occultation had not quite reached the center of the visible nebula...". An examination of the data in Reference 1 shows that this lack of coincidence holds whether one interprets "the center of the visible nebula" as the optical center (maximum brightness), or as the central star.*

We have found the possible lack of coincidence of the X-ray source with the optical source in conflict with the hypothesis that the X-ray emission from the Crab is of the same nature as the optical emission, viz., synchrotron radiation (References 2, 3, 4). As noted in Reference 4, large lower-energy fluxes (i.e., optical radiation) must accompany the emission of synchrotron X-radiation, and this in turn implies spatial correlation between the two types of sources.

On re-examining the published data concerning the lunar occultation of TauXR-1 we have found that, if the effect of the rocket motion is properly included in the occultation computation, both the optical center and the "central star" are well within the half-power-width of the reported X-ray source.

---

*One of a pair of double stars near the apparent geometric center of the nebula.

The results of our calculation are illustrated in Figure 1, which shows the position of the lunar limb during the time of interest as calculated in this paper (solid lines) and as given by Bowyer et al (1) (dashed lines). Bowyer et al state that the peak of the X-ray emission occurred at 230 sec and the width of X-ray emission region was about one arc minute. We have found the lunar limb at 230 seconds to be within 5 and 12 arc seconds of the central star and the center of optical intensity, respectively. Furthermore, we find the occultation rate to be about twice that shown by Bowyer et al which would double the width of the emission region.

The remainder of this paper reports in some detail how we obtained our results.

COMPUTATIONAL PROCEDURE

Apparent Selenocenter of Date

The celestial coordinates of the selenocenter were taken from the ephemeris (Reference 6) using a linear interpolation over the one hour tabular interval (maximum error that could be introduced over the interval of interest is on the order of $0^s.01$ in R.A. and $0''.2$ in dec.). The tabular values (apparent) are as seen from the geocenter with reference to the true equinox of date and include planetary aberration of the moon.

The cartesian coordinates of the moon were then computed in this system by determining the lunar geocentric radius from the tabulated lunar semi-diameter for the times of interest. The error introduced by linear interpolation of the semi-diameter is effectively zero. The lunar radius was taken as 1738.2 km (actually the current estimates are, polar radius 1737.8 ± 0.2 and equatorial radius 1738.6 ± 0.2, thus producing maximum errors near the poles and equator of $0''.2$ and much less near the region of interest).

Technical Approach

Because of the suspected error in lunar limb position as a function of time in Reference 1, we developed a computation technique for occultation predictions from any point in space. The method used is based on Reference 5, whereby the sensor-moon vector is computed in the equatorial system of date and the observed lunar limb is traced out on the celestial sphere. The lunar limb coordinates computed in this manner are accurate to better than $1''.0$ in either coordinate. As a check on this method we computed the 1955 occultation as viewed from Dwingeloo (Reference 8) with no discernible error.

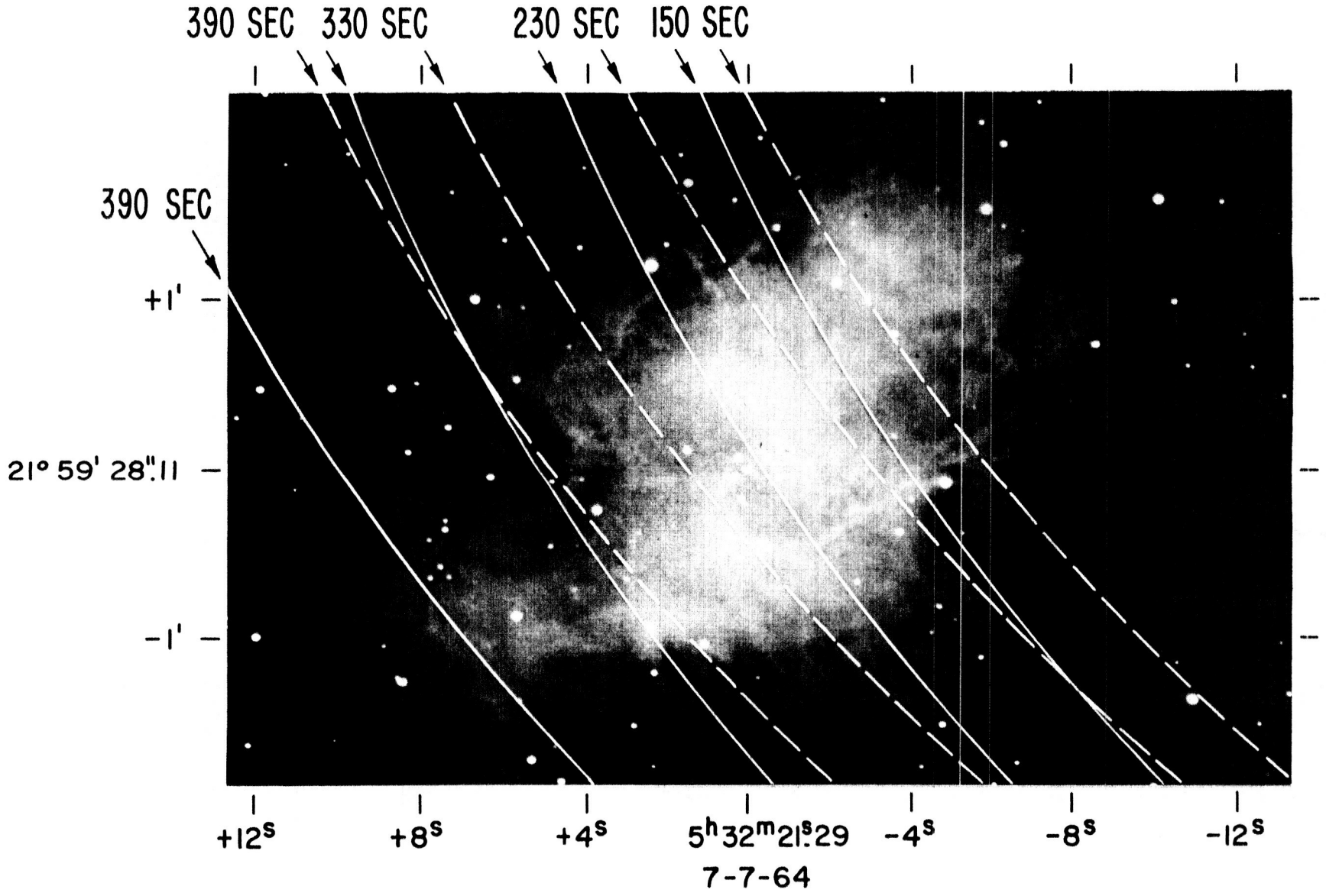


Fig. 1 Position of Lunar Limb During Crab Occultation

(Photograph Courtesy of California Institute of Technology)

Apparent Sensor Coordinates

The sensor coordinates in the celestial system were obtained by transforming the topocentric vehicle coordinates (referenced to White Sands, N. M.), to the geocentric celestial system. For the times of interest, the vehicle coordinates (7, 11) to within $\pm$ .5 km (producing errors of less than 0."3) are:

T	X (East)*	Y (North)*	Z (Vertical)*
150 sec	-3.5 km	31 km	175 km
230	-6.7	52	220
330	-11.0	77	192
390	-12.8	91	132

The transformation from geocentric rotating coordinates to celestial coordinates (x-axis through Greenwich meridian to x-axis through equinox of date) was accomplished with our library subroutine and ephemeris data for the hour angle of the vernal equinox. Linear interpolation of the hour angle introduces no error. The conversion from Greenwich (Universal) time to Ephemeris time was taken to be 35 seconds (ET = UT + 35 sec.).

Sensor-Moon Vector Components and Vehicle Apparent Semi-Diameter

The cartesian coordinates of the sensor and the moon were used to determine the components of the line-of-sight from sensor to the moon. These components provide the "look angles" in the celestial system, i.e., vehicle-moon apparent right ascension and declination referenced to the equinox of date. The only error of note introduced is the neglect of vehicular and diurnal aberration. These were not included however, since their total effect was estimated to be less than 0."5. The angular semi-diameter of the moon as seen from the vehicle was recomputed using the vehicle-moon distance and the lunar radius.

Lunar-Limb Computation

The coordinates of the lunar limb were computed in a spherical astronomy routine using the apparent semidiameter as seen from the vehicle. The limb coordinates as a function of central angle were thus plotted to provide the limb projection of the celestial sphere. In

---

* References 7 and 11

reproducing the limb curves in Figure 1, it was assumed that a constant cosine correction for right ascension as a function of declination in a cartesian plot (thus producing a Plate Carreé projection) does not differ noticeably over the declination range of the Crab nebula.

Crab Nebula Coordinates

The celestial coordinates of the Crab nebula were obtained from Reference 8. This reference provides the 1950.0 coordinates for the reference central double stars. The lower right central star was used as origin and its coordinates

$$\alpha_{1950} = 5^h\,31^m\,31.^s\,46$$

$$\delta_{1950} = 21^\circ\,58'54.''8$$

were updated to 1965.0 with the rigorous reduction using Newcomb's expressions. Nutation, aberration and precession back to 7 July 1965 were obtained through the Besselian Day Numbers tabulated in Reference 6. The 7 July 1965 coordinates of the reference star are

$$\alpha_{7/7/64} = 5^h 32^m 21.^s\,29$$

$$\delta_{7/7/64} = 21^\circ 59'28.''\,1$$

These coordinates in conjunction with Figure 2 of Reference 9 indicate that the point of maximum photographic luminosity of the Crab had the approximate coordinates (updated in the manner above).

$$\alpha_{oc} = 5^h 32^m 20.^s\,6$$

$$\delta_{oc} = 21^\circ 59'39''$$

on 7 July 1964.

COMPARISON OF RESULTS

Since our results differ considerably from those in Reference 1, we felt it necessary to determine what conditions would duplicate these

results. All computations were carried out on an IBM 1620 Computer using trajectory-astronomical reduction techniques developed or adapted by us. If it is assumed that the rocket vehicle is stationary directly above the launch site at an altitude of 200 km rather than taking account of the correct trajectory, during all computations and that the cosine correction for right ascension as a function of declination (22^{o}) is neglected, our computational technique produces the curves presented in this reference with reasonable accuracy (11).

Luminosity Curves

The luminosity versus time curve of the Crab Nebula during the occultation was obtained by superimposing the lunar limb on Figure 2 of Reference 9. The areas within the photographic isophotes were summed with a planimeter and were used to produce our Figure 2. From this figure we determined that the center of the half power region as measured in visible light was traversed at approximately 214 seconds after launch.

The smoothed X-ray curves of Reference 1 are reproduced in Figure 3 along with an accurate indication of the occultation as determined from Figures 1 and 2. For the occultation as viewed from the moving rocket, the lunar limb traversed the west to east direction of an average rate of 45"/minute of time. The half-power width of the X-ray emission region is about 40" and the 90% power width about 105". If the curves in Reference 1 are used, the half-power width appears to be about 25" and the 90% width about 55". The ratio between the half-power width and the 90% power width differs in the two cases because of non-linear effects introduced by the motion of the vehicle.

According to our calculations, the central star was occulted at 241 sec. (Point C on the curve in Figure 3) and the optical center of the nebula at 214 sec. (Point B), both times being well within the half power points (A, A'). On the other hand, the limb positions given by Bowyer et al in Reference 1 indicate that the central star was occulted at about 300 sec. (Point C') and the optical center at about 270 sec. (Point B'), both of which lie outside the half-power region. It thus appears that the use of the more correct occultation parameters yields better agreement between the optical center of the Crab nebula and the X-ray emission center, and increases the width of the X-ray region as well.

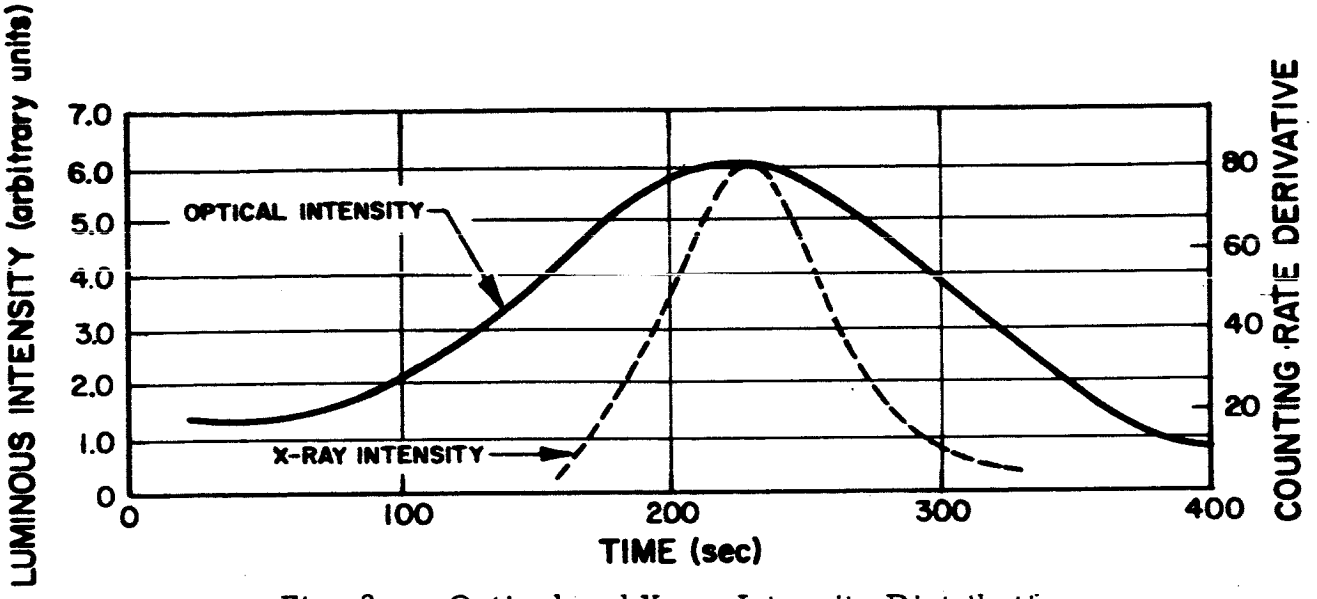


Fig. 2 Optical and X-ray Intensity Distributions

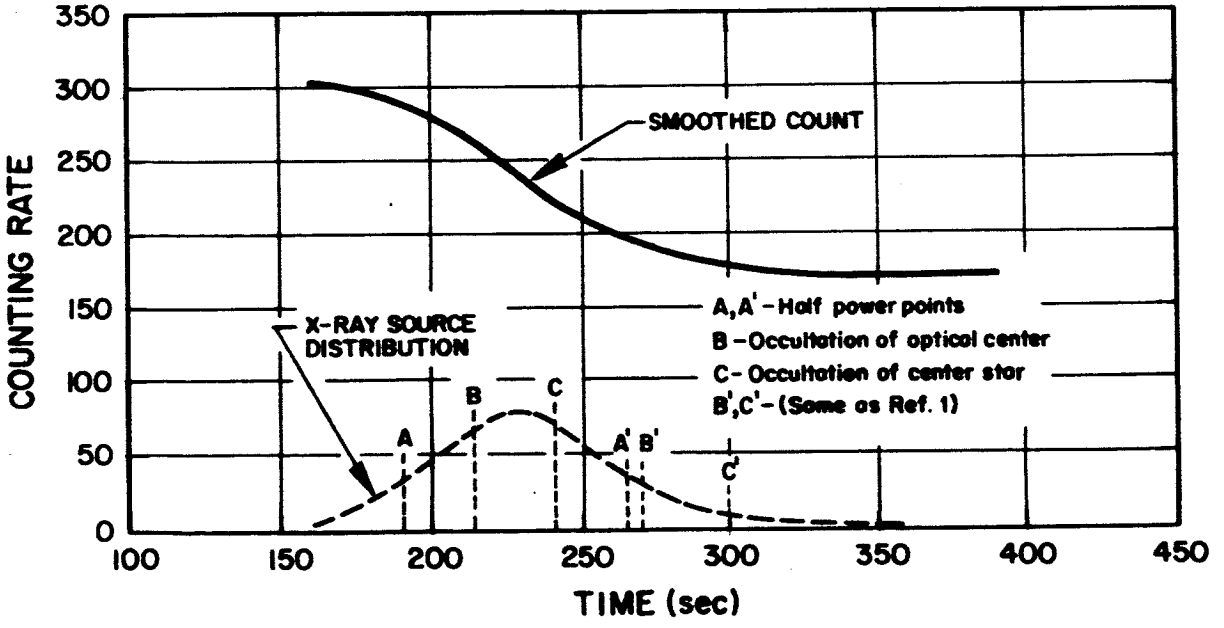


Fig. 3 Occultation Experiment Data

REFERENCES

1. Bowyer, S.; Byram, E. T.; Chubb, T. A.; Friedman, H.; Science 146, 912, 1964.

2. Shklovskii, I. S., quoted in Reference 1.

3. Woltjer, L., Ap. J. 140, 1309, 1964.

4. Burbidge, G. R., et al., Phys. Rev. Letters 14, 289, 1965.

5. Ouellette, G. A., Lecture Notes on Celestial Mechanics AS 301, Boston University

6. American Ephemeris and Nautical Almanac 1964, Government Printing Office, Washington, D. C.

7. Brezezenski, D.; Oullette, G.; Sexton, J.; H. Q., AFCRL, Bedford, Massachusetts. Final Report, Contract AF 19 (628)-3278.

8. Seeger, C. L.; Westerhout, G.; Bulletin of the Astronomical Institutes of the Netherlands, Vol. XIII, No. 478, (p. 313) Sept. 1957.

9. Woltjer, L., IBID, (p. 301).

10. Matreenko, Martirosyan, Sorochenko, Soviet Astronomy, 9, No. 2, (p. 247) Sept. - Oct. 1965. (English Translation)

11. Dr. Herbert Friedman of NRL, in private communication with the authors, has verified that the rocket trajectory data used here are correct and that an occultation prediction was used in their published article (Reference 1) that did not take complete account of the rocket motion.

APPENDIX I

COMPUTER PROGRAMMING

To support the data reduction and analysis, a set of computer programs was written for use on the IBM 1620 computer at AS&E. This machine is a Model 2 1620, equipped with a disk drive, and is operated using the Monitor I executive system. These programs were written in 1620 Fortran II-D and utilize the AS&E subroutine library. They could be easily rewritten for other versions of Fortran and for other computers. This appendix describes the most important programs that were implemented for this project. They are:

1. STDFCR, star finder differential corrector for spinning yawing rocket.
2. MSDFCR, spin axis magnetometer differential correction for spinning yawing rocket.
3. M9DFCR, 90° magnetometer differential correction for spinning yawing rocket.
4. SPAXIS, spin axis tracer for spinning yawing rocket.
5. MASDEN, atmospheric mass-density along line of sight.

The first three programs are used for aspect determination. The fourth program may be used to assist in aspect determination, but is generally used to study the motion of the rocket after aspect has been determined. The fifth program is used to compute the effect of the atmosphere.

These computer programs are available through Michael W. Bate at AS&E.

NAME: STDFCR, star finder differential corrector for spinning yawing rocket.

PURPOSE/ABSTRACT: Differential corrects aspect parameters for a spinning, yawing rocket, by using the star finder data. Corrects in order to minimize difference between observed star positions (as derived from aspect parameters and time of star acquisition) and known star positions, from star catalogs. Correction may use any of three coordinate systems to represent star positions:

α, δ Pole is north pole (right ascension, declination)

a_s, d_s Pole is current value of rocket spin axis

a_y, d_y Pole is current value of rocket yaw axis

Parameters to be corrected may be selected by either manual or automatic means. In either case, program repeatedly corrects the same parameter set, until result converges or diverges. Program may also be used simply to print observed star position, without doing any differential correction.

PROGRAM DESCRIPTION:

1. Aspect Parameters

The following set of parameters is used throughout the program. Given the parameter set, and a time, it is possible to uniquely determine rocket orientation:

α_y Right ascention of yaw axis, degrees.

δ_y Declination of yaw axis, degrees.

t_{oy} Time of closest approach of spin axis to north celestial pole, seconds.

ω_y Rate of yaw, in degrees per second, counter clockwise on the celestial sphere, as viewed from the earth.

r Radius of yaw cone, in degrees

t_{os} Time, in seconds, of closest approach, during rocket spin, of a line of zero azimuth on the rocket to the yaw axis.

ω_s Rate of spin, (where 1 rotation is from yaw axis to yaw axis) in degrees per second, counter-clockwise on the celestial sphere, as viewed from the earth.

$\dot{\omega}_s$ Time derivative of rate of spin, in degrees per second per second.

2. Star Acquisitions

The program assumes that the star finders are of a photo-electric type, and that their scan will show a sharp peak when a star enters the field of view. Star acquisition information required is as follows:

a) time of star acquisition (peak) in seconds

b) coordinates of the star finder. These tell the orientation of the star finder axis on the rocket. They are:

ϕ star finder declination. This is angular distance in degrees from rocket axis to star finder axis.

θ star finder azimuth. This is measured counter-clockwise from the line of zero azimuth on the rocket to the star finder axis, as seen from the bottom of the rocket looking up in the sky. It is given in degrees.

c) Right ascension and declination of star, as given in star catalog. These are given in degrees. Equinox and epoch should agree with that used for specifying position of yaw axis in aspect parameter set. These quantities need not be given if no differential correction is being performed; i.e., if the program is being run under options 1, 2, or 3, as described below.

3. Observed star positions

Note that, given a set of aspect parameters and the first 3 items (time and star finder coordinates) of a star acquisition, a point on the celestial sphere where the star finder is pointed may be computed, in any of the three coordinate systems (α, δ; a_s, d_s; or a_y, d_y). This is the <u>observed</u> star position.

4. Differential correction process

Differential correction consists of solving a set of equations of the form:

$$\Delta a_i = \sum_{j=1}^{N} \left(\frac{\partial a_i}{\partial p_j} \right) \Delta p_j \qquad i = 1, M$$

where Δa_i is the residual in star coordinate, and is equal to true (catalog) minus observed value of one of the star coordinates.

$\frac{\partial a_i}{\partial p_j}$ are partial derivatives of observed star coordinate value with respect to one of the aspect parameters.

Δp_j are corrections to the aspect parameters for Δp_j. Since two coordinates are used to represent the position of a star, each star acquisition generates two equations of the

above form (two values of i). Note that Δa_i and $\left(\frac{\partial a_i}{\partial p_j}\right)$ are known. Each partial derivative is computed numerically by varying the appropriate parameter slightly and recomputing the coordinate value.

In each pass through the star acquisitions, any number of the aspect parameters (p_j) may be included in the above equation set, and thus be corrected. After each pass, a standard deviation, referring to the aspect parameters before correction, may be computed as:

$$\sigma = \sqrt{\sum_{i=1}^{M} \Delta a_i / M}$$

When, for two successive passes, or corrections, the change in standard deviation is small compared to the value of standard deviation itself, the differential correction process is said to have converged. The user may use the result of this set of corrections to do a new set of corrections, using the same set of star acquisitions, but this time correcting more of the aspect parameters.

Since observed star position is extremely sensitive to the spin aspect parameters (t_{os}, ω_s, $\dot{\omega}_s$), the user will usually want to correct these first, and then proceed to correct the other parameters.

The user specifies the numerical criterion for convergence of standard deviation. If the corrections or any one set of parameters do not converge after 8 passes, the solution is said to diverge.

5. Automatic Rejection of Bad Star Acquisitions

On the first differential correction in a run, all star acquisitions are rejected which give a value of coordinate residual (Δa_i) greater than 1 radian. On succeeding corrections, the residual value criterion is 3 times the standard deviation computed during the previous correction.

6. Weighting

The star finders used generally have a field of view that is very narrow in the direction of rocket spin (azimuthal direction) and wide in the vertical direction. For this reason, especially when using a_s, d_s, or a_y, d_y coordinate sets to represent star position, it will often be desirable to weight the differential correction equations involving one coordinate of the pair (usually a_s, a_y) over that involving the other (usually d_s, d_y). This is done uniformly for all star acquisitions. The program allows the user to read in weighting factors for the two coordinates. If the user wants to bypass weighting, he must still enter weights of 1.0 and 1.0. The program multiplies each differential correction equation by the appropriate weighting factor, before solving the set by least squares.

7. Running Options

The program may be run under any of 9 options, summarized as follows:

	STAR COORDINATE SET		
	α, δ	a_s, d_s	a_y, d_y
No differential correction Print observed star coordinates only	1	2	3

	α, δ	a_s, d_s	a_y, d_y
Differential correction with automatic selection of parameters	4	5	6
Differential correction with manual selection of parameters	7	8	9

Under options 1, 2, and 3, the program performs no differential correction; rather it computes and prints, for each star acquisition that it is given, the observed position in one of the three coordinate systems.

Under options 4, 5, and 6; the program first differentially correct the spin parameters t_{os}, ω_s, $\dot{\omega}_s$. When this converges or diverges, the program then adds yaw cone radius and yaw rate, correcting ω_y, r, t_{os}, ω_s, $\dot{\omega}_s$. When this converges or diverges, the program then corrects all aspect parameters.

Under options 7, 8, and 9; the user specifies the parameter set that he wants to correct. The program corrects these until the result converges or diverges.

INPUT DECK MAKEUP:

1. The first card is the aspect parameter card:

Columns

1-10	α_y	right ascension of yaw axis, degrees.
11-20	δ_y	declination of yaw axis, degrees.
21-30	t_{oy}	time of closest approach of spin axis (rocket axis) to north celestial pole, in seconds.
31-40	ω_y	yaw rate, in degrees per second, measured counter-clockwise as seen from earth looking at celestial sphere.

41-50	r	radius of yaw cone, degrees
51-60	t_{os}	time of closest approach of line of zero azimuth on rocket to yaw axis, seconds.
61-70	ω_s	rate of spin, degrees per second, clockwise as seen from earth looking at celestial sphere.
71-79	$\dot{\omega}_s$	time derivative of rate of spin, in degrees per second per second.

All the above quantities should be punched with explicit decimal point.

2. The second card gives perturbations to the parameters. These perturbations are used in the computation of the partial derivatives, as described in PROGRAM DESCRIPTION, above. The format is the same as for the parameter card, and these values must be punched with explicit decimal point. There is a one to one correspondence between the card field used for the parameter in the parameter card, and the card field used for the perturbation on this card. The units, however, are changed. Wherever the parameter card uses degrees, this card uses radians.

3. The third card is the option selector and run parameter card:

Columns

1-8	Each of these 8 columns corresponds to one of the eight aspect parameters, in the same order as they appear on the aspect parameter card. When running with option 7, 8, or 9, the digit 1 or 0 should be punched in each of these columns to select which

	of the aspect parameters are to be corrected. The digit 1 in any column means that the corresponding parameter is to be corrected, while 0 means that it is not to be corrected.
10	Option number 1-9
11-20	Weight to be assigned to the azimuthal coordinate (α, a_j, or a_y) when doing differential corrections. Each of the differential correction equations involving this star coordinate will be multiplied by this factor. This number must be punched with with decimal point.
21-30	Weight to be assigned to the elevation coordinate (δ, d_s, or d_y) when doing differential corrections. Each of the differential correction equations involving this star coordinate will be multiplied by this factor. This number must be punched with decimal point.
31-40	Convergence criterion. When the difference between the standard deviation resulting from two successive differential corrections of the same parameter set, divided by the most recent standard deviation, is less than this number, the solution is considered to have converged. This number must be punched with decimal point.

4. The next group of cards are the star acquisition cards. Each card has the following format:

Columns

1-10	ϕ, star finder declination, in degrees. This is the angle from the rocket spin axis to the star finder axis.
11-20	θ, star finder azimuth. This is measured counter-clockwise from the line of zero azimuth on the rocket to the star finder axis, as seen from below the rocket, looking up in the sky. It is punched in degrees.
21-30	Time of star acquisition, in seconds.
31-40	α, right ascension of star, in degrees.
41-50	δ, declination of star, in degrees.

Note that these cards always give right ascension and declination of stars, even when another coordinate system is used internally. All the fields in this card must be punched with explicit decimal points.

5. The end of the input deck is signaled by the appearance of a card with -200. or less punched in columns 1-10.

NAME: MSDFCR, spin axis magnetometer differential corrector for spinning yawing rocket

PURPOSE: Given initial estimates of aspect parameters describing the yaw of a spinning yawing rocket, and a set of readings of a single axis magnetometer that is parallel to the spin axis, differentially corrects the aspect parameters to describe the yaw more accurately.

INPUT DECK MAKEUP:

1. The first card is the aspect parameter card:

Columns

1-10	d	great circle distance from magnetic field vector to yaw axis on celestial sphere, in degrees.
11-20		ignored
21-30	t_{oy}	time of closest approach of spin axis to magnetic field vector, in seconds.
31-40	ω_y	angular rate of yaw, clockwise on celestial sphere as seen from earth, in degrees per second.
41-50	r	great circle radius of yaw cone, in degrees.

All the above quantities must be punched with decimal points.

2. The second card gives magnetometer coefficients, magnetic field strength, and convergence criterion:

Columns

1-10	B	Total magnetic field strength in vicinity of rocket, in gauss
11-20	v_o	magnetometer bias, in arbitrary voltage units.
21-30	a	magnetometer calibration coefficient, in gauss per arbitrary voltage units.
31-40		convergence criterion. When the quantity; $\frac{\lvert\Delta\sigma\rvert}{\sigma}$ where $\Delta\sigma$ is change in standard deviation on two consecutive corrections, is less than this number, the solution is considered to have converged, and the program terminates.

All the above quantities must be punched with decimal points.

3. The third and following cards are the observed voltage values. Up to 400 of these cards may be given:

Columns

1-6	v	spin axis magnetometer readout, in arbitrary voltage units. Decimal point either punched explicitly, or else assumed between columns 3 and 4.
7-14	t	time of voltage reading, in seconds. Decimal point either punched explicitly or else assume between columns 10 and 11. t must never be -999. or less.

4. These cards are followed by a card with:

Columns

7-14 Any number less than or equal to -999., punched with decimal point.

to terminate the input deck.

SENSE SWITCHES: The program will give detailed printout for each voltage point as long as sense switch 1 is on. It should usually be off.

NAME: M9DFCR, 90° magnetometer differential corrector for spinning yawing rocket

PURPOSE: Given initial estimates of aspect parameters describing the attitude of a spinning yawing rocket relative to the magnetic field vector, and a set of readings of a single axis magnetometer with axis 90° from the spin axis, corrects the aspect parameters to fit the magnetometer data more closely.

INPUT DECK MAKEUP:

1. The first card contains the aspect parameters and magnetometer bias:

Columns

1-10	d	great circle distance from magnetic field vector to yaw axis on celestial sphere, in degrees.
11-20	t_{oy}	time of closest approach of spin axis to magnetic field vector, in seconds.
21-30	ω_y	angular rate of yaw, counter-clockwise on celestial sphere, as seen from earth, in degrees per second.
31-40	r	radius of yaw cone in degrees.
41-50	t_{os}	time of closest approach of 90° magnetometer axis (positive side) to yaw axis, in seconds. IF SENSE SWITCH 3 is on, this should be time of closest approach to magnetic field (time of maximum field reading).

51-60	ω_s	angular rate of spin, yaw axis to yaw axis, counter-clockwise on the celestial sphere as seen from earth, in degrees per second.
61-70	$\dot{\omega}_s$	rate of change of ω_s, in degrees per second per second.
71-80	v_o	magnetometer bias, in arbitrary voltage units.

All the above quantities must be punched with decimal point.

2. The second card gives the range in time during which the parameters are valid:

1-10	T_{low}	minimum time, seconds, with decimal point.
11-20	T_{high}	maximum time, seconds, with decimal point.

3. The third card gives perturbations to the parameters. These are used to numerically compute the partial derivatives $(\partial v/\partial p)$ of the parameters. Of the eight partial derivatives that must be computed, only the first four are computed numerically:

Columns

1-10	Δd	perturbation to d, in radians
11-20	Δt_{oy}	perturbation to t_{oy}, in seconds
21-30	$\Delta \omega_y$	perturbation to ω_y, in radians per second
31-40	Δr	perturbation to r, in radians

The above quantities must all be punched with decimal points.

4. The fourth card gives:

Columns		
1-10	a	magnetometer calibration coefficient, in gauss per arbitrary voltage units.
11-20	B	total magnetic field strength in vicinity of rocket in gauss.
21-30		Rejection criterion for first pass through data, in arbitrary voltage units. Any magnetometer readout which produces a residual whose absolute value is greater than this number will be rejected on the first pass through the data.
31-40		Convergence criterion. When on two successive passes, the standard deviations (σ) are close enough so that the fraction $\frac{\left\|\sigma_{i-1} - \sigma_i\right\|}{\sigma_i}$ is less than this number, the solution is considered to have converged, and the program terminates.
41-50		Blank or zero if magnetometer readings are on cards (6, below). If they are on a 1620 MONITOR I DIMREC-generated disk file, this field contains DIM number.

Records in the file must have logical length 10, of which only the first two words are used:

1) Time of voltage reading, in seconds. Must be greater than -900.

2) Voltage reading, in arbitrary voltage units.

Both quantities must be in floating point.

51-60 This field is usually zero or blank, but may contain an integer telling the number of magnetometer readings to skip between each reading that is processed. Thus, 1. means process every other reading, 2. means process every third, etc. This is primarily used when magnetometer readings are on the disk file.

61-70 Must be blank.

All quantities on this card must be punched with decimal points.

5. The fifth card gives parameter selection digits:

Columns

1-8 Each of these 8 columns corresponds to one of the 8 aspect parameters, in the same order as they appear on the aspect parameter card. The digit 1 or 0 should be punched in each of these columns, to select which of the aspect parameters are

to be corrected. The digit 1 in any column means that the corresponding parameter is to be corrected, while 0 means that it is not to be corrected.

6. If magnetometer readings are on a disk file, this is the end of the input deck. If they are on cards however, the following cards each give an observed magnetometer readout:

Columns

1-20	Time of voltage reading, in seconds. Must not be less than or equal to -900. Decimal point is punched or else assumed to be between columns 12 and 13.
21-40	Voltage reading, in arbitrary voltage units. Decimal point is punched or else assumed to be between columns 32 and 33.

7. These cards are followed by a card with:

Columns

1-20	Any number less than or equal to -900., punched with decimal point.

SENSE SWITCHES: If sense switch 1 is on, the program will give printout for each voltage point (off line). This switch should ordinarily be off. Sense switch 3 is used as described under INPUT DECK MAKEUP: (first card) above.

NAME: SPAXIS, spin axis tracer for spinning yawing rocket

PURPOSE: During a single spin of a spinning yawing rocket, the total field of view of any instrument on board is an annulus on the celestial sphere. The center of this annulus is the spin axis of the rocket. The annulus is bounded by two small circles described by the projection on the celestial sphere of the vectors of maximum and minimum elevation, with respect to the spin axis, that the instrument can see. During the yaw period, this annulus remains fixed in position with respect to the spin axis; but the spin axis rotates around the yaw axis. Thus the annulus moves on the celestial sphere. This program provides means of tracing the position of the spin axis during the yaw period; and, given a set of reference objects on the sphere, gives their position relative to the center of the annulus described by an instrument at a given position. Elevation with respect to this small circle allows the user to determine whether an object falls within the field of view of the instrument. Phase, or azimuth along the annulus, tells the user at what portion of the spin period the object should appear.

PROGRAM DESCRIPTION:

1. Aspect parameters

Five parameters are used to describe the motion of the spin axis. This set of parameters is a subset of the 8 aspect parameters used to completely describe rocket aspect in program STDRCR (Star finder differential corrector) and other AS&E rocket

programs. The five aspect parameters are:

- α_y, Right ascension of yaw axis, degrees
- δ_y, Declination of yaw axis, degrees
- t_{oy}, Time of closest approach of spin axis to north celestial pole, seconds.
- ω_y, Rate of yaw, in degrees per second, counter-clockwise on the celestial sphere, as viewed from the earth.
- r, Radius of yaw cone, degrees.

Given the parameter set, and a time, it is possible to uniquely determine the position of the spin axis on the celestial sphere.

2. Reference objects

The program can handle a large number of reference objects. Specifically, up to 200 may be read from input cards, and also a 1620 Monitor I DIMREC-generated disk file containing any number of reference objects may be specified. The following information is read for each reference object:

number (up to 5 digits, arbitrary numbering system)
name (up to 8 characters)
right ascension, in degrees
declination, in degrees

3. Program computations and output.

In addition to the above, the program reads a value which is one-half the vertical field of view of all sensors in degrees. This tells how far away from the annulus on the celestial sphere the sensors can see.

The program reads a list of times and associated sensor declinations (angular distance from sensor axis to spin axis).

For each time, the program computes and outputs the right ascension and declination of the spin axis. For each of the reference objects, the program computes and outputs the following:

ABS. PHASE	this is the angle, measured at the spin axis, clockwise from the reference object to the yaw axis.
REL. PHASE	this is the angle, measured at the spin axis, clockwise from the reference object to the first reference object.
DIST TO SENSOR	this is the great circle distance from the reference object to the center of the field of view of the instrument, at the closest approach during the spin period of the instrument to the reference object. It is positive when the reference object is between the sensor and the spin axis, negative otherwise.
DIST TO AXIS	this is the great circle distance from the reference object to the spin axis, and is always positive.

This information is only printed when the value DIST TO SENSOR is less than or equal to the value of 1/2 the vertical field of view of the sensor (i.e., when the object comes in the field of view of the sensor during the spin period). The user

specifies a large value of vertical field of view if he wishes to have the information printed for all reference objects at each input time.

INPUT DECK MAKEUP:

1. The first card read is the parameter card:

   Columns

   1-10 α_y, right ascension of yaw axis, degrees.

   11-20 δ_y, declination of yaw axis, degrees.

   21-30 t_{oy}, time of closest approach of spin axis to north celestial pole, seconds.

   31-40 ω_y, rate of yaw, in degrees per second, counter clockwise on the celestial sphere, as viewed from earth.

   41-50 r, radius of yaw cone, degrees.

   The above quantities should all be punched with explicit decimal points. The rest of the card is not read, and will usually contain the other three parameters of the AS&E aspect parameter set.

2. The second card read has one field:

   1-10 1/2 the vertical field of view for all sensors, in degrees, punched with decimal point.

3. The third card read has two fields:

   1-4 n, number of reference objects on cards, as right adjusted integer.

   5-8 DIM number of DIMREC-generated disk data file containing reference objects in AS&E disk star catalog format. File must have logical record length of 10. Only the first 5 words of each record

are read. These are:

1	Catalog number (floating point)
2-3	Name (alphanumeric in floating point word)
4	Right ascension, radians, flo-pt.
5	Declination, radians, flo-pt.

No correction is made for precession or proper motion.

The two quantities on this card are punched as right adjusted integers.

4. The next n cards (where n is integer read above) specify reference objects. Each card has the format:

Columns

2-6	reference object number, integer
8-9	hours of right ascension, integer
11-12	minutes of right ascension, integer
13-17	seconds of right ascension, punched with explicit decimal point
25	sign of declination
26-27	degrees of declination, integer
29-30	minutes of declination, integer
32-33	seconds of declination, integer
63-70	name of reference object (any alphameric characters)

All integers in the above card must be right adjusted. Columns 18-24 and 34-62 may contain any information.

5. There follow any number of cards giving times and sensor declinations for which printout is requested. Each card has two fields:

1-10 ϕ , sensor declination, in degrees. This is the angle from the rocket spin axis to the center of the sensor field of view.

21-30 time, in seconds

Both fields must be punched with decimal points. Note that this format is compatible with the acquisition card format used by program STDFCR (star finder differential corrector).

6. A blank card terminates the list of time requests, and may be followed by another complete input deck, starting with a parameter card (1, above).

OPERATING INSTRUCTIONS:

The program is operated under control of 1620 Monitor I, in the usual manner.

NAME: MASDEN, atmospheric mass-density along line-of-sight

PURPOSE: Given a sensor location and angle of view, integrates through the atmosphere to determine the total atmospheric density through which it looks and also provides the total mass per square centimeter along the line-of-sight.

HOW TO USE: The first card gives the topocentric origin of coordinates:

Columns

1-10 East terrestrial longitude, degrees

11-20 Geodetic latitude, degrees

21-30 altitude, kilometers

The above quantities should all be punched with decimal points.

The second card gives phase angle of diurnal bulge, in degrees, punched with decimal point, in columns 1-10.

The third card gives the orientation angle option, 1-4 (explained below), punched with decimal point, in columns 1-10.

The fourth card gives integration control parameters:

Columns

1-10 s, size of integration step, in kilometers

11-20 s_{max}, maximum value of distance along line-of-sight, in kilometers

21-30 h_{max}, maximum value of h (altitude), in kilometers

31-40 h_{low}, value of h (altitude), below which sensor is considered to be looking into the earth, in kilometers

All the above quantities must be given with decimal points. Integration will be stopped when altitude exceeds h_{max}, or when distance along line-of-sight exceeds s_{max}, whichever occurs first. It will also be stopped when altitude is less than h_{low}.

The fifth card gives the date, time, and topocentric sensor coordinates.

Columns

1-2	Month, as right adjusted integer.
4-5	Day of month as right adjusted integer.
7-10	Year, as right adjusted integer.
11-20	Greenwich Universal Time, in days.
21-30	Topocentric sensor coordinate X, kilometers.
31-40	Topocentric sensor coordinate Y, kilometers.
41-50	Topocentric sensor coordinate Z, kilometers.

The last 4 above quantities should be punched with decimal points. The following cards specify the orientation angle (sensor angle of view), and their format depends on the option number read above:

OPTION 1 - Azimuth and elevation

Any number of cards follow, each specifying an orientation angle. Each card has the following format:

Columns

1-10 Type of azimuth indicator, punched with decimal point.

=	0	Azimuth is measured ccw from East
	1	ccw from North
	2	cw from N
	3	ccw from S
	4	cw from S

11-20	Azimuth, in degrees, with decimal point.
21-30	Elevation, in degrees, with decimal point.

OPTION 2 - Right ascension and declination

Any number of cards follow, each specifying an orientation angle.

Columns

1-10 Right ascension, degrees, with decimal point.

11-20 Declination, degrees, with decimal point.

OPTION 3 - Longitudinal axis direction right ascension and declination, plus vehicle roll angle from north-vertical plane, plus sensor altitude from longitudinal axis angle.

Any number of cards follow, each specifying an orientation angle.

Columns

1-10 Right ascension, degrees, of longitudinal (rocket) axis, punched with decimal point.

11-20 Declination, degrees, of longitudinal axis, with decimal point.

21-30 Vehicle roll angle (from north and vertical plane), degrees, with decimal point.

31-40 Sensor altitude, degrees, from longitudinal plane, with decimal point.

OPTION 4 - Rocket aspect parameters

An aspect parameter set follows, of the same format as used with the star finder differential corrector program (see writeup).

With this option, several integrations are performed, during a single rocket spin, at times equally spaced during the spin.

The aspect parameter card is followed by a card:

Columns

1-10 Look angle declination. This is the angle from the rocket axis to the angle of view, in degrees, with decimal point.

11-20 Look angle azimuth. This is measured counter-clockwise from the line of zero azimuth on the rocket to the angle of view, as seen from the bottom of the rocket looking up in the sky. It is given in degrees, with decimal point.

21-30 Time of spin, in seconds. This is in the time system of the aspect parameters. This time is taken to be the Greenwich Universal Time of the day, and supersedes the information punched in the time card above. Punched with decimal point.

31-40 Angular increment between successive integrations, in degrees, with decimal point.

When the program has performed all the OPTION 4 integrations, it reads another time card.

APPENDIX J

ATMOSPHERIC MASS COMPUTATION

Gerald Ouellette

American Science and Engineering, Inc.
Cambridge, Massachusetts 02142

ATMOSPHERIC MASS COMPUTATION

The total atmospheric mass per unit area in any direction relative to some point in space can be determined with reasonable accuracy using the AS&E MASDEN computer program. This program utilizes an approximation to the atmospheric density that includes the effects of diurnal heating. The total mass is obtained by determining the altitude above the reference earth spheroid along the line of sight, the diurnal bulge angular distance, the altitude–angular bulge density and summing to some limiting altitude. The summation (integration) technique used is a simple rectangular rule-type approach. Results indicate that for the rockets of interest, it is not necessary to include the atmosphere above 1000 km, since it contributes less than 0.1% to the average total mass.

The atmosphere model used in the program is that recommended by Luigi Jacchia* and is of the form

$$\rho = a_2 \left[1 + a\left(e^{bh} + d\right) \cos^6 \left(\frac{\psi}{2}\right) \right] \quad (gm/cm^3)$$

where

$$a_2 = me^{a_1}$$

$$a_1 = f + gh + ke^{lh}$$

For altitudes below 120 km, where the diurnal variations in the atmospheric density are small, the U. S. Standard Atmosphere, 1962, is used. In the atmosphere equation, a, b, d, f, g, k, l, and m are constant coefficients, ψ is the geocentric angle between the diurnal atmospheric bulge and the point of interest and h is the altitude above the reference earth spheroid in kilometers. This equation does not account for fluctuations in the solar flux associated with variations in solar activity. It represents the daily mean average of the 20 cm solar flux and produces a reference night-time density when $\psi = 180^\circ$. Although not extremely

---

* Private communication

accurate, the results obtained using this model are probably good to within several percent.

The total mass along a line of sight is obtained by

1. determining the geocentric coordinates of the sensor
2. selecting a line of sight direction
3. computing the altitude above the reference earth ellipsoid for points along the line of sight and the diurnal bulge distance
4. determining the density along the line of sight and integrating with some selected step size out to the integration limits.

The primary source of inaccuracy in this approach is the uncertainty in atmospheric density. Near the altitudes of interest, the sensor – line of sight – ellipsoid computations are accurate to better than 100 meters and introduce negligible error. Varying the integration step size over a nominal range has little effect on the results. The coefficients in the density equation should be changed to correspond with current sunspot activity. The coefficients used in the program hold approximately over the 1962-65 period.

With this program, it is possible to determine the total mass per unit area along a line of sight extending out through the atmosphere. The line of sight can be specified either as an azimuth elevation or by specifying the equatorial celestial coordinates of the line of sight terminator. In either case, local topocentric coordinates and the Greenwich civil time are required to make the necessary geometric and time transformations. For application of the program to problems where accurate (better than several percent) solutions are required, it would be necessary to replace the density equation with up-to-date tabular data. For applications similar to those in the present report, the atmosphere above 400 km has little effect on the results since the contribution, even for zero line-of-sight altitude, is less than the uncertainty in the atmospheric model.

March 1966
American Science and Engineering, Inc.
11 Carleton Street
Cambridge, Massachusetts 02142